Transport Properties of a single molecular transistor and also across a metal-semiconductor interface

A Thesis submitted in partial fulfillment of the award of the degree of Doctor of Philosophy

by

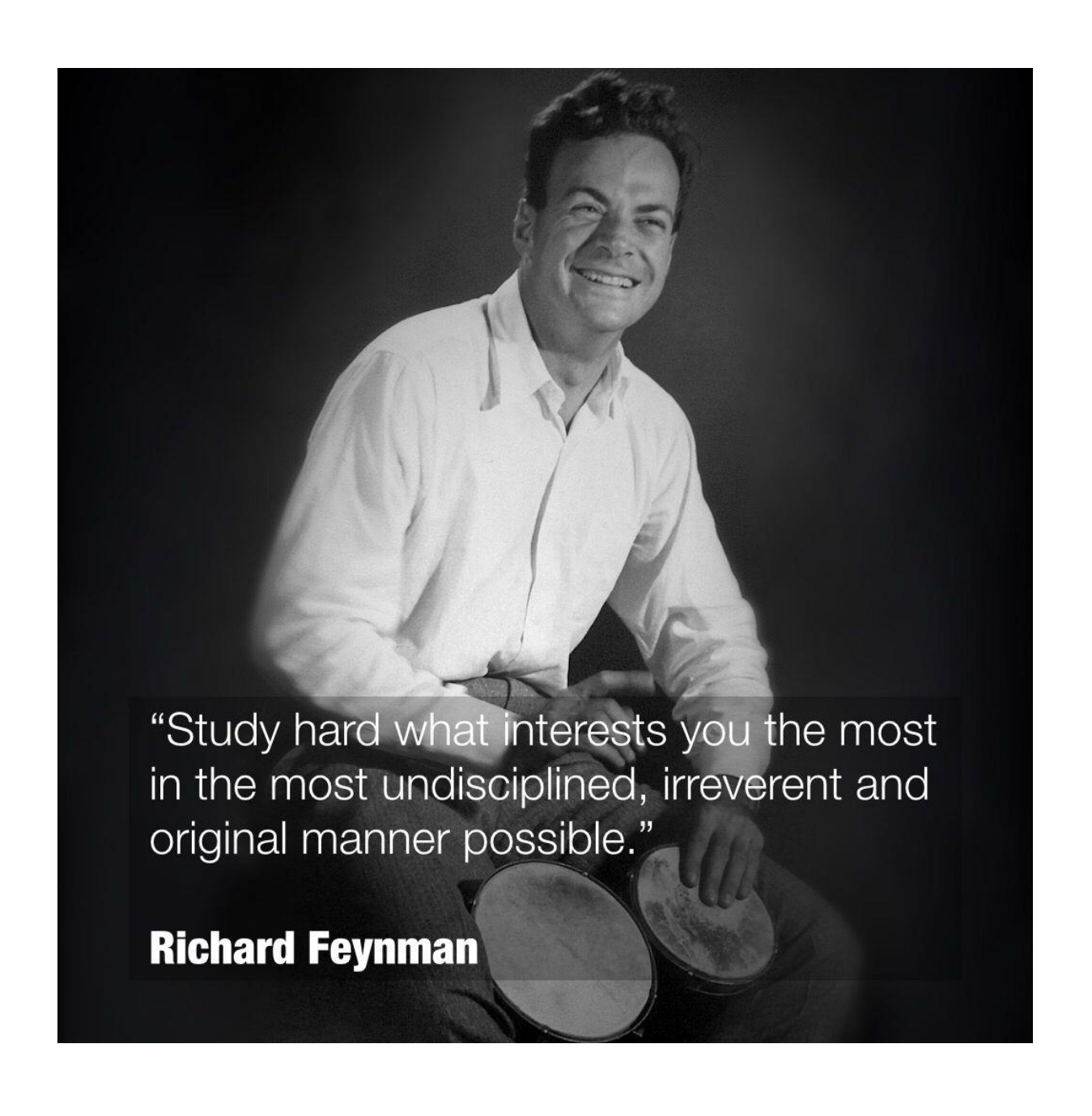
Manasa Kalla

15PHPH22



School of Physics
University Of Hyderabad
Hyderabad- 500046
India

Supervisor: Prof. Ashok Chatterjee



Declaration

I hereby declare that the work detailed in this thesis has been done by me

autonomously in the School of Physics, University of Hyderabad, under

Prof. Ashok Chatterjee, School of Physics, University of Hyderabad. I

additionally declare that this is my own work and exertion, and it has not

been submitted at any other University or institution for any degree. Each

endeavor is taken to plainly demonstrate where other people's

contributions are included, with satisfactory reference to literature and

affirmation of collective exploration and conversations.

Place: Hyderabad

Date: 24 | 03 | 2022

K-mourager Manasa Kalla



Certificate

This is to certify that the thesis work entitled "Transport Properties of a single molecular transistor and also across a metal-semiconductor interface" is being submitted to the University of Hyderabad by Manasa Kalla with Reg. No. 15PHPH22, in partial fulfillment for the award of Doctor of Philosophy in physics, is a bona fide work done by her under my supervision.

This thesis is free from plagiarism and has not been submitted previously in part or in full to this or any other University or Institution for award of any degree or diploma.

The student has the following publications and conference proceedings before the thesis for adjudication.

- 1. **Manasa Kalla**, Narasimha Raju Chebrolu and Ashok Chatterjee, Magneto-transport properties of a single molecular transistor in the presence of electron-electron and electron-phonon interactions and quantum dissipation, *Sci. Rep. 9*, 16510(2019).
- 2. **Manasa Kalla**, Narasimha Raju Chebrolu and Ashok Chatterjee, Quantum transport properties of a single molecular transistor at finite temperature, *Sci. Rep.* 11, 10458 (2021).
- Manasa Kalla, Sanjeev Kumar, Sreekanth Sil and Ashok Chatterjee, Double Refraction and tunneling conductance across the metal-semiconductor junction in the presence of Rashba and Dresselhaus spin-orbit interaction: A spin filtering device, Super lattices and Microstructures 156, 106951 (2021).

- 4. **Manasa Kalla**, Swathi. T.S, Narasimha Raju Chebrolu and Ashok Chatterjee Transport properties of a single-molecular transistor at finite temperature. *IJIIP*, *Vol. 1, Issue 2, (2020)*.
- Manasa Kalla, Ashok Chatterjee Magneto-transport in an Interacting Single Molecular Transistor using Anderson-Holstein model. AIP Conference Proceedings 1942, 110027 (2018).
- Manasa Kalla, Narasimha Raju Chebrolu and Ashok Chatterjee Magnetotransport properties of a single molecular transistor: Anderson-Holstein-Caldeira-Leggett model. AIP Conference Proceedings 2115, 030450 (2019).

Further, the student has passed the following courses towards the fulfillment of the course required for Ph. D

Course Code	Name	Credits	Pass/Fail
PY801	Advanced Quantum Mechanics	4	Pass
PY803	Advanced Statistical Mechanics	4	Pass
PY804	Advanced Electromagnetic Theory	4	Pass
PY821	Research Methodology	4	Pass

Dean

School of physics

DEAN

School of Physics University of Hyderabad HYDERABAD - 500 046 Prof. Ashok Chatterjee Supervisor

Prof. ASHOK CHATTERJEE SCHOOL OF PHYSICS UNIVERSITY OF HYDERABAD HYDERABAD - 500 046, INDIA

Acknowledgments

I consider myself extremely fortunate to have had a chance to work with Prof. Ashok Chatterjee. He has always been encouraging, guiding, while at the same time, he gave me enough freedom to pursue my research interests. He always helped me morally and mentally. Without his guidance, this thesis would not have been possible. I express my gratitude to Prof. Soma Mukhopadhyay for her support during hard times. I want to express my gratitude to my Ph.D. review committee members, Prof. Srinath and Prof. S. V. S. Nageswara Rao, for their insightful comments during doctorate review presentations. I am incredibly grateful to my collaborator and senior colleague, Dr. Narasimha Raju, for his valuable suggestions and discussions. He was always available for me to help whenever needed.

I am thankful to the School of Physics office staff Deepika madam, Abraham Sir, Vijayalakshmi madam, Sudarshan Sir for their help in administrative matters.

I thank all my seniors and colleagues, Uma lavanya, Luhluh Jahan, Dr. Sanjeev kumar, Dr.Shankar, Dr.Aalu Boda, Zahid Malik, Hemant Kumar Sharma, Pooja Saini, Kuntal Bhattacharya and Debika Debnath. I especially thank my childhood friends Lakshmi Chaithanya, Saigeetha, Ramya Sravani, Syed Basha and Parthu for their constant encouragement over the years. I am also grateful to my friends Leelashree, Avisek Das, Muhammed Razi for their constant support. I thank all my batch mates and seniors Naresh, Bappa, Sujai, Rajesh, Taher, Nilanjan, Vinod, Praneetha, Shivaraju, Rashmi, Sharif, Shiva Kumar, Sai Krishna, Dr. Ravi Kumar, Dr. Binoy Hazra, Dr. Anupama, Dr. Nisha and Dr. Atiya. I thank my friends, Amulya, Roja, Chandravathi, Sajidha, Poorvaja, Rajesh, Koti, Nagendra and Surendra for their moral support.

I am thankful to my school teachers Ramu sir, Priyadarshini madam, Sudakar sharma sir, Vijayasharada Madam and Padma Madam for their immense support. I express my sincere thanks to my School, Jawahar Navodaya Vidyalaya, Banavasi, Kurnool (Dist) where I discovered myself.

I want to dedicate this thesis work to my parents K. Srinivasulu, K. Eswari, and my sisters K. Sulochana and Dr. K. Aparna, who supported me and believed in my abilities. Lastly, I would like to acknowledge my nieces Medhasree, Devika, and Parinitha for their unconditional love.

I acknowledge the financial assistance provided by the CSIR-JRF fellowship (09/414(1100)/2015-EMR-I).

Preface

The primary aim of this thesis is to study quantum transport in a single molecular transistor (SMT) and also across a metal-semiconductor interface.

In the first part of the thesis, we consider the problem of an SMT device. An SMT system consists of a central molecule or a quantum dot (QD) with discrete energy levels and coupled to two metal electrodes, one acting as Source (S) and the other as Drain (D). We assume that the source and the drain have continuous energy levels and the central QD has a single energy level and a single phonon mode. An electron can move from the source to the drain through QD by the hopping process. An electron on QD can have local repulsive Coulomb interaction with another electron on the QD by the usual onsite Hubbard interaction. We also consider a QD electron to interact with the QD phonon with the local electron-phonon (el-ph) interaction. We employ Holstein Hamiltonian to model this interaction. Thus the aforementioned SMT system can be described by the Anderson-Holstein model.

The el-ph interaction effects on the transport properties of an SMT device have been studied by several researchers. Chen et al. have investigated non-equilibrium transport in an SMT device using the Keldysh Green function method in the presence of el-ph interaction. They have shown that the current reduces with increase in el-ph coupling due to the polaronic effect. Later, the transport in an SMT system has been examined by Raju and Chatterjee incorporating dissipation and Coulomb correlation in addition to el-ph interaction using Keldysh formalism. They have considered an SMT system based on an insulating substrate that acts as a bath of phonons and incorporated a coupling between the substrate phonons and the QD phonon

using the linear Caldeira-Leggett model which takes care of the dissipative effect. Raju and Chatterjee have employed the Anderson-Holstein-Caldeira-Leggett (AHCL) model to describe whole system and observed that dissipation causes an enhancement in the current through SMT.

In the present thesis, we first investigate how a magnetic field influences the transport properties in the aforementioned dissipative SMT system. work is described in Chapter 2 of thesis. We model our system using the AHCL Hamiltonian. The dissipative interaction between the substrate phonons and the local QD phonon modeled by the Caldeira-Leggett is treated by using a unitary transformation. This results in a reduction in the frequency of the QD phonon, which is precisely the dissipative effect. The el-ph coupling term is dealt with by first performing the Lang-Firsov transformation and then carrying out an expectation value with respect to the zero-phonon state. We calculate the spectral density, the current, the differential conductance and the spin polarization parameter using the Keldysh Green function method. The magnetic field removes the spin degeneracy and this leads to the splitting of QD energy levels and gives rise to peaks of the spectral functions. The el-ph interaction reduces the spin-polarised current densities. The spin-down current density is reduced by the magnetic field whereas the spin-up current density initially increases as the magnetic field increases and beyond a certain field it decreases with increasing field and finally drops to zero. The differential conductance graphs also exhibit the splitting of peaks due to the magnetic field, implying the availability of additional energy levels for transport. As the magnetic field increases, the spin polarization decreases and finally vanishes. The damping is shown to increase the spin-polarised currents. differential conductance, and spin-polarization parameter. This system can have potential application as a spin filter.

Next, we study, in Chapter 3, the effect of temperature on the spectral density, current and differential conductance in an SMT system in the presence of el-

ph interaction, Coulomb correlation and quantum dissipation. Here also we model the system using the AHCL Hamiltonian and study aforementioned transport properties at finite temperature using the Keldysh approach and the equation of motion method. We show that dissipation increases the current density at finite temperature but the increase is less significant than at zero temperatures. The current density is found to decrease as temperature increases, and the behaviour of the differential conductance is found to be similar.

In Chapter 4 of the thesis we study Double refraction and Tunneling conductance of electron spin across a metal-semiconductor interface. We assume an infinite two-dimensional (2D) system in the x - y plane, where a 2D metallic lead fills the region x < 0 and a semiconductor system with Rashba and Dresselhaus spin-orbit interactions occupies the region x > 0. At x = 0, the two materials are separated by an interface. Khodas et al. (*Phys.* Rev. Lett. 92, 086602 (2004)) have used the spin-orbit interaction effect to cause electron polarisation in nonmagnetic semiconductor heterostructures and Dargys (Superlattices Microstruct. 48, 221, (2010)) has explored the phenomenon of electron reflection by an infinite barrier in a 2D device. Extending the works of Khodas et al. and Dargys, we investigate the reflection and refraction of electrons at a metal/semiconductor interface where the semiconducting material can be considered as a semi-infinite 2D electron gas with non-zero spin-orbit interactions. The current density and differential conductance are also calculated. We calculate experimentally measurable quantities such as spin-up and spin-down currents and corresponding differential conductances, as well as spin-polarization current in the metallic and semiconductor region and investigate the role of incident angle, incident energy, applied voltage, and spin-orbit interactions on them. We show that the Dresselhaus interaction reduces the angle of refraction of spin-up and spin-down electrons, with the spin-down electrons undergoing a more

significant reduction. When both the spin-orbit interactions are considered, the spin polarization is found to increase significantly, improving the spin-filtering effect observed in the presence of Rashba coupling alone. We find that increasing the incident energy increases the angle of refraction of spin-up electrons and decreases the angle of refraction of spin-down electrons. Therefore, the spin-filtering effect can be controlled by tuning the incident energy. The currents corresponding to spin-up and spin-down electrons reduce as the Fermi energy is increased. However, they increase as the applied voltage is increased. In the semiconductor region, the spin polarisation current turns out to be negative in the presence of both Rashba and Dresselhaus interactions, and it decreases with increasing Dresselhaus interaction. In contrast, the spin polarisation current in the metallic region turns out to be positive and decreases with increasing Dresselhaus coupling. The present work can have potential applications in spin-filtering and spin-polarising devices.

List of Publications based on which the thesis has been written

- 1. **Manasa Kalla**, Narasimha Raju Chebrolu and Ashok Chatterjee, Magneto-transport properties of a single molecular transistor in the presence of electron-electron and electron-phonon interactions and quantum dissipation, *Sci. Rep. 9*, 16510(2019).
- 2. **Manasa Kalla**, Narasimha Raju Chebrolu and Ashok Chatterjee, Quantum transport properties of a single molecular transistor at finite temperature, *Sci. Rep.* 11, 10458 (2021).
- 3. **Manasa Kalla**, Sanjeev Kumar, Shreekantha Sil and Ashok Chatterjee, Double Refraction and tunneling conductance across the metalsemiconductor junction in the presence of Rashba and Dresselhaus spinorbit interaction: A spin filtering device, *Super lattices and Microstructures* 156, 106951 (2021).
- 4. **Manasa Kalla**, Swathi. T.S, Narasimha Raju Chebrolu and Ashok Chatterjee Transport properties of a single-molecular transistor at finite temperature. *IJIIP*, *Vol. 1*, *Issue 2*, (2020).

Other publications (not included in the thesis)

- 1. **Manasa Kalla**, Narasimha Raju Chebrolu and Ashok Chatterjee, Transient dynamics of a single molecular transistor in the presence of electron-phonon interaction at zero temperature (Under review).
- 2. H. K. Sharma, **Manasa Kalla** and A. Chatterjee, Non-equilibrium Quantum transport through a Quantum dot dimer in the presence of electron-electron interaction, electron-phonon interaction, magnetic field and quantum dissipation (to be communicated).
- 3. Kuntal Bhattacharya, **Manasa Kalla** and A.Chatterjee, Quantum transport in a dissipative single molecular transistor in the presence of electron correlations and polaronic interaction at a finite temperature and external magnetic field (to be communicated).

List of Publications in Conference proceedings

- 1. **Manasa Kalla**, Ashok Chatterjee Magneto-transport in an Interacting Single Molecular Transistor using Anderson-Holstein model. *AIP Conference Proceedings* 1942, 110027 (2018).
- Manasa Kalla, Narasimha Raju Chebrolu and Ashok Chatterjee Magnetotransport properties of a single molecular transistor: Anderson-Holstein-Caldeira-Leggett model. AIP Conference Proceedings 2115, 030450 (2019).
- 3. Kuntal Bhattacharya, **Manasa Kalla** and A.Chatterjee, Effect of finite temperature and external magnetic field on the non-equilibrium transport in a single molecular transistor with quantum dissipation: Anderson-Holstein-Caldeira-Leggett model, *Materials today: Proceedings*(2021).

List of Conferences and workshops attended

- Poster Presentation: Manasa Kalla and Ashok Chatterjee, "Magneto-transport in an Interacting Single Molecular Transistor using Anderson-Holstein model", 'DAE SSPS 2017', December 26-30 2017, BARC Mumbai, Maharashtra.
- Oral presentation: Manasa Kalla, Narasimha Raju Chebrolu, Ashok Chatterjee, "Magneto-transport properties of a single molecular transistor: Anderson-Holstein-Caldeira-Leggett Model", International Conference on Advanced basic sciences, February 7-9, 2018, GDC Memorial College, Bahal, Bhiwani district, Haryana.
- Poster presented: Manasa Kalla, Narasimha Raju Chebrolu and Ashok Chatterjee, "Magneto-transport properties of a single molecular transistor: Anderson-Holstein-Caldeira-Leggett Model", 'DAE SSPS 2018', December 18-22 2018, Guru Jambeshwar University of Science and Technology, Hisar, Haryana.
- Workshop attened: Manasa Kalla, "Integrable systems in Mathematics, Condensed matter and Statistical physics", July 16 – August 10, 2018, ICTS, Bangalore, Karnataka.
- Poster presented: Manasa Kalla, D. Sanjeev Kumar, Shreekantha Sil, and Ashok Chatterjee, "Double refraction of electron spin across metalsemiconductor junction with spin-orbit interactions" 2nd Annual Conference on Quantum Condensed Matter, July 8-10, 2019, IISc, Bangalore.
- Oral presentation: Manasa Kalla, Swathi.T.S, Narasimha Raju Chebrolu and Ashok Chatterjee, "Transport properties of a single molecular

transistor at finite temperature", International Conference on Condensed Matter Physics, November 14 -16, 2019, Department of Basic Science and Humanities, Institute of Engineering & Management, Kolkata.

Contents

	Declaration form	I
	Certificate	II
	Acknowledgments	III
	Preface	IV
	List of publications	V
	Contents	VI
1.	Introduction	
	1.1 Single molecular transistor	
	1.1.1 What is an SMT device and its importance	1
	1.1.2 Anderson-Holstein-Caldeira-Leggett model	3
	1.2 Tunneling across a Metal-Semiconductor Interface	8
	1.3 Organization of thesis	10
	1.4 References	11
2.	Magneto-transport properties: Keldysh Formalism	
	2.1 Introduction	16
	2.2 Model Hamiltonian	17
	2.3 Decoupling of bath phonons	19
	2.4 Effective Hamiltonian: Lang-Firsov transformation	21
	2.5 Current density, Differential conductance and Spin polarization	23
	2.6 Results and discussions	37
	2.7 Conclusions	62
	2.8 References	64
3.	Temperature effect on the transport	
	3.1 Introduction	66
	3.2 Model and Calculations	66

	3.3 Results and discussions	71
	3.4 Summary	84
	3.5 References	85
4.	Double Refraction: Metal-Semiconductor interface	
	4.1 Introduction	87
	4.2 Model and Hamiltonian Descriptions	88
	4.3 Formalism	91
	4.4 Results and discussions	99
	4.5 Conclusions	118
	4.6 References	119
5.	Conclusions	124

Chapter 1

Introduction

In this thesis we mainly study the transport properties of a Single Molecular Transistor. We also study the Tunneling Conductance of electron spin across a metal-semiconductor interface in the presence of Rashba and Dresselhaus spin-orbit interactions in the semiconductor medium.

1.1 Single molecular transistor (SMT)

1.1.1 Introduction

In the last four decades, we have seen the shift from the employment of bulk systems to nanosystems, semiconductor systems, and magnetic systems in material science applications. The quantum effects become extremely important for the nanosystems. Early studies have provided us with a number of important and interesting features about the physics of nanosystems, their quantum transport properties, and device applications. The field has been adequately discussed by Datta [1]. In recent years, due to advances in fabrication techniques and the availability of instrumentation facilities, detailed investigations have been carried out on the electronic, optical, transport and magnetic properties of various nanosystems.

In 1974, Aviram and Ratner [2] have given the theoretical design of a molecular device using a single organic molecule and observed that the response of this device in an applied field works as a rectifier. Later, a few research groups fabricated a single molecular transistor [3, 4] using organic molecules. An SMT device usually consists of a central molecule or any nanosystem like a quantum dot (QD) that would have discrete energy levels. It is connected to two metallic electrodes, one being the Source (S) and the other the Drain (D). In an SMT device [5, 6], the current can be successfully regulated by adjusting the gate voltage.

Considering the potential applications of molecular electronic devices, research on SMTs [7-9] has received significant attention in the last few decades and provided many interesting results. It has been suggested that SMTs can have important applications in micro-electronic technology as spin-filtering devices [10], switching devices [11], sensors [12] etc. At low temperature, an SMT device shows very many interesting properties such as non-equilibrium effects of el-ph interaction during the charge tunneling like phonon-assisted tunneling transport [13, 14], Coulomb blockade [15], Kondo effect [16-18], hysteresis-induced bistability [19- 21], local heating [22, 23], molecular switching and negative differential conductance [24, 25]. If a polar QD is considered as a central molecular in an SMT device, transport mechanism will be additionally influenced by polarons which are

quasi-particles consisting of electrons dressed with a cloud of virtual phonons and form because of the el-ph interaction. Thus, the quantum transport phenomena in an SMT device are influenced by both *el-el* and *el-ph* interactions. The transport properties of SMT have been investigated by using different theoretical and numerical methods like kinetic equation method [26, 27], rate equation approach [28], slave-boson mean-field method [29], non-crossing approximation method [30], numerical renormalization method [31-33] and non-equilibrium Green's function approaches [34-38].

1.1.2 Anderson-Holstein-Caldeira-Leggett model

The schematic representation of an SMT system that we have investigated in this thesis is shown in Fig. 1. It is connected to two metallic electrodes, one being the Source (S) and the other the Drain (D).

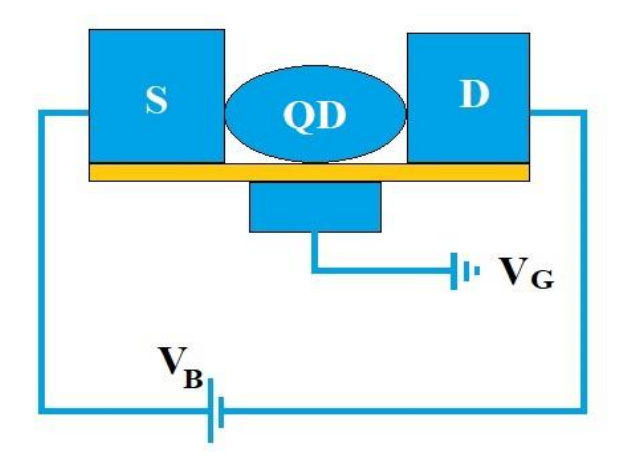


Fig.1 Schematic representation of an SMT device

Since the Source (S) and the Drain (S) contain free electrons, they can be described by the Hamiltonian

$$H_{S,D} = \sum_{k,\sigma \in S,D} \varepsilon_{k\sigma} n_{k\sigma} , \qquad (1.1)$$

where $\varepsilon_{k\sigma}$ is the energy of a free electron in S or D with momentum k and spin σ and $n_{k\sigma}(=c_{k\sigma}^{\dagger}c_{k\sigma})$ represents the number operator corresponding to these electrons, $c_{k\sigma}^{\dagger}(c_{k\sigma})$, referring to the corresponding creation (annihilation) operator.

We consider the QD to have a single energy level of energy ε_d . We also include the el-el interaction in the QD. Such a QD can be modelled by the Hubbard model which is described by the Hamiltonian

$$H_{QD} = \sum_{\sigma} (\varepsilon_d - eV_g) n_{d\sigma} + U n_{d,\uparrow} n_{d,\downarrow}$$
 (1.2)

where $n_{d\sigma}(=c_{d\sigma}^{\dagger}(c_{d\sigma}))$ is the number operator for the QD electrons of spin σ with ε_d as the onsite energy, $c_{d\sigma}^{\dagger}(c_{d\sigma})$ being the creation (annihilation) operator for the QD electrons and V_g is the gate voltage that can be used to tune the energy level. U denotes the onsite el-el interaction strength in QD.

We consider the electron to move from one site to anther by hopping and the hopping Hamiltonian (H_h) can be written as

$$H_h = \sum_{\sigma, k\alpha \in S, D} V_k (c_{k\alpha}^{\dagger} c_{d\sigma} + h.c)$$
 (1.3)

where V_k represents the hybridization coefficient that governs the tunnelling strength for the electron to tunnel between the QD and the leads.

The system described above can be modelled by the Anderson Hamiltonian [39]. Many research groups have employed the Anderson model to investigate different solid state systems like mixed valence systems, superconductors, Heavy fermions, negative tunneling centers in semiconductor glasses, etc.. Thus the Anderson Hamiltonian corresponding to our system described above is given by

$$H = H_{S,D} + H_{QD} + H_{h}$$

$$= \sum_{k\alpha} \varepsilon_{k} n_{k\alpha} + \sum_{\sigma} \varepsilon_{d} n_{d\sigma} + U n_{d,\uparrow} n_{d,\downarrow} + \sum_{\sigma,k\alpha \in S,D} V_{k} (c_{k\sigma}^{\dagger} c_{d\sigma} + h.c)$$
(1.4)

The QD is assumed to have a single local phonon mode of dispersionless frequency ω_0 which can be described by the free phonon Hamiltonian

$$H_{QD-ph} = \hbar \omega_0 b^{\dagger} b \,. \tag{1.5}$$

where $b^{\dagger}(b)$ represents the creation (annihilation) operator of the QD phonon. The above phonon mode is assumed to interact with the local QD electrons through el-ph interaction which can be described by the Holstein model:

$$H_{QD-ep} = \lambda \hbar \omega_0 (b^{\dagger} + b) \sum_{\sigma} n_{d\sigma}. \tag{1.6}$$

where λ gives the *el-ph* coupling constant. Thus the SMT system consisting of S, D and QD can be described by the Anderson-Holstein Hamiltonian which can be written as

$$H = H_{S,D} + H_{QD} + H_h + H_{QD-ph} + H_{QD-ep}$$

$$= \sum_{k\alpha} \varepsilon_k n_{k\alpha} + \sum_{\sigma} \varepsilon_d n_{d\sigma} + U n_{d\uparrow} n_{d\downarrow} + \sum_{\sigma, k\alpha \in S, D} V_k (c_{k\alpha}^{\dagger} c_{d\sigma} + h. c)$$
$$+ \hbar \omega_0 b^{\dagger} b + \lambda \hbar \omega_0 (b^{\dagger} + b) \sum_{\sigma} n_{d\sigma} . \tag{1.7}$$

Many research groups have examined the el-ph interaction effects on transport in an SMT system. Chen et al. [40] have found that el-ph coupling generates side bands in the spectral density and makes the width of the zero-phonon peak narrower. They have also analysed how the chemical potentials of the leads influence the tunnelling current and differential conductance at zero temperature. Later, Raju and Chatterjee (RC) [41] have examined, for the first time, the dissipative effect on the transport properties of an SMT system at zero temperature using the Keldysh technique incorporating the effects of el-ph interaction and Coulomb correlation. RC have considered an arrangement in which the SMT device is mounted on a substrate which is an insulator and acts as a phonon bath. They have assumed that the single phonon mode of the QD interacts with the substrate phonons leading to quantum dissipation in the SMT current. RC have incorporated the coupling of the QD phonon with the substrate phonons using the Caldeira-Leggett (CL) model. The bath Hamiltonian (H_B) considered by RC is given by

$$H_B = \sum_{j=1}^{N} \left[\frac{p_j^2}{2m_j} + \frac{1}{2} m_j \omega_j^2 x_j^2 \right] + \sum_{j=1}^{N} \beta_j x_j x_0 , \qquad (1.8)$$

where $x_{j's}$ and x_0 refer to the position coordinates of the substrate oscillators and the QD, respectively, ω_j denotes the frequency of the j-th substrate oscillator and β_j represents coupling strength of interaction between the QD oscillator and the j-th substrate oscillator. Hence, the

whole system is modeled using Anderson-Holstein-Caldeira-Leggett (AHCL) Hamiltonian. Thus the total Hamiltonian studied by RC is given by

$$H = H_{S,D} + H_{QD} + H_h + H_{QD-ph} + H_{QD-ep} + H_B$$

$$= \sum_{k\alpha} \varepsilon_k n_{k\alpha} + \sum_{\sigma} \varepsilon_d n_{d\sigma} + U n_{d,\uparrow} n_{d,\downarrow} + \sum_{\sigma,k\alpha\epsilon S,D} V_k (c_{k\alpha}^{\dagger} c_{d\sigma} + h.c)$$

$$+ \hbar \omega_0 b^{\dagger} b + \lambda \hbar \omega_0 (b^{\dagger} + b) \sum_{\sigma} n_{d\sigma} + \sum_{j=1}^{N} \left[\frac{p_j^2}{2m_j} + \frac{1}{2} m_j \omega_j^2 x_j^2 \right]$$

$$+ \sum_{j=1}^{N} \beta_j x_j x_0.$$
(1.9)

RC have used the the non-equilibrium Keldysh formalism and the Equation of motion technique to study el-ph interaction effect on the spectral density, tunnelling current and differential conductance in the presence of quantum dissipation. According to their calculations, the local phonon frequency of QD gets renormalized because of phonon dissipation. Furthermore, the el-ph interaction decreases the tunnelling current whereas the phononic dissipation increases it.

In the present thesis we consider the aforementioned SMT device in a magnetic field and study its magneto-transport properties using the Keldysh technique and the Equation of motion method within the framework of the Green function formalism. We furthermore examine the effect of temperature on the quantum transport in an SMT system at zero magnetic field.

1.2 Tunneling across a Metal-Semiconductor Interface

In the second part of the thesis, we study double refraction and tunneling current across a metal-semiconductor interface. The system we consider is an infinite 2D system in the x - y plane, where a 2D metallic lead fills the negative-x region and a semiconductor system fills the positive-x region. At x = 0, the two materials are separated by an interface.

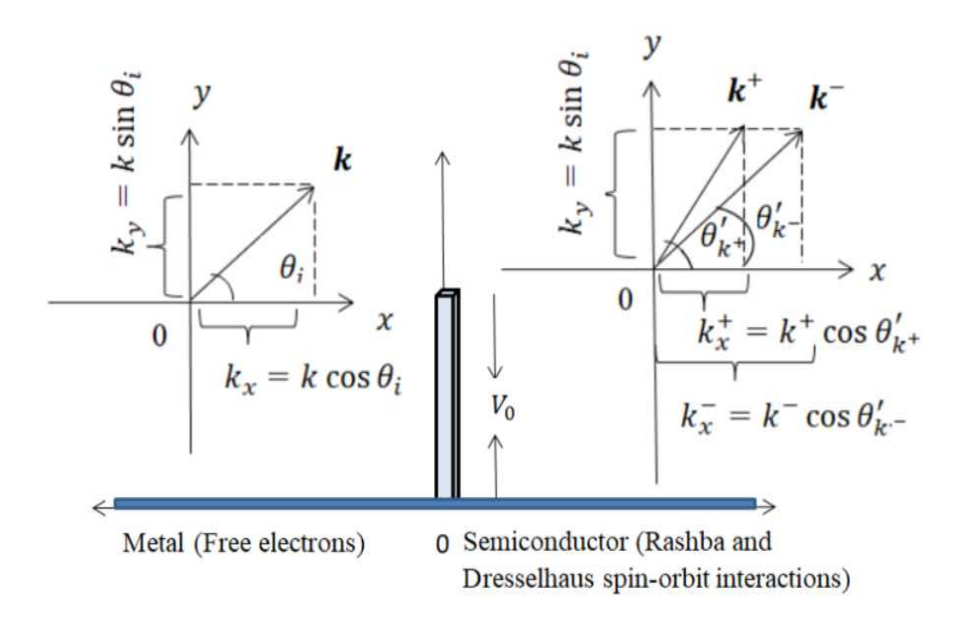


Fig.2 Schematic sketch of the system

This problem has been earlier studied by Khodas et al. [42] by incorporating the Rashba spin-orbit interaction (RSOI) in the semiconductor medium.

The Dirac theory provides a term known as the Thomas term (H_T) which is given by

$$H_T = -\frac{e\hbar\sigma. (\mathbf{E} \times \mathbf{p})}{4m^2c^2} \ . \tag{1.10}$$

where p refers to the electron momentum and σ the spin. In an electric field $E = E \hat{z}$, the system loses the inversion symmetry at the surface and the Thomas term reads

$$H_T = H_R = -\frac{e\hbar\sigma \mathbf{E}.(\hat{\mathbf{z}}\times\mathbf{p})}{4m^2c^2} = -\frac{\alpha}{\hbar}\left(\sigma_y p_x - \sigma_x p_y\right). \tag{1.11}$$

Eq. (11) is the well-known Rashba spin-orbit interaction (RSOI) where $\alpha = \frac{e\hbar^2 E}{4m^2c^2}$ denotes the RSOI strength which in certain systems can be significantly large. It has been shown by Khodas et al. that in the presence of RSOI in region II, there will be a split in the path of the spin-up and spin-down electrons which suggests that the system under consideration can have potential application as a spin-filtering device.

In systems which have zinc blend structure, such as a GaAs system, the bulk inversion symmetry is also broken. This gives rise to another important spin-orbit interaction known as the Dresselhaus SOI (DSOI) and is given by

$$H_D = \frac{\beta}{\hbar} \left(\sigma_x p_x - \sigma_y p_y \right) . \tag{1.12}$$

DSOI can have sizable effect on spin transport and therefore in the present thesis, we study the transport across the metal-semiconductor interface incorporating both RSOI and Dresselhaus spin-orbit interactions (DSOI). More specifically, we explore the RSOI and DSOI effects on the tunnelling current, differential conductance and the spin polarization. We show that in the presence of the Dresselhaus interaction, the spin-filter effect is enhanced significantly.

1.3 Organization of Thesis

In the present thesis, we mainly study the transport properties of a single molecular transistor. We also study the spin transport across a metal-semiconductor interface. The organization of the thesis as follows.

In the present chapter i. e., Chapter 1, we have introduced the subject of Single Molecular Transistor and briefly touched upon the problem of Transport across a Metal-Semiconductor junction.

In the following chapter i. e., in Chapter 2, we study magneto-transport in an SMT device incorporating the effects of el-el interaction, el-ph interaction and quantum dissipation. We deal with the problem using the non-equilibrium Green function method. We present, in detail, the derivation of the current density using the Equation of motion method and the Keldysh formalism. We model the system using the AHCL Hamiltonian introduced in this chapter. We study, in particular, the magnetic field on the tunneling current, spectral density, differential conductance, and spin-polarization parameter at zero temperature.

In Chapter 3, we investigate quantum transport through SMT at finite temperature. In particular, we consider an SMT system with el-ph interaction, Coulomb correlation and quantum dissipation at finite temperature and zero magnetic field and obtain the spectral density, tunneling current and differential conductance using the temperature-dependent Keldysh formalism.

Next, in Chapter 4, we delineate our work on the spin transport across a

metal-semiconductor interface. We incorporate Rashba and Dresselhaus spin-orbit interactions in the semiconductor region of the system. Because of the spin-orbit interactions the up-spin and down-spin electrons have different angles of refraction. This gives rise to a double refraction phenomenon leading to the spin-filtering effect. We show that Dresselhaus interaction significantly increases the spin-filtering effect caused by the Rashba interaction alone.

Finally, in Chapter 5, we summarize the main results of the present thesis and make concluding remarks.

1.4References

- 1. S. Datta, Electronic Transport in Mesoscopic Systems. (Cambridge University Press, 1997).
- 2. A. Aviram, M. A. Ratner. Molecular Rectifiers. *Chem. Phys. Lett.* **29**, 277(1974).
- 3. W. Liang, M. P. Shores, M. Bockrath, J. R. Long. & H. Park. Kondo resonance in a single-molecule transistor. *Nature* **417**, 725-729(2002).
- 4. H. Park *et al.* Nanomechanical oscillations in a single-C60 transistor. *Nature* **407,** 57-60 (2000).
- 5. Tans Sander. J, Verschueren Alwin. R. M. & Cees Dekke. Room-temperature transistor based on a single carbon nanotube, Nature, **393**, 49-52 (1998);
- 6. Makoto. Y *et al.* Molecular floating-gate single-electron transistor. *Sci. Rep* 7, 1589 (2017).

- 7. Mickael, L. P, Enrique, B and Herre S. J. van der Zant. Single-molecule transistors. *Chem. Soc. Rev.* **44**, 902 (2015).
- 8. Abdelghaffar N, Aïmen. B, Bilel. H, Wassim. K and Adel. K. High-sensitivity sensor using C60-Single molecule transistor. IEEE Sensors journal **18** 1558-1748(2018)
- 9. Stokbro. K. First-principles modeling of molecular single-electron transistors. *J. Phys. Chem. C* **114**, 20461 (2010).
- 10. Costi. T. A. Magneto-transport through a strongly interacting quantum dot. *Phys. Rev.* B **64**, 241310(R) (2001).
- 11. Meded. V, Bagrets. A Arnold. A, and Evers. F, Molecular Switch Controlled by Pulsed Bias Voltages, *Small* **5**, 2218 (2009).
- 12. Ray. S. J. Single molecular transistor as a superior gas sensor. J. *Appl. Phys.* **118**, 034303 (2015).
- 13. Chen. Z. Z, Lü. H, Lu. R and Zhu. B. Phonon-assisted Kondo Effect in a Single-Molecule Transistor out of Equilibrium. *J. Phys.: Condens. Matter* **18** 5435 (2006).
- 14. Jeon. G. S, Park. T. H & Choi. H. Y. Numerical renormalization-group study of the symmetric Anderson-Holstein model: Phonon and electron spectral functions. *Phys. Rev. B* **68**, 045106 (2003).
- Pipit. U. V, Yasuo. A, Masanori. S, Toshiharu. T, Yutaka. M. Coulomb blockade and Coulomb staircase behavior observed at room temperature. *Mater. Res. Express* 4, 024004 (2017).
- 16. Gordon. D. G, *et al.* Kondo effect in a single-electron transistor. *Nature* **391**, 156 (1998).

- 17. Yu. L. H & Natelson. D. The Kondo Effect in C₆₀ Single-Molecule Transistors. *Nano Lett.* **4,** 79(2003).
- 18. Gonzalez. G, Leuenberger. M. N & Mucciolo. E. R. Kondo effect in single-molecule magnet transistors. *Phys. Rev. B* **78**, 054445 (2008).
- Li. C, Zhang. D, Liu. X, Han. S, Tang. T, Zhou. C, Fan. W, Koehne. J, Han. J, Meyyappan. M, et al. Fabrication approach for molecular memory arrays, *Appl. Phys. Lett.* 82, 645 (2003).
- Liljeroth. P, Repp. J, and Meyer. G, Current-Induced Hydrogen Tautomerization and Conductance Switching of Naphthalocyanine Molecules, *Science* 317, 1203 (2007).
- 21. Huang. Z, Xu. B, Chen. Y, Di Ventra. M, and Tao. N, Measurement of Current-Induced Local Heating in a Single Molecule Junction, *Nano Lett.* **6**, 1240 (2006).
- 22. Choi. B. Y, Kahng. S. J, Kim. S, Kim. H, Kim. H. W, Song. Y. J, Ihm. J, and Kuk. Y, Conformational Molecular Switch of the Azobenzene Molecule: A Scanning Tunneling Microscopy Study, *Phys. Rev. Lett.* **96**, 156106 (2006).
- 23. Sapmaz. S, Jarillo-Herrero. P, Blanter. Ya. M, Dekker. C, and van der Zant. H. S. J, Tunneling in Suspended Carbon Nanotubes Assisted by Longitudinal Phonons, *Phys. Rev. Lett.* **96**, 026801(2006).
- 24. Gaudioso. J, Lauhon. L. J, and Ho. W, Vibrationally Mediated Negative Differential Resistance in a Single Molecule, *Phys. Rev. Lett.* **85**, 1918 (2000).

- 25. Pop. E, Mann. D, Cao. J, Wang. Q, Goodson. K, and Dai. H, Negative Differential Conductance and Hot Phonons in Suspended Nanotube Molecular Wires, *Phys. Rev. Lett.* **95**, 155505 (2005).
- 26. Boese, D. & Schoeller, H. Influence of nanomechanical properties on single-electron tunneling: a vibrating single-electron transistor. *Europhys. Lett.* **54**, 668 (2001).
- 27. McCarthy, K. D, Prokof 'ev, N. & Tuominen, M. T. Incoherent dynamics of vibrating single-molecular transistor. *Phys. Rev. B* **67**,245415–6 (2003).
- 28. Mitra. A Aleiner. I. & Millis. A. Phonon effects in molecular transistors: quantal and classical treatment. J. *Phys. Rev. B* **69**, 245302–21(2004).
- 29. Meir. Y, Wingreen. N. S and Lee. P. A. Low-temperature transport through a quantum dot: The Anderson model out of equilibrium. *Phys. Rev.* Lett. 70, 2601 (1993).
- 30. Wingreen. N. S and Meir.Y. Anderson model out of equilibrium: Noncrossing-approximation approach to transport through a quantum dot. *Phys. Rev.* B 49, 11 040 (1994).
- 31. Hewson. A. C & Meyer. D. Numerical renormalization group study of the Anderson-Holstein impurity model. *J. Phys. Cond. Matter* 14, 427 (2002).
- 32. Khedri. A Costi. T.A, Meden V. Exponential and power-law renormalization in phonon-assisted tunneling, *Phys. Rev.B* **96**, 195155 (2017).
- 33. Khedri. A Costi. T.A, Meden V. Influence of phonon-assisted tunneling on the linear thermoelectric transport through molecular quantum dots, *Phys. Rev.B* **96**, 195156 (2017).
- 34. Khedri. A Costi. T.A, Meden V. Nonequilibrium thermoelectric transport through vibrating molecular quantum dots, *Phys. Rev.B* **98**, 195138 (2018).

- 35. Keldysh. L. V. Diagram technique for nonequilibrium processes. *Sov. Phys. JETP* **20**, 1018–1026 (1965).
- 36. Datta, S. Quantum Transport: Atom to Transistor. (Cambridge University Press, 2005).
- 37. Haug, H. & Jauho, A. P. Quantum Kinetics in Transport and Optics of Semiconductors (Springer, 1996).arXiv:0711.4881v1.
- 38. Song. J, Sun. Q. F, Gao. J and Xie. X. C. Measuring the phonon-assisted spectral function by using a non-equilibrium three-terminal single-molecular device. *Phys. Rev B.***75**, 195320(2007).
- 39. Anderson. P. W, Localized Magnetic States in Metals, *Phys. Rev.* **124**, 41(1961).
- 40. Chen. Z. Z, Lü. R, Zhu B. F. Effects of electron-phonon interaction on nonequilibrium transport through a single-molecule transistor. *Phys, Rev. B* **71**, 165324 (2005).
- 41. Narasimha Raju. Ch. and Ashok. C. Quantum dissipative effects on non-equilibrium transport through a single-molecular transistor: The Anderson-Holstein-Caldeira-Leggett model. Scientific Reports. 6, 18511 (2016).
- 42. Khodas. M, Shekhter. A, Finkel'stein. A. M, *Phys. Rev. Lett.* **92**, 086602, (2004).

Chapter 2

Magneto-transport properties of a single molecular transistor

2.1 Introduction

In this chapter, we study quantum magneto-transport in an SMT system using the non-equilibrium Green function theory due to Keldysh. Costi [1] has demonstrated using Wilson's renormalization group method that a magnetic field can influence the electron transport properties of a QD in an SMT system. They have also proposed that a strongly coupled QD in a magnetic field can be used as a spin-filtering device. The properties of the device can also be tuned by controlling the gate voltage. According to Dong et al. [2], the magnetic field reduces the linear conductance at zero-temperature. It has also been reported that when the magnetic field is sufficiently increased, the conductance develop side peaks. The SMT system has been recently studied in the presence of quantum dissipation by Raju and Chatterjee [12] (RC). In the presence of el-ph interaction, Coulomb correlation, quantum dissipation and an external magnetic field.

To model the system, we add to the AHCL Hamiltonian introduced in Chapter 1, the Zeeman term (arising because of the presence of the magnetic field) and calculate the current density using the equation of motion method. We also explore the effect of the magnetic field on the SMT properties namely, the spectral density (SD) function and the spin-polarized currents and differential conductances.

2.2 The Model

The SMT device, under consideration, consists of a single-level QD as a central molecule which is connected to two metallic electrodes, one being the Source (S) and the other the Drain (D). The entire system is placed on a substrate which is an insulator and which can act as a bath of independent oscillators. Electrons from S can hop to QD and from QD to D. The central QD is assumed to have one phonon mode that can interact with the bath phonons through the linear Caldeira-Leggett (CL) interaction [3] and also with the local QD electrons though the Holstein interaction. The electrons on QD can also interact with each other

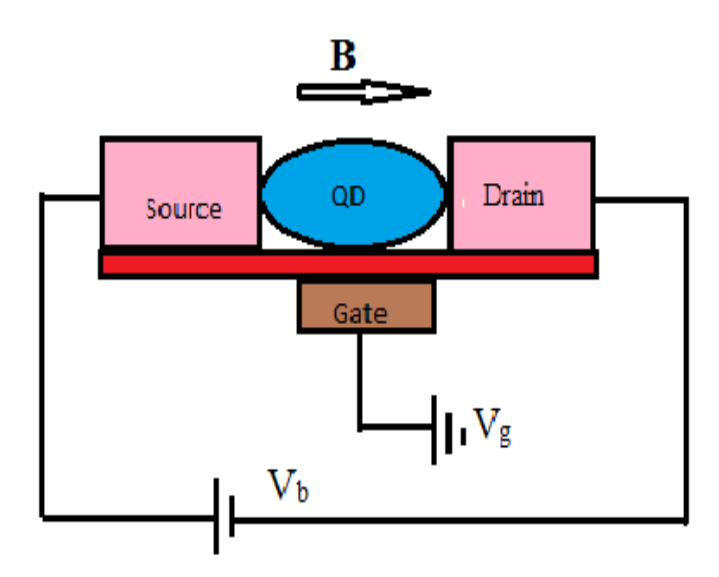


Fig.1 Schematic representation of an SMT device.

through the onsite Hubbard interaction. The CL interaction [3] causes a dissipation in the SMT current. Fig.1 shows a schematic diagram of an SMT device placed in a external magnetic field. The external field applied to QD is expected to modify its transport properties, and such effects have indeed been observed [4, 5].

As the external field lifts the QD's spin-degeneracy, the QD configuration acts as a spin filter producing spin-polarized currents. Because of the external magnetic field, we will have an additional term H_M in the AHCL Hamiltonian introduced in Sec. 1.1.2 of Chapter 1. H_M is given by

$$H_M = \frac{1}{2}g\mu_B B S_d^Z \quad , \tag{2.1}$$

where $\mathbf{B}(0,0,B) = \mathbf{\hat{z}}B$ and S_d^z refers to the z component of the total spin of the QD electrons. The SMT Hamiltonian is thus given by

$$H = H_{S,D} + H_{QD} + H_h + H_{QD-ph} + H_{QD-ep} + H_B + H_M$$

$$= \sum_{k\alpha} \varepsilon_k n_{k\alpha} + \sum_{\sigma} \varepsilon_d n_{d\sigma} + U n_{d,\uparrow} n_{d,\downarrow} + \sum_{\sigma,k\alpha\in S,D} V_k (c_{k\alpha}^{\dagger} c_{d\sigma} + h.c)$$

$$+ \hbar \omega_0 b^{\dagger} b + \lambda \hbar \omega_0 (b^{\dagger} + b) \sum_{\sigma} n_{d\sigma}$$

$$+ \sum_{j=1}^{N} \left[\frac{p_j^2}{2m_j} + \frac{1}{2} m_j \omega_j^2 x_j^2 \right] + \sum_{j=1}^{N} \beta_j x_j x_0 + \frac{1}{2} g \mu_B B S_d^z . \tag{2.2}$$

The spectral function $(J(\omega))$ for the substrate phonons can be represented as:

$$J(\omega) = \sum_{j=1}^{N} \left[\frac{\beta_j^2}{2m_j \omega_j} \right] \delta(\omega - \omega_j). \tag{2.3}$$

2.3 Decoupling of the substrate oscillators

We first consider the following vibrational part of Eq. (2.2):

 $H_{OD-nh} + H_B$

$$= \left(\frac{p_0^2}{2m_0} + \frac{1}{2} m_0 \omega_0^2 x_0^2\right) + \sum_{j=1}^N \left[\frac{p_j^2}{2m_j} + \frac{1}{2} m_j \omega_j^2 x_j^2\right] + \sum_{j=1}^N \beta_j x_j x_0, \quad (2.4)$$

where the first term denotes the free phonon part of the QD Hamiltonian $\hbar\omega_0 b^{\dagger}b$ and perform the following canonical transformations

$$\tilde{x}_j = \left[x_j + \frac{\beta_j x_0}{\left(m_j \omega_j^2 \right)} \right],\tag{2.5}$$

$$\tilde{p}_j = -i\hbar \, \frac{\partial}{\partial \tilde{x}_i} = -i\hbar \, \frac{\partial}{\partial x_i} = p_j \,. \tag{2.6}$$

Eq. (2.6) then transforms to

$$H_{QD-ph} + H_B = \left(\frac{p_0^2}{2m_0} + \frac{1}{2} m_0 \widetilde{\omega}_0^2 x_0^2\right) + \sum_{j=1}^N \left(\frac{\widetilde{p}_j^2}{2m_j} + \frac{1}{2} m_j \omega_j^2 \widetilde{x}_j^2\right), \quad (2.7)$$

where

$$\widetilde{\omega}_0 = [\omega_0^2 - (\Delta \omega)^2]^{1/2} \quad ; \qquad \Delta \omega = \left(\sum_{j=1}^N \frac{{\beta_j}^2}{m_0 m_j \omega_j^2}\right)^{1/2}.$$
 (2.8)

Eq. (2.7) suggests that the QD phonon and the bath phonons are approximately separated by the canonical transformations (5) and (6).

The role of the interaction between the bath phonons and the QD phonon is to renormalize the frequency of the QD phonon from ω_0 to $\widetilde{\omega}_0$. From now onwards, we will concentrate on SMT only.

Using Eq. (3) for the spectral density, $(\Delta\omega)^2$ can be written as

$$(\Delta\omega)^2 = \frac{2}{m_0} \int_0^\infty \frac{J(\omega)}{\omega} d\omega, \qquad (2.9)$$

In the Ohmic situation, the spectral density $J(\omega)$ follows the relationship:

$$J(\omega) = 2m_0 \gamma \omega \tag{2.10}$$

for all frequencies, where the Ohmic damping coefficient can be expressed as

$$\gamma = \frac{1}{2m_0} \sum_{j=1}^{N} \left(\frac{\beta_j^2}{2m_j \omega_j^2} \right) \delta(\omega - \omega_j) . \qquad (2.11)$$

One can see from Eq. (2.11) that γ diverges in the limit: $\omega \to \infty$ and therefore the form of γ given by (2.11) is not a realistic expression for a pue Ohmic spectral density. To salvage the situation, one introduces a cut-off frequency. In this regard, various forms have been proposed. We employ the Lorentz-Drude form [6], which gives $J(\omega)$ as follows:

$$J(\omega) = \frac{2m_0\gamma\omega}{\left[1 + \left(\frac{\omega}{\omega_c}\right)^2\right]},\tag{2.12}$$

where ω_c denotes the cut-off frequency. It is evident that in the limit: $\omega \to \infty$, $J(\omega) \to 0$, and in the limit: $\omega \to 0$, one obtains the pure Ohmic spectral density. Finally, we can express the change in the frequency of QD phonon as:

$$\Delta\omega^2 = 2\pi\gamma\omega_c \,. \tag{2.13}$$

The SMT Hamiltonian now reads

$$H = \sum_{k\sigma\in S,D} \varepsilon_k n_{k\sigma} + \sum_{\sigma} (\varepsilon_d - eV_g) n_{d\sigma} + U n_{d,\uparrow} n_{d,-\downarrow} + g\mu_B B S_d^z + \hbar \widetilde{\omega}_0 b^{\dagger} b$$
$$+ \lambda \hbar \widetilde{\omega}_0 (b^{\dagger} + b) \sum_{\sigma} n_{d\sigma} + \sum_{k\sigma\in S,D} (V_k c_{k\sigma}^{\dagger} c_{d\sigma} + h.c) . \quad (2.14)$$

where $b^{\dagger}(b)$ is now considered to represent the creation (annihilation) operator of QD phonon of frequency $\widetilde{\omega}_0$.

2.4 Elimination of phonons

In order to treat the el-ph coupling term, we perform on the transformed QD Hamiltonian \overline{H} , the celebrated unitary Lang-Firsov transformation [7] by the operator:

$$U = e^{s}, S = \lambda(b^{\dagger} - b) \sum_{\sigma} n_{d\sigma}. (2.15)$$

The transformed Hamiltonian can be written as

$$\widetilde{H} = e^S H e^{-S} \quad , \tag{2.16}$$

The electron operators of the system are transformed as follows:

$$\tilde{c}_{d\sigma} = c_{d\sigma}\hat{\chi}, \qquad \tilde{c}_{d\sigma}^{\dagger} = c_{d\sigma}^{\dagger}\hat{\chi}^{\dagger} , \qquad (2.17)$$

where,

$$\hat{\chi} = e^{-\lambda(b^{\dagger} - b)}, \qquad \hat{\chi}^{\dagger} = e^{+\lambda(b^{\dagger} - b)}, \qquad (2.18)$$

and the phonon operators are transformed as:

$$\tilde{b} = b - \sum_{\sigma} \lambda n_{d\sigma} , \qquad \tilde{b}^{\dagger} = b^{\dagger} - \sum_{\sigma} \lambda n_{d\sigma} .$$
 (2.19)

Thus the effective Hamiltonian of the SMT system reads

$$\widetilde{H} = \sum_{k\sigma} \varepsilon_k \, n_{k\sigma} + \sum_{\sigma} \widetilde{\varepsilon}_d \, n_{d\sigma} + \widetilde{U} n_{d,\uparrow} n_{d,-\downarrow} + \hbar \omega_0 b^{\dagger} b$$

$$+ \sum_{k\sigma} \left(V_k c_{k\sigma}^{\dagger} \widetilde{c}_{d\sigma} + h.c \right) , \qquad (2.20)$$

where the system parameters get renormalized as

$$\tilde{\varepsilon}_d = \varepsilon_d - eV_G - \lambda^2 \hbar \omega_0, \tag{2.21}$$

$$\widetilde{U} = U - 2\hbar\omega_0\lambda^2,\tag{2.22}$$

$$\widetilde{V}_k = V_k \hat{\chi} = V_k e^{\lambda(b-b^{\dagger})} . \tag{2.23}$$

2.5 Tunnelling current: The non-equilibrium Keldysh Green function formalism

We calculate the expression for the current density employing Keldysh method. We shall present here the derivation of the tunneling current expression in the presence of the el-el, el-ph interactions and quantum dissipation. Then the current from the source to the quantum dot in a single molecular transistor can be written as the average value of the rate of change of charge operator

$$Q = -eN_{\rm s} \tag{2.24}$$

where N_s is the operator corresponding to the number of electrons in the source and is given by

$$N_S = \sum_{k\sigma \in S} c_{k\sigma}^{\dagger} c_{k\sigma}. \tag{2.25}$$

Thus the current from S to QD is given by

$$J_S = -e \left\langle \frac{dN_S}{dt} \right\rangle = -\frac{ie}{\hbar} \left\langle \left[\widetilde{H}, N_S \right] \right\rangle, \qquad (2.26)$$

where \widetilde{H} refers to the effective Hamiltonian given by Eq. (2.20). Since N_s commutes with all but the hybridization term of \widetilde{H} , we obtain

$$J_{S} = \frac{ie}{\hbar} \sum_{k\sigma \in S} \left[\tilde{V}_{k} \langle c_{k\sigma}^{\dagger} c_{d\sigma} \rangle - h.c \right] \qquad (2.27)$$

Let us now define the following Green functions.

$$G_{k\sigma,d}^{\leq}(t,t') = i\langle 0|c_d^{\dagger}(t')c_{k\sigma}(t)|0\rangle, \tag{2.28a}$$

$$G_{d,k\sigma}^{\leq}(t,t') = i\langle 0|c_{k\sigma}^{\dagger}(t')c_d(t)|0\rangle\rangle, \tag{2.28b}$$

where $G^{>}(t,t')$ ($G^{<}(t,t')$) is the Keldysh greater (lesser) Green function, $G^{r(a)}(t,t')$ is the usual retarded (advanced) Green function, $|0\rangle$ denotes the actual ground state of the whole system and

$$c_{d\sigma}(t) = e^{-i\tilde{H}_{el}t}c_{d\sigma}e^{i\tilde{H}_{el}t} , \qquad (2.29)$$

where $\tau = (t - t')$. Using the property

$$G_{k\sigma,d}^{<}(t,t) = -[G_{d,k\sigma}^{<}(t,t)]^{*}$$
, (2.30)

the current from S to QD can be written as

$$J_{S} = \frac{2e}{\hbar} Re \left\{ \sum_{k\sigma \in S} \widetilde{V}_{k} G_{d,k\sigma}^{\leq}(t,t) \right\} . \tag{2.31}$$

 $G_{d,k\sigma}^{\leq}(t)$ can be obtained through the equation of motion (EOM) method. Due to the structural similarity between the non-equilibrium theory and the equilibrium theory, we consider the zero temperature time-ordered Green function and its equation of motion. So, let us define the retarded and the advanced tunnelling Green functions as

$$G_{d,k\sigma}^{r(a)}(t-t') = \mp i\theta(\pm t \mp t')\langle 0|\{\tilde{c}_d(t), c_k^{\dagger}(t')\}|0\rangle, \qquad (2.32)$$

which satisfies the following (inhomogeneous) EOM

$$\left(-i\frac{\partial}{\partial t'} - \varepsilon_k\right) G_{d,k}^{r(a)}(t - t') = V_k^* G_{dd}^{r(a)}(t - t') , \qquad (2.33)$$

where,

$$G_{dd}^{r(a)}(t-t') = \mp i \,\theta(\pm t \mp t')\langle 0| \{\tilde{c}_d(t), \tilde{c}_d^{\dagger}(t')\}|0\rangle \ . \tag{2.34}$$

The Green functions for the non-interacting lead electrons is given by

$$g_{k\sigma}^{r(a)}(t-t') = \mp i\theta \left((\pm t \mp t') \right) \left\langle \left\{ c_{k\sigma}^{\dagger}(t), c_{k\sigma}(t') \right\} \right\rangle$$
$$= \mp i\theta \left((\pm t \mp t') \right) e^{-i\varepsilon_k (t-t')} . \tag{2.35}$$

where the averaging state is the ground state of the non-interacting electron system. $g_{k\sigma}^{r(a)}$ satisfies the equation

$$\left(-i\frac{\partial}{\partial t} - \varepsilon_k\right) g_{k\sigma}^{r(a)}(t) = \delta(t) . \qquad (2.36)$$

Therefore, Eq. (2.33) can be easily solved to give

$$G_{d,k\sigma}^{r(a)}(\tau) = \int d\tau \, V_k^* G_{dd}^{r(a)}(\tau) g_{k\sigma}^{r(a)}(\tau) \quad .$$
 (2.37)

According to the analytical continuum rule,

$$C(\tau) = A(\tau)B(\tau) , \qquad (2.38)$$

which can be explicitly written as

$$C(t,t') = \int dt_1 A(t,t_1)B(t_1,t') , \qquad (2.39)$$

and the real axis of the $C(\tau)$ is given as

$$C^{<}(t,t') = \int \left[A^{<}(t,t_1)B^{(a)}(t_1,t') + A^r(t,t_1)B^{<}(t_1,t') \right] dt_1 . \quad (2.40)$$

So we can write

$$G_{d,k\sigma}^{\leq}(t,t') = \int dt_1 V_k^* [G_{dd}^{\leq}(t,t_1) g_{k\sigma}^a(t_1,t') + G_{dd}^r(t,t_1) g_{k\sigma}^{\leq}(t_1,t')], \quad (2.41)$$

where

$$g_{k\sigma}^{<}(t-t') = i\langle c_{k\sigma}^{\dagger}(t')c_{k\sigma}(t)\rangle = i f(\varepsilon_k)e^{-i\varepsilon_k(t-t')}$$
 , (2.42)

 $f(\varepsilon_k)$ denoting the Fermi-Dirac (FD) distribution function. The Fourier transforms of the different Green functions are defined as

$$G_{d,k\sigma}^{\leq}(\tau) = \frac{1}{2\pi} \int d\varepsilon \ e^{-i\varepsilon\tau} \ G_{d,k\sigma}^{\leq}(\varepsilon), \tag{2.43}$$

$$G^{r}_{dd}(\tau) = \frac{1}{2\pi} \int d\varepsilon \, e^{-i\varepsilon\tau} G^{r}_{dd}(\varepsilon) \,, \tag{2.44}$$

$$G_{dd}^{<}(\tau) = \frac{1}{2\pi} \int d\varepsilon \ e^{-i\varepsilon\tau} G_{dd}^{<}(\varepsilon), \tag{2.45}$$

$$g_{k\sigma}^{a}(\tau) = \frac{1}{2\pi} \int d\varepsilon \ e^{-i\varepsilon\tau} \ g_{k\sigma}^{a}(\varepsilon) \,,$$
 (2.46)

where $G_{dd}^{r(a)}(\varepsilon)$ and $G_{dd}^{<}(\varepsilon)$ represent the retarded (advanced) and lesser Keldysh Green functions respectively for the QD electron in the energy space and $g_{k\sigma}^{a}(\varepsilon)$ refers to the advanced Green function for the non-interacting electrons in the ε -space. The first term of $G_{d,k\sigma}^{<}(t,t')$ can be calculated as follows.

$$G_{d,k\sigma}^{\leq}(t,t') = \int dt_1 V_k^* G_{dd}^{\leq}(t,t_1) g_{k\sigma}^a(t_1,t')$$

$$= \left(\frac{1}{2\pi}\right)^2 \int dt_1 V_k^* \int d\varepsilon \, e^{-i\varepsilon(t-t_1)} G_{d,k\sigma}^{\leq}(\varepsilon) \int d\varepsilon' \, e^{-i\varepsilon'(t_1-t')}$$

$$= \frac{1}{2\pi} \int d\varepsilon \, V_k^* \, G_{d,k\sigma}^{\leq}(\varepsilon) g_{k\sigma}^a(\varepsilon) \, e^{-i\varepsilon(t-t')}$$
(2.47)

Similarly, we can calculate the second term of $G_{d,k\sigma}^{\leq}(t,t')$ and thus $G_{d,k\sigma}^{\leq}(t,t')$ is given by

$$G_{d,k\sigma}^{<}(t,t') = \int \frac{d\varepsilon}{2\pi} V_k^* \left[G_{d,k\sigma}^{<}(\varepsilon) g_{k\sigma}^a(\varepsilon) + G_{dd}^r(\varepsilon) g_{k\sigma}^{<}(\varepsilon) \right] e^{-i\varepsilon(t-t')}. \tag{2.48}$$

The current expression then becomes

$$J_{s} = \frac{2e}{\hbar} \int \frac{d\varepsilon}{2\pi} Re \left\{ \sum_{k} \tilde{V}_{k} V_{k}^{*} [G_{dd}^{r}(\varepsilon) g_{k\sigma}^{<}(\varepsilon) + G_{dd}^{<}(\varepsilon) g_{k\sigma}^{a}(\varepsilon)] \right\}$$
(2.49)

where $g_{k\sigma}^{<}(\varepsilon)$ is given by:

$$g_{k\sigma}^{<}(\varepsilon) = \int d\tau \ e^{i\varepsilon\tau} \ g_{k\sigma}^{<}(\tau) = 2\pi i \ f(\varepsilon_k) \delta(\varepsilon - \varepsilon_k) \ .$$
 (2.50)

The first term in the current expression that contains $G_{dd}^{r}(\varepsilon)$ is calculated as follows.

$$J_{s}(1) = \frac{2e}{\hbar} \int \frac{d\varepsilon}{2\pi} Re \left\{ \sum_{k} \tilde{V}_{k} V_{k}^{*} [G_{dd}^{r}(\varepsilon) g_{k\sigma}^{<}(\varepsilon)] \right\}$$
 (2.51)

We convert the momentum summation into energy integration and get

$$J_{S}(1) = \frac{2e}{\hbar} \int \frac{d\varepsilon}{2\pi} \int d\varepsilon_{k} \, \Gamma_{S}(\varepsilon_{k}) \, Re[G_{dd}^{r}(\varepsilon)i\delta(\varepsilon - \varepsilon_{k})f_{S}(\varepsilon_{k})] \quad (2.52)$$

where

$$\Gamma_{S}(\varepsilon_{k}) = 2\pi \varrho_{S}(\varepsilon_{k}) \tilde{V}_{k} V_{k}^{*} , \qquad (2.53)$$

 $\rho_{S(D)}$ and $f_{S(D)}(\varepsilon)$ are respectively the density of states and the FD distribution function of S(D) and the chemical potentials of S and D are related to the bias voltage (V_B) and mid-voltage (V_m) as:

$$(\mu_S - \mu_D) = eV_B, \qquad (\mu_S + \mu_D)/2 = eV_m.$$
 (2.54)

Integration over ε_k gives

$$J_{S}(1) = \frac{2e}{\hbar} \int \frac{d\varepsilon}{2\pi} f_{S}(\varepsilon) \Gamma_{S}(\varepsilon) Re\{iG_{dd}^{r}(\varepsilon)\}$$

$$= -\frac{2e}{\hbar} \int \frac{d\varepsilon}{2\pi} f_{S}(\varepsilon) \Gamma_{S}(\varepsilon) Im\{G_{dd}^{r}(\varepsilon)\}$$

$$= \frac{ie}{\hbar} \int \frac{d\varepsilon}{2\pi} f_{S}(\varepsilon) \Gamma_{S}(\varepsilon) [G_{dd}^{r}(\varepsilon) - G_{dd}^{a}(\varepsilon)] . \qquad (2.55)$$

Since

$$G_{dd}^r(\varepsilon) = [G_{dd}^a(\varepsilon)]^*$$
, (2.56)

the other part of the current expression can be manipulated similarly. Finally, one obtains

$$J_{S(D)} = \frac{ie}{\hbar} \int \frac{d\varepsilon}{2\pi} \Gamma^{S(D)}(\varepsilon) \{ G_{dd}^{<}(\varepsilon) + f_{S(D)} [G_{dd}^{r}(\varepsilon) - G_{dd}^{a}(\varepsilon)] \}, \quad (2.57)$$

where $\Gamma_{S(D)}(\varepsilon)$, the hybridization interaction of the quantum dot with the source (drain) is given by

$$\Gamma_{S(D)} = 2\pi \rho_{S(D)}(\varepsilon) |V_k|^2 e^{-\lambda (b^{\dagger} - b)} . \tag{2.58}$$

In steady-state, the current will be uniform, and we have:

$$J = J_S = -J_D , (2.59)$$

and after symmetrizing, we can write

$$J = \frac{(J_S - J_D)}{2}$$

$$= \frac{ie}{2\hbar} \int \frac{d\varepsilon}{2\pi} [(\Gamma^S - \Gamma^D) G_{dd}^{<}(\varepsilon) + (f_S \Gamma^S - f_D \Gamma^D) \{G_{dd}^r(\varepsilon) - G_{dd}^a(\varepsilon)\}]. \tag{2.60}$$

The SD function which gives a possible excitation is defined as

$$A(\varepsilon) = i \left[G_{dd}^{r}(\varepsilon) - G_{dd}^{a}(\varepsilon) \right] = i \left[G_{dd}^{>}(\varepsilon) - G_{dd}^{<}(\varepsilon) \right]. \tag{2.61}$$

Finally, the current through QD assumes the expression [8 - 10]

$$J = \frac{e}{2h} \int [\{f_S(\varepsilon)\Gamma_S - f_D(\varepsilon)\Gamma_D\} A(\varepsilon) + \{(\Gamma_S - \Gamma_D)G_{dd}^{\leq}(\varepsilon)\}] d\varepsilon. \quad (2.62)$$

The occupation number of the quantum dot is given by

$$\langle n_{d\uparrow} \rangle = \int \frac{d\varepsilon}{2\pi\Gamma} \{ f_S(\varepsilon) \Gamma_S + f_D(\varepsilon) \Gamma_D \} A(\varepsilon). \tag{2.63}$$

For a symmetric quantum dot,

$$\Gamma_{S(D)}(\varepsilon) = \frac{\Gamma_S(\varepsilon) + \Gamma_D(\varepsilon)}{2} = \Gamma,$$
(2.64)

which we approximate Γ as

$$\Gamma \cong \pi \rho(0) |V_k|^2 \langle n | e^{-\lambda (b^{\dagger} - b)} | n \rangle, \tag{2.65}$$

where

$$\rho_S = \rho_D = \rho \quad , \tag{2.66}$$

and $|n\rangle$ is an n-phonon state. The above approximation should be plausible when the el-ph interaction energy is much weaker than the hopping energy. In the limit $T \to 0$ K, we can write

$$\left\langle n \left| e^{-\lambda (b^{\dagger} - b)} \right| n \right\rangle = e^{-\frac{1}{2}\lambda^2} \left\langle n \left| e^{-\lambda b^{\dagger}} e^{\lambda b} \right| n \right\rangle \cong e^{-\lambda^2 \left(n + \frac{1}{2} \right)}$$
 (2.67)

where

$$|n\rangle = \frac{(a^{\dagger})^n |0\rangle}{\sqrt{n!}} \tag{2.68}$$

is an n – phonon state, so that we have

$$\Gamma \cong \pi \rho(0) |V_k|^2 e^{-\lambda^2 \left(n + \frac{1}{2}\right)}. \tag{2.69}$$

 $G_{dd}^{r(a)}(t,t')$ can be expressed as:

$$G_{dd}^{r(a)}(t,t') = \mp i \,\theta(\pm t \mp t') \langle \{\tilde{c}_{d}(t), \tilde{c}_{d}^{\dagger}(t')\} \rangle_{\tilde{H}}$$

$$= \mp i \,\theta(\pm t \mp t') \,\langle \{c_{d\sigma}(t), c_{d\sigma}^{\dagger}(t')\} \rangle_{el} \,\langle X^{\dagger}(0)X(\tau) \rangle_{ph},$$

$$= \left[\tilde{G}_{dd}^{r(a)}(t,t')\right]_{el} \,\langle X^{\dagger}(0)X(\tau) \rangle_{ph}. \tag{2.70}$$

where,

$$c_{d\sigma}(t) = e^{-i\tilde{H}_{el}t}c_{d\sigma}e^{i\tilde{H}_{el}t}, \chi(t) = e^{-i\tilde{H}_{ph}t}\chi e^{i\tilde{H}_{ph}t}.$$
 (2.71)

Now we shall calculate $\langle \chi(t)\chi^{\dagger}(t')\rangle_{ph}$.

$$\langle \chi(t)\chi^{\dagger}(t')\rangle_{ph} \equiv F(t,t') = \frac{\sum_{n=0}^{\infty} \langle n | e^{-\beta \tilde{H}_{ph}} \chi(t) \chi^{\dagger}(t') | n \rangle}{\sum_{n=0}^{\infty} \langle n | e^{-\beta \tilde{H}_{ph}} | n \rangle} , \qquad (2.72)$$

where $\sum_{n=0}^{\infty} \langle n | e^{-\beta \widetilde{H}_{ph}} | n \rangle$ is given by

$$\sum_{n=0}^{\infty} \langle n | e^{-\beta \widetilde{H}_{ph}} | n \rangle = \sum_{n=0}^{\infty} e^{-n\beta \hbar \widetilde{\omega}_0} = \frac{1}{(1 - e^{-\beta \hbar \widetilde{\omega}_0})} = e^{\beta \hbar \widetilde{\omega}_0} f_p, \qquad (2.73)$$

where

$$f_p = \frac{1}{(e^{\beta\hbar\widetilde{\omega}_0} - 1)} \tag{2.74}$$

is the phonon distribution function. We obtain

$$\langle \chi(t)\chi^{\dagger}(t')\rangle_{ph} = e^{-\varphi(-\tau)} = \sum_{n=-\infty}^{\infty} L_n e^{in\widetilde{\omega}_0 \tau}$$
 (2.75)

where

$$\varphi(\mp\tau) = \lambda^{2} \left[\left(2f_{ph} + 1 \right) \right]^{1/2} 2\cos(\hbar \widetilde{\omega}_{0}(\mp \tau + i/2k_{B}T)) \right]$$

$$+ \left[f_{ph} (1 + f_{ph}) \right]^{1/2} 2\cos(\hbar \widetilde{\omega}_{0}(\mp \tau + i/2k_{B}T)) \right]$$

$$+ \left[2.76 \right]$$

$$+ \left[(2\lambda^{2} \left[f_{ph} (1 + f_{ph}) \right]^{1/2} \right] .$$

$$+ \left[(2\lambda^{2} \left[f_{ph} (1 + f_{ph}) \right]^{1/2} \right] .$$

$$+ \left[(2\lambda^{2} \left[f_{ph} (1 + f_{ph}) \right]^{1/2} \right] .$$

$$+ \left[(2\lambda^{2} \left[f_{ph} (1 + f_{ph}) \right]^{1/2} \right] .$$

$$+ \left[(2\lambda^{2} \left[f_{ph} (1 + f_{ph}) \right]^{1/2} \right] .$$

$$+ \left[(2\lambda^{2} \left[f_{ph} (1 + f_{ph}) \right]^{1/2} \right] .$$

$$+ \left[(2\lambda^{2} \left[f_{ph} (1 + f_{ph}) \right]^{1/2} \right] .$$

$$+ \left[(2\lambda^{2} \left[f_{ph} (1 + f_{ph}) \right]^{1/2} \right] .$$

$$+ \left[(2\lambda^{2} \left[f_{ph} (1 + f_{ph}) \right]^{1/2} \right] .$$

$$+ \left[(2\lambda^{2} \left[f_{ph} (1 + f_{ph}) \right]^{1/2} \right] .$$

$$+ \left[(2\lambda^{2} \left[f_{ph} (1 + f_{ph}) \right]^{1/2} \right] .$$

$$+ \left[(2\lambda^{2} \left[f_{ph} (1 + f_{ph}) \right]^{1/2} \right] .$$

$$+ \left[(2\lambda^{2} \left[f_{ph} (1 + f_{ph}) \right]^{1/2} \right] .$$

$$+ \left[(2\lambda^{2} \left[f_{ph} (1 + f_{ph}) \right]^{1/2} \right] .$$

$$+ \left[(2\lambda^{2} \left[f_{ph} (1 + f_{ph}) \right]^{1/2} \right] .$$

$$+ \left[(2\lambda^{2} \left[f_{ph} (1 + f_{ph}) \right]^{1/2} \right] .$$

$$+ \left[(2\lambda^{2} \left[f_{ph} (1 + f_{ph}) \right]^{1/2} \right] .$$

$$+ \left[(2\lambda^{2} \left[f_{ph} (1 + f_{ph}) \right]^{1/2} \right] .$$

$$+ \left[(2\lambda^{2} \left[f_{ph} (1 + f_{ph}) \right]^{1/2}] .$$

$$+ \left[(2\lambda^{2} \left[f_{ph} (1 + f_{ph}) \right]^{1/2}] .$$

$$+ \left[(2\lambda^{2} \left[f_{ph} (1 + f_{ph}) \right]^{1/2}] .$$

$$+ \left[(2\lambda^{2} \left[f_{ph} (1 + f_{ph}) \right]^{1/2}] .$$

$$+ \left[(2\lambda^{2} \left[f_{ph} (1 + f_{ph}) \right]^{1/2}] .$$

$$+ \left[(2\lambda^{2} \left[f_{ph} (1 + f_{ph}) \right]^{1/2}] .$$

where, I_n refers to the Modified Bessel function of the second kind and $L_{+n}(L_{-n})$ represents the spectral weight corresponding to the +n (-n)-th phonon side band. Eq. (2.70) now reads

$$G_{dd}^{r(a)}(t,t') = \left[\tilde{G}_{dd}^{r(a)}(t,t')\right]_{el} \langle \chi(t)\chi^{\dagger}(t')\rangle_{ph}$$

$$= \left[\tilde{G}_{dd}^{r(a)}(t,t')\right]_{el} \sum_{n=-\infty}^{\infty} L_n(z)e^{-in\hbar\tilde{\omega}_0\tau}.$$
(2.78)

Thus the energy-dependent Green function $G_{dd}^{r(a)}(\varepsilon)$ is given by

$$\begin{split} G_{dd}^{r(a)}(\varepsilon) &= \int \left[\tilde{G}_{dd}^{r(a)}(\tau) \right]_{el} F(\tau) \, e^{i\varepsilon\tau} \, d\tau \\ &= \int e^{-\lambda^2 \left(1 + 2f_p \right)} \sum_{n = -\infty}^{\infty} I_n(z) e^{n\hbar \widetilde{\omega}_0 \beta/2} \left[\tilde{G}_{dd}^{r(a)}(\tau) \right]_{el} e^{-in\hbar \widetilde{\omega}_0 \tau} e^{i\varepsilon\tau} d\tau \\ &= \sum_{n = -\infty}^{\infty} e^{-\lambda^2 \left(1 + 2f_p \right)} e^{n\hbar \beta \widetilde{\omega}_0/2} I_n(z) \int \left[\tilde{G}_{dd}^{r(a)}(\tau) \right]_{el} \, e^{i \, (\varepsilon - n\hbar \widetilde{\omega}_0) \tau} d\tau \end{split}$$

$$= \sum_{n=-\infty}^{\infty} L_n(z) \left[\tilde{G}_{dd}^{r(a)} (\varepsilon - n\hbar \tilde{\omega}_0) \right]_{el} . \qquad (2.79)$$

 $\left[\tilde{G}_{dd}^{r(a)}(\varepsilon)\right]_{el}$ can be determined from EOM method within the mean-field approximation (MFA). We obtain

$$i\frac{\partial}{\partial t'} \left[\tilde{G}_{dd}^{r(a)}(\varepsilon) \right]_{el} = \delta(\pm t \mp t') \mp i\theta(\pm t \mp t') \langle \left\{ c_{d}(t), \left[c_{d}^{\dagger}, \tilde{H}_{el} \right] \right\} \rangle$$

$$= \delta(\pm t \mp t') \mp i\theta(\pm t \mp t') \langle \left\{ c_{d\sigma'}(t), \left[c_{d\sigma'}^{\dagger}(t'), \sum_{\sigma} \tilde{\varepsilon}_{d} n_{d\sigma} + \right] \right\} \rangle$$

$$+ \sum_{k\sigma} \left(\tilde{V}_{k} c_{k\sigma}^{\dagger} c_{d\sigma} + h.c \right)$$

$$(2.80)$$

$$=\delta(\pm t\mp t')\mp i\theta(\pm t\mp t')$$

$$\times \left\langle \left\{ c_{d\sigma'}(t), \left(\tilde{\varepsilon}_{d} c_{d\sigma'}^{\dagger}(t') - \widetilde{U} \langle n_{d\downarrow} \rangle c_{d\uparrow}^{\dagger}(t') - \sum_{k} (\widetilde{V}_{k} c_{k\sigma'}^{\dagger}(t') + h.c.) \right) \right\} \right\rangle$$
(2.81)

$$= \delta(\pm t \mp t') + \tilde{\varepsilon}_d \tilde{G}_{dd}^{r(a)}(t,t') + \tilde{U}\langle n_{d\downarrow} \rangle \tilde{G}_{dd}^{r(a)}(t,t') + \tilde{V}_k \tilde{G}_{dk}^{r(a)}(t,t'),$$
(2.82)

which gives

$$\tilde{G}_{dd}^{r(a)}(\varepsilon \mp n\hbar\widetilde{\omega}_{0}) = \frac{1 + \tilde{V}_{k}\tilde{G}_{d,k\sigma}^{r(a)}(\varepsilon \mp n\hbar\widetilde{\omega}_{0})}{\left[(\varepsilon \mp n\hbar\widetilde{\omega}_{0}) - \tilde{\varepsilon}_{d} - \tilde{U}\langle n_{d\downarrow}\rangle\right]},$$
(2.83)

where $\tilde{G}_{d,k\sigma}^{r(a)}(\varepsilon \mp n\hbar \tilde{\omega}_0)$ is the Fourier transform of $\tilde{G}_{d,k\sigma}^{r(a)}(t,t')$. We obtain the EOM for $\tilde{G}_{d,k\sigma}^{r(a)}(t,t')$ in a similar way.

$$i\frac{\partial}{\partial t'}\tilde{G}_{d,k\sigma}^{r(a)}(t,t') = \mp i\theta(\pm t \mp t')\langle\{c_d(t),[c_k^{\dagger},\tilde{H}]\}\rangle$$

$$= \mp i\theta(\pm t \mp t')\langle\{c_d(t),[c_k^{\dagger},\sum_{k\sigma}\varepsilon_k n_{k\sigma} + \sum_{k\sigma}(\tilde{V}_k c_{k\sigma}^{\dagger} c_d + h.c)]\}\rangle$$

$$= \varepsilon_k \tilde{G}_{d,k\sigma}^{r(a)}(t,t') + \tilde{V}_k^* \tilde{G}_{dd}^{r(a)}(t,t')$$

$$(2.85)$$

Multiplying by $e^{i(\varepsilon \mp n\hbar \tilde{\omega}_0)(\tau)}$ and integrating over τ , we have after some algebraic manipulation

$$\tilde{G}_{d,k\sigma}^{r(a)}(\varepsilon \mp n\hbar\widetilde{\omega}_0) = \left[\frac{\tilde{V}_k^*}{(\varepsilon - \varepsilon_k)}\right] \tilde{G}_{dd}^{r(a)}(\varepsilon \mp n\hbar\widetilde{\omega}_0) \quad . \tag{2.86}$$

Substituting for $\tilde{G}_{dk}^{r(a)}(\varepsilon \mp n\hbar \tilde{\omega}_0)$ in the expression of $\tilde{G}_{dd}^{r(a)}(\varepsilon \mp n\hbar \tilde{\omega}_0)$, we obtain

$$\tilde{G}_{dd}^{r(a)}(\varepsilon \mp n\hbar \widetilde{\omega}_0) = \frac{1}{\left[(\varepsilon \mp n\hbar \widetilde{\omega}_0) - \tilde{\varepsilon}_d - \widetilde{U}\langle n_{d\downarrow}\rangle - \Sigma^{r(a)}\right]}$$
(2.87)

where $\Sigma^{r(a)}(\varepsilon)$ represents the retarded (advanced) self-energy arising due to el-ph interaction and hybridization and can be written as

$$\Sigma^{r(a)}(\varepsilon) = \sum_{k \in S, D} \frac{\left|\tilde{V}_k\right|^2}{\left(\varepsilon - \varepsilon_k \pm i0^+\right)} = \Lambda(\varepsilon) \mp i\Gamma(\varepsilon) , \qquad (2.88)$$

In Eq. (2.87), the real part of $\Sigma^{r(a)}(\varepsilon)$ can be absorbed into the onsite energy of QD. $G_{dd}^{<,>}(\tau)$ can be calculated as follows.

$$G_{dd}^{<,>}(\tau) = \pm i \langle \tilde{c}_d^{\dagger}(0) \tilde{c}_d(\tau) \rangle$$

$$= \pm i \langle c_d^{\dagger}(0) c_d(\tau) \rangle_{el} \langle X^{\dagger}(0) X(\tau) \rangle_{nh} \cong \tilde{G}_{dd}^{<,>}(\tau) e^{-\varphi(\mp \tau)}. \quad (2.89)$$

The lesser and greater Green's functions are expanded as

$$G^{<,>}(\varepsilon) = \sum_{n=-\infty}^{\infty} L_n(z) \, \tilde{G}^{<,>}(\varepsilon + n\hbar \tilde{\omega}_0). \tag{2.90}$$

The SD function can now be written as

$$A(\varepsilon) = \sum_{n=-\infty}^{\infty} i L_n(z) \big[\tilde{G}^{>}(\varepsilon - n\hbar \tilde{\omega}_0) - \tilde{G}^{<}(\varepsilon + n\hbar \tilde{\omega}_0) \big]. \quad (2.91)$$

To calculate lesser (greater) Green function, we can use the Keldysh formalism [11]. We can write the Dyson equations for $\tilde{G}^{<,>}(\varepsilon)$ using Langreth analytical continuation rules,

$$\tilde{G}^{<,>}(\varepsilon) = \tilde{G}_{dd}^{r}(\varepsilon) \, \Sigma^{<,>}(\varepsilon) \, \tilde{G}_{dd}^{a}(\varepsilon) \tag{2.92}$$

with

$$\Sigma^{<}(\varepsilon) = i \Gamma [f_{S}(\varepsilon) + f_{D}(\varepsilon)], \qquad (2.93a)$$

$$\Sigma^{>}(\varepsilon) = -i \Gamma [2 - f_{S}(\varepsilon) - f_{D}(\varepsilon)]. \qquad (2.93b)$$

For the symmetric case, we obtain

$$J = \frac{e\Gamma}{2h} \int [\{f_S(\varepsilon) - f_D(\varepsilon)\}A(\varepsilon)] d\varepsilon, \qquad (2.94)$$

where $A(\varepsilon)$ is given by (Eqn. 2.61). $\tilde{G}_{dd}^{r(a)}$ now reads

$$\tilde{G}_{dd}^{r(a)}(\varepsilon \mp n\hbar \widetilde{\omega}_0) = \frac{1}{\left[(\varepsilon \mp n\hbar \widetilde{\omega}_0) - \tilde{\varepsilon}_d - \widetilde{U} \langle n_{d\downarrow} \rangle \mp i\Gamma \right]} \quad , \quad (2.95)$$

and thus $A(\varepsilon)$ reduces to

$$A(\varepsilon) = \sum_{n=-\infty}^{\infty} L_n(z) \frac{2\Gamma}{\left[\left((\varepsilon \mp n\hbar \widetilde{\omega}_0) - \widetilde{\varepsilon}_d - \widetilde{U} \langle n_{d\downarrow} \rangle \right)^2 + \Gamma^2 \right]}. \quad (2.96)$$

I can be obtained by substituting for $A(\varepsilon)$ in Eq. (2.94) where

$$f_S(\varepsilon) = \frac{1}{1 + e^{-\frac{(\varepsilon - \mu_S)}{KT}}} \quad ; \quad \mu_S = \left(eV_m + \frac{eV_B}{2}\right), \tag{2.97}$$

and

$$f_D(\varepsilon) = \frac{1}{1 + e^{-\frac{(\varepsilon - \mu_D)}{KT}}} \quad ; \quad \mu_S = \left(eV_m - \frac{eV_B}{2}\right). \tag{2.98}$$

At zero temperature, we have

$$\Gamma \cong \pi \rho(0) |V_k|^2 e^{-\frac{\lambda^2}{2}} \; ; \; L_n = \begin{cases} \frac{\lambda^{2n}}{n!} e^{-\lambda^2} & n \ge 0\\ 0 & n < 0 \end{cases}$$
 (2.99)

The onsite Correlation term is treated using the Hartree-Fock (HF) MFA. So, the results obtained by us are expected to be valid away from the

Kondo regime. Now $\tilde{G}^{>(<)}(\varepsilon)$ and $A(\varepsilon)$ can be easily determined and consequently, one can obtain the the current flowing through QD. The differential conductance is calculated using the following equation

$$G = \frac{dJ}{dV_b},\tag{2.100}$$

and spin polarization parameter from:

$$P_{\sigma,-\sigma} = \frac{(J_{\sigma} - J_{-\sigma})}{(J_{\sigma} + J_{-\sigma})}.$$
 (2.101)

2.6 Results and Discussions

For simplicity, we consider a single-level QD (with energy $\varepsilon_d=0$) that is symmetrically coupled to S and D. Also we measure energy in units of $\hbar\omega_0$ which is the phonon energy and set $\Gamma=0.2, eV_g=0, k_BT=0, \hbar\omega_0=1$. In addition, we take r U=5 for major part of our computations. U=5 might appear to be a bit large from the point of view of MFA that is employed here, but as the on-site the Hubbard term is modified by the polaronic effect to a much smaller effective interaction, the HF MFA may be a reasonable approach for the current situation. In addition, it is assumed that the density of electron states of S and D that participate in transport is constant.

RC [12] have investigated the SD function A for non-zero values of λ and γ for B=0. We have recently examined the SD function for $B \neq 0$. We present our results in Fig. 2. The inset displays the behaviour of the function A for $\lambda = 0 = \gamma$ when U = 0, and B = 0. Clearly one observes a Lorentzian behavior with single central resonance peak structure. The presence of a peak in the SD function indicates an excitation. Fig. 2 also

shows the results of RC obtained for $\lambda \neq 0$ and at B = 0. One can see that in this case, side peaks appear in addition to the central peak due to the polaronic effect [12]. Our results for $B \neq 0$ show that the central peak is split when $B \neq 0$ and the side peaks shift towards left. In the case of B = 0, the electronic states of QD are spin-degenerate and the magnetic field removes this spin degeneracy. As a result of the lifting if this spin-degeneracy, the central peak of the SD function undergoes a splitting.

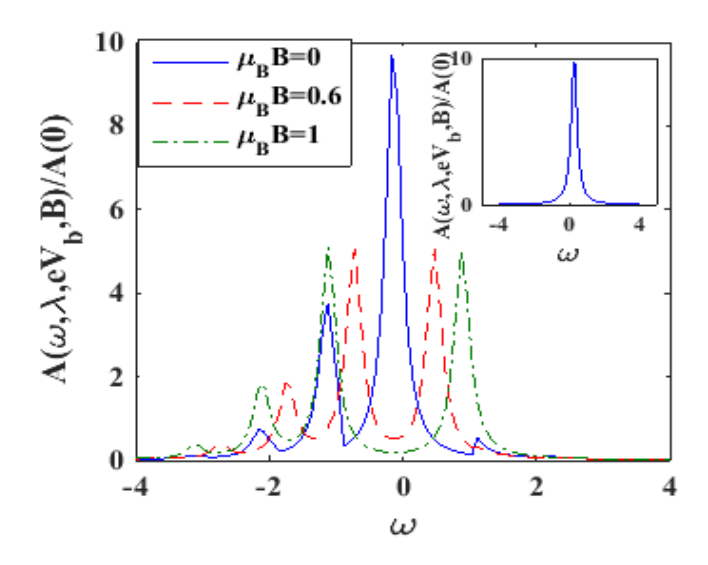


Fig. 2 *A* vs. ω for a few values of $\mu_B B$.

To figure out the role of magnetic field further, we display the spinresolved SD functions in Figs. 3 (a-b). Fig. 3(a) depicts how the downspin SD function $A_{\downarrow}(\omega)$ varies with ω , whereas Fig. 3(b) shows the behaviour of up-spin SD function $A_{\uparrow}(\omega)$. As shown in Fig. 3(a), as $\mu_B B$ increases, the peaks of $A_{\downarrow}(\omega)$ increase in height and move to the higher values of ω . The side peaks, however, increase only marginally. It is observed from Fig. 3(b) that for $A_{\uparrow}(\omega)$ also, peaks grow higher with B but shift to the lower values of ω . However, for up-spin SD function, side peaks show a sizable increase.

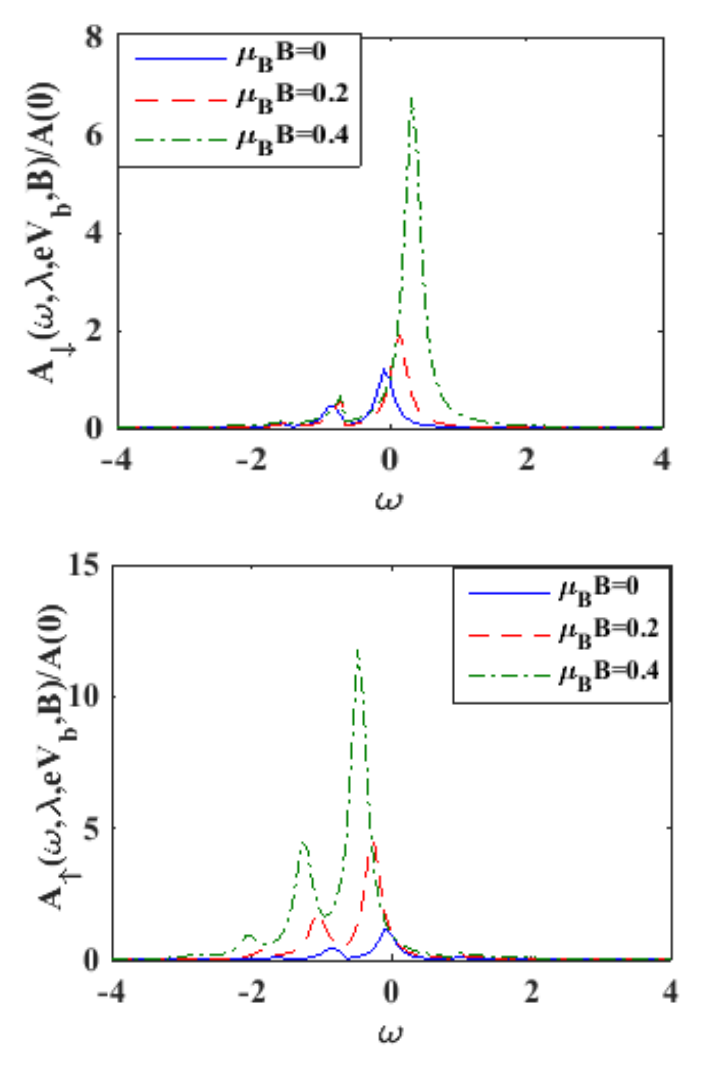


Fig. 3 A_{\uparrow} and A_{\downarrow} vs. ω for a few values of $\mu_B B$.

In Figs. 4(a-b), the behaviour of A_{\uparrow} and A_{\downarrow} is shown with the bias voltage V_b for different B values. The qualitative behavior of A_{\uparrow} and A_{\downarrow} with V_b is similar in general. At small V_b , both A_{\uparrow} and A_{\downarrow} increase slowly with V_b while at large V_b , the rate of increase is a little more. The non-Ohmic effect at large V_b is probably responsible for the quicker increase in A_{\uparrow} and A_{\downarrow} at large V_b . We find that though at B=0, A_{\uparrow} and A_{\downarrow} behave

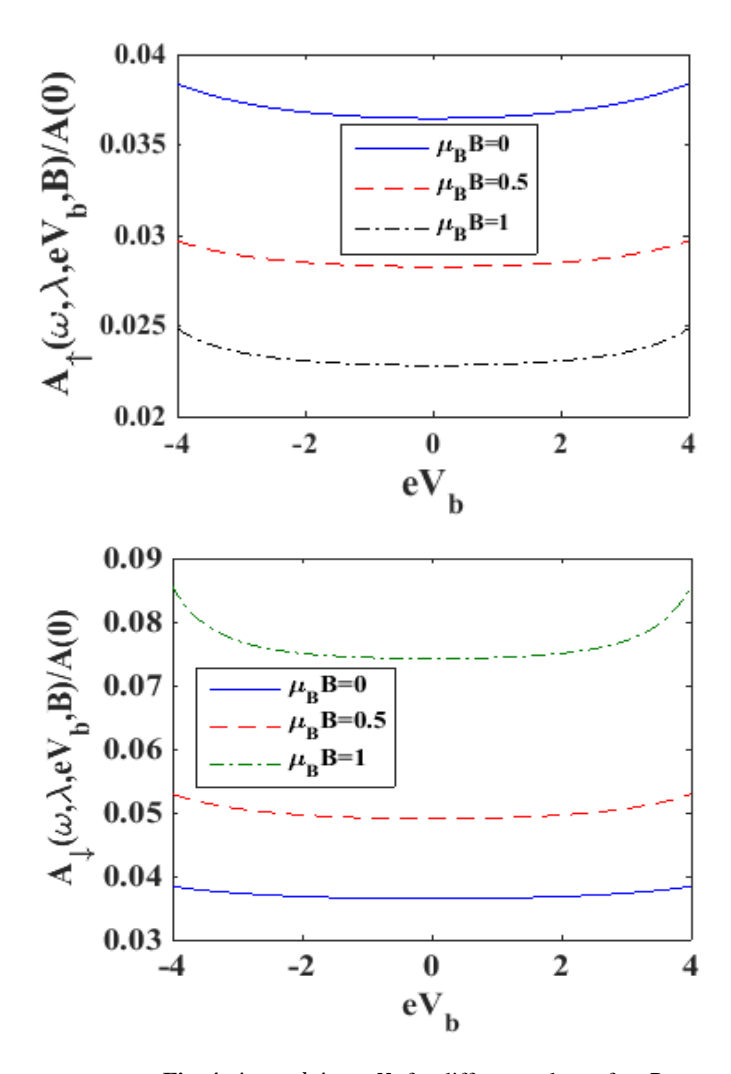


Fig. 4 A_{\uparrow} and A_{\downarrow} vs. V_b for different values of $\mu_B B$.

in the same way, as $\mu_B B$ increases, A_{\uparrow} and A_{\downarrow} behave differently. While A_{\uparrow} is found to decrease with increasing $\mu_B B$, A_{\downarrow} is found to increase as $\mu_B B$ increases. This is due to the magnetic field-induced removal of degeneracy with respect of electron spin. The down-spin level is raised by the magnetic field raises while the up-spin level is lowered.

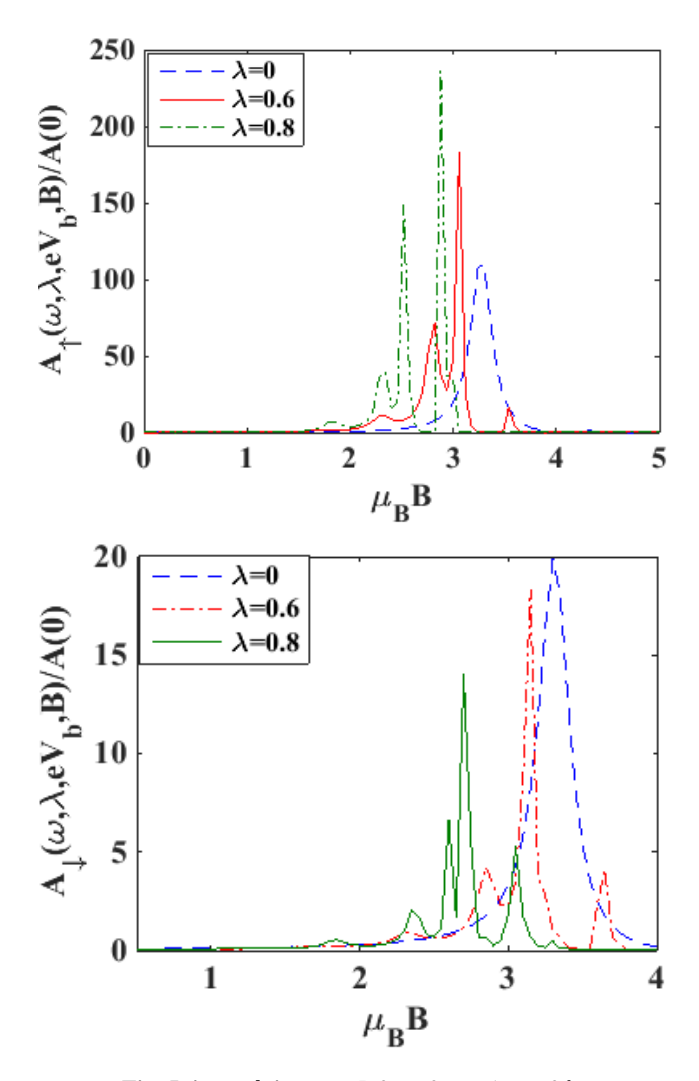


Fig. 5 A_{\uparrow} and A_{\downarrow} vs. $\mu_B B$ for a few values of λ .

In Fig. 5, we present the behaviour of A_{\uparrow} and A_{\downarrow} with respect B for a few λ values. As can be seen from Fig. 5(a), for $\lambda = 0$, A_{\uparrow} exhibits a peak-structure at some specific value of $\mu_B B$. With increasing λ , the peak-width becomes narrower and the peak moves to the lower B values. Around the prominent peak, also a few side peaks form. Fig. 5(b) demonstrates that the behaviour of A_{\downarrow} is more or less same as A_{\uparrow} , though now the height of the main peak decreases as λ increases.

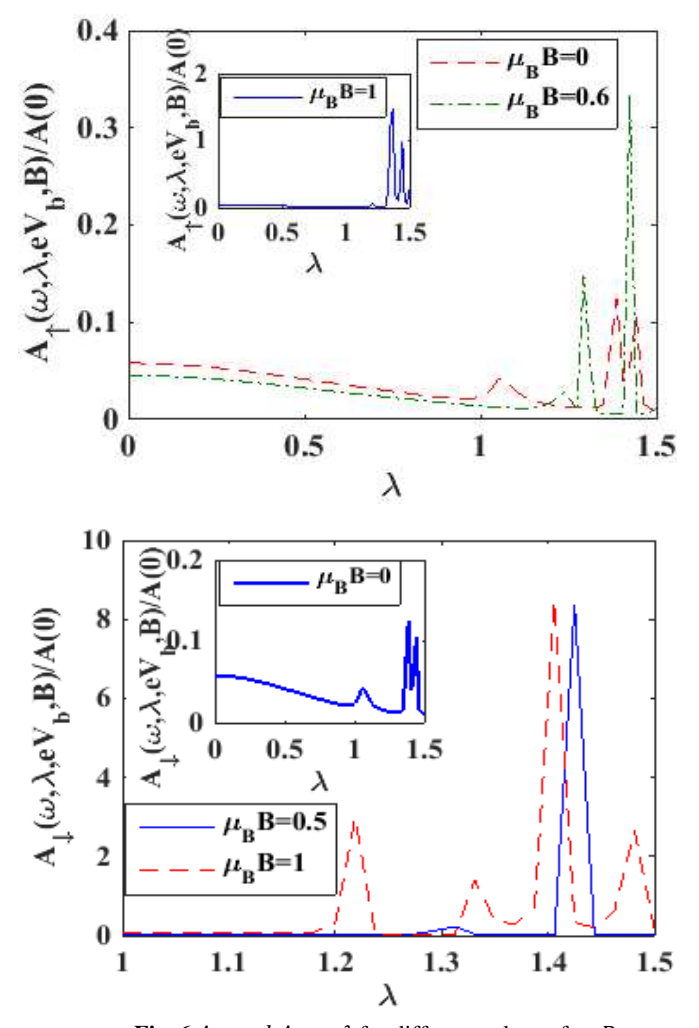
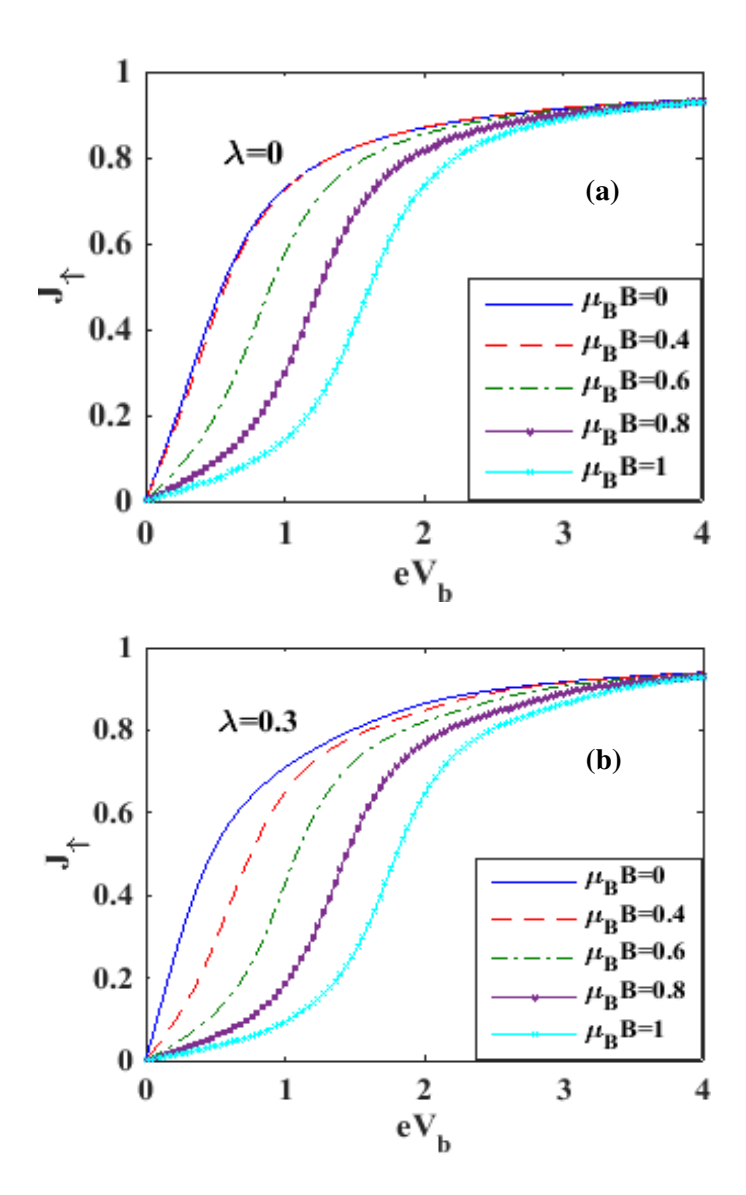


Fig. 6 A_{\uparrow} and A_{\downarrow} vs. λ for different values of $\mu_B B$.

We present in Figs. 6(a-b) the variation of A_{\uparrow} and A_{\downarrow} with λ for $\mu_B B = 0.5$ and 1.0 to unravel the effect of SD functions on the el-ph interaction. When B = 0, the behaviour of A_{\uparrow} and A_{\downarrow} is similar, but for non-zero $\mu_B B$, the qualitative behaviour of A_{\uparrow} is different from that of A_{\downarrow} .

Figs. 7 (a-d) show the nature of the variation of the up-spin current J_{\uparrow} with V_b . The behaviour for $\lambda = 0$ is shown in Fig. 7(a) for a few values of B. When B = 0, J_{\uparrow} turns out to be ohmic at low V_b and seems to saturate

asymptotically to a constant at large V_b . As V_b is increased, the Fermi goes up and this makes it easier for electrons to tunnel from S into QD and consequently the current increases. However, since the number of electrons the QD can hold is limited, it is only natural that the current should saturate if V_b increases beyond a particular value. The two-fold spin-degeneracy of the QD-level is lifted in the case of $B \neq 0$ and consequently, the spin-up energy level goes down and spin-down energy



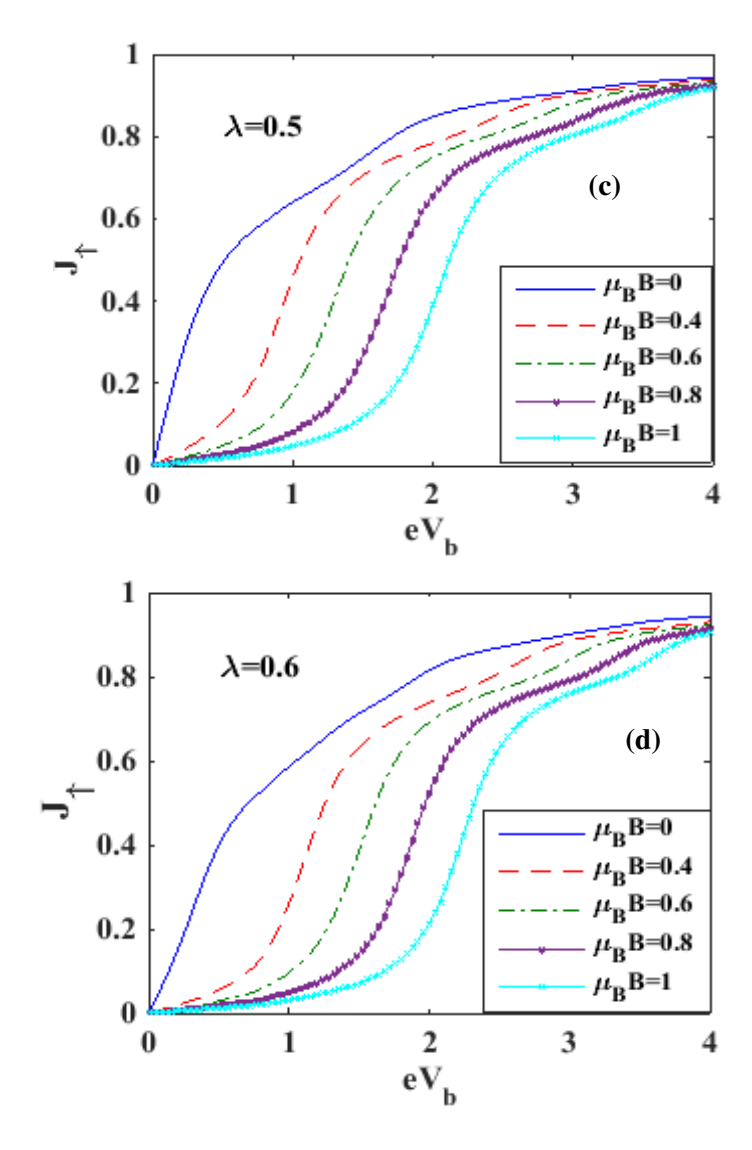
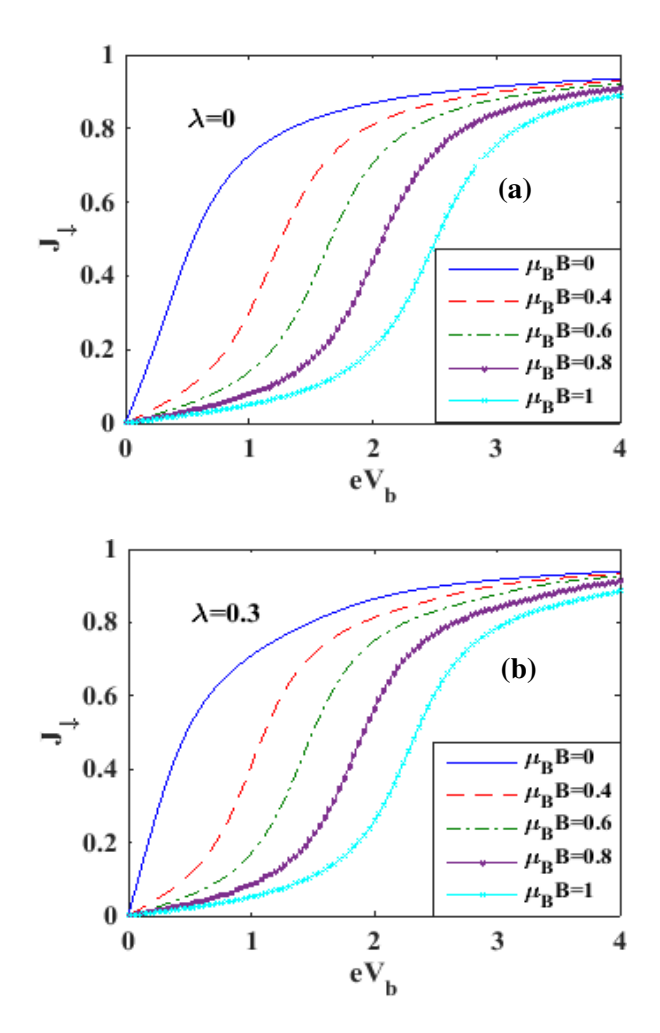


Fig. 7 J_{\uparrow} vs. V_b for different values of $\mu_B B$.

level goes up. As a result of this, unless V_b is sufficiently increased to bring down the Fermi level of D to the spin-up level of QD, the spin-up electrons from QD will not be able to tunnel into D and consequently the spin-up current flowing through the drain channel will be zero. As, with increase in V_b , the Fermi level in D falls below the spin-up electron level

of QD, the spin-up tunnelling current acts more or less in an ohmic manner, eventually reaching saturation for the same reason as happens for B=0. The splitting of QD-level grows as $\mu_B B$ is increased. As a result, J_{\uparrow} remains zero up to a greater V_b value. The behavior for $\lambda=0.3$ is shown in Fig. 7(b). The qualitative behaviour of current is same as seen in Fig.7 (a), save for it is now slightly lower due to the decline in electron mobility caused by polaron formation. Figs. 7(c) and 7(d) show that at large λ , the decrease in the electron mobility is more significant due to the polaronic effect.



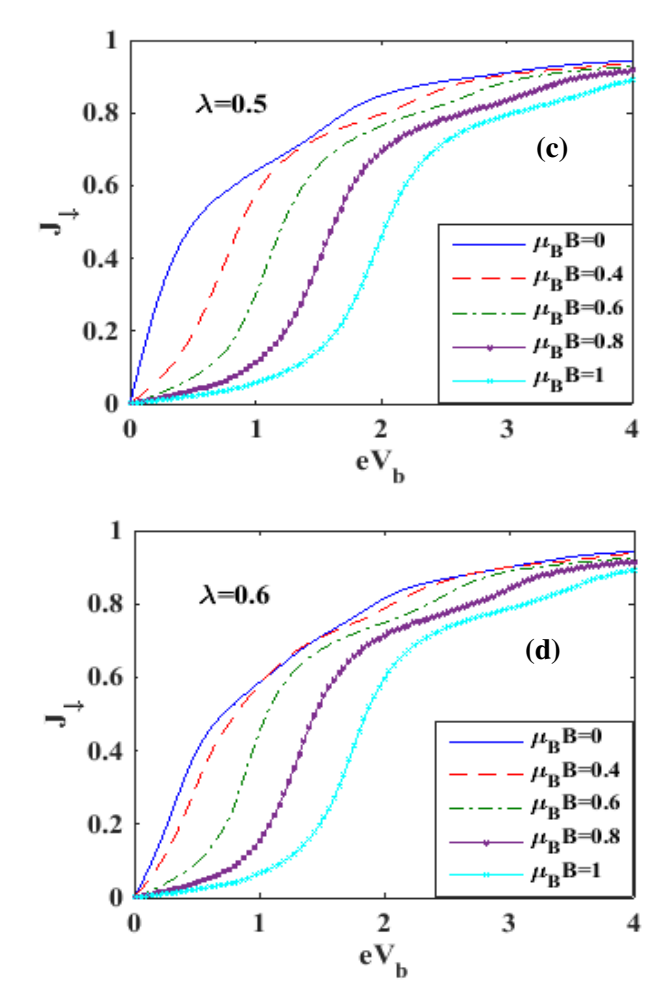


Fig. 8 J_{\downarrow} vs. V_b for different values of $\mu_B B$.

Figs.8 (a-d) show the behaviour of λ both for $\lambda = 0$ and $\lambda \neq 0$, for various $\mu_B B$ values. Again, J_{\downarrow} increases with V_b and ultimately reaches saturation. Of course, this is the expected behavior. As λ increases, λ is found to develop shoulders. Khedri et al. [13-16] and Luffe et al. [17] have examined the appearance of these shoulders.

Fig. 9 provides a comparison between the spin-up and spin-down currents. One can observe that for $\lambda = 0$, the value of J_{\uparrow} is less than that

of J_{\downarrow} up to a particular V_b . This has a simple explanation. The magnetic field lowers the spin-up electron levels while it raises the spin-down

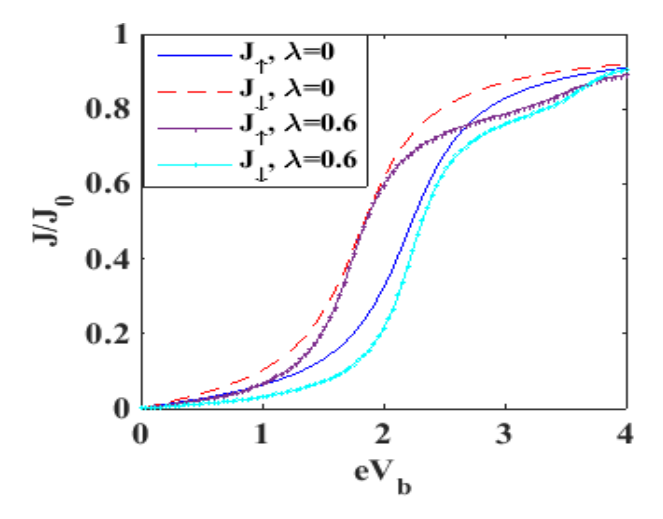


Fig. 9 *J* vs. V_b for a few λ values at $\mu_B B = 1$.

electron levels, resulting in a lower value of J_{\uparrow} due to the reduced probability of tunnelling of the spin-up electrons from QD to D. For $\lambda \neq 0$, the behaviour of the current density appears a bit complex. J_{\uparrow} is found to be higher at lower bias voltages. However, there is a crossover behavior at a specific value of V_b and J_{\uparrow} increases beyond this bias voltage. We do not have a clear explanation for this strange behaviour.

Figs.10 (a-b) show direct plots of J_{\uparrow} and J_{\downarrow} vs. B for various damping coefficients with $\lambda=0.6$. Fig. 10(a) shows the results for J_{\uparrow} , whereas Fig. 10(b) shows those for J_{\downarrow} . According to Fig. 10(a), J_{\uparrow} initially increases with increasing magnetic field, but then drops and eventually reaches zero at a specific magnetic field. Again, the explanation is straightforward. As B increases, spin-up levels decrease, allowing a larger number of electrons to participate in conduction and consequently the current flow increases. However, when the magnetic field reaches a critical value, two factors inhibit the current. The first is that the accessibility of vacant levels

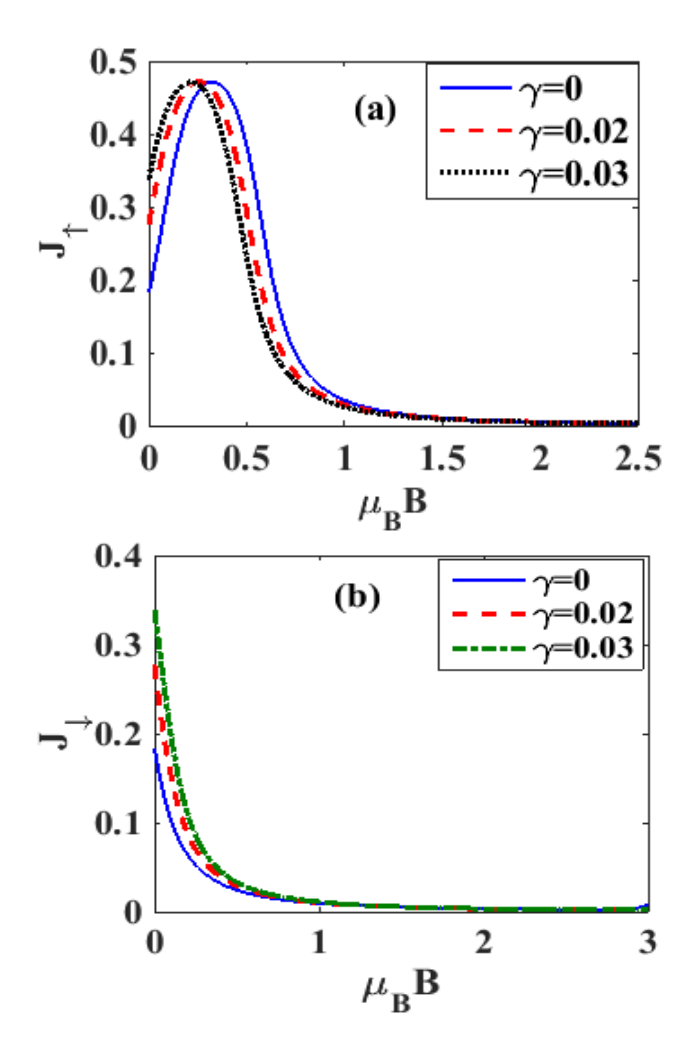


Fig. 10 J_{\uparrow} and J_{\downarrow} vs. $\mu_B B$ for different values of γ .

in QD becomes less. The second is that the probability of electrontunnelling from the QD to D also becomes less. As a consequence, above a specific magnetic field, the current begins to diminish and finally vanishes. As one can see from Fig. 10(b), J_{\downarrow} monotonically decreases as $\mu_B B$ increases. As $\mu_B B$ increases, the spin-down levels rise and this makes the electron tunnelling from S to QD more difficult. This causes the current to decrease as the magnetic field increases.

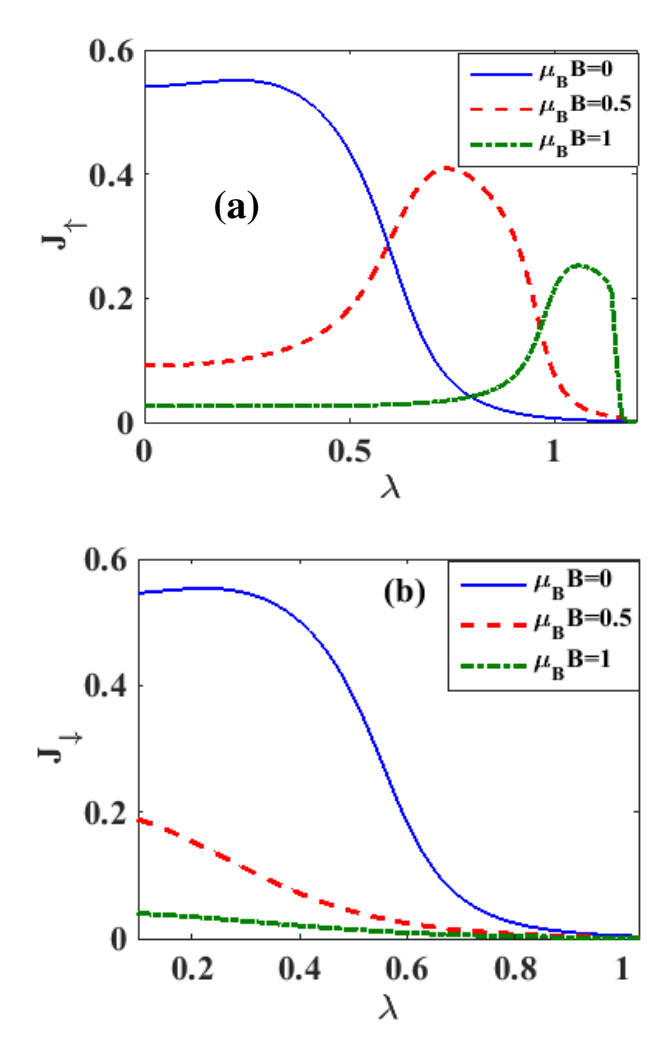


Fig. 11 J_{\uparrow} and J_{\downarrow} vs λ for different values of $\mu_B B$ at $eV_b = 0.5$, $\gamma = 0.02$.

It is expected that the dissipation of the type considered here should raise the current. Figures 11(a-b) explicitly display how J_{\uparrow} and J_{\downarrow} depend on λ for a $\mu_B B$ values. Fig. 11(a) presents the behaviour of J_{\uparrow} . The spin-up electron levels decrease in the presence of a magnetic field, promoting electron tunnelling. The polaronic interaction has two effects. One is that it lowers the electronic level causing an enhancement in the current and secondly, it limits the mobility owing to polaron formation. As a result, numerous competing processes lead to the most remarkable structure in J_{\uparrow} .

The polaronic interaction gives rise to a factor: $\lambda^2 e^{-\lambda^2}$ in J_{\uparrow} . So at small values of λ , λ^2 being the dominant factor, J_{\uparrow} undergoes a quadratic rise, whereas at large λ , J_{\uparrow} is expected to fall in a Gaussian way. Thus, J_{\uparrow} exhibits a maximum in J_{\uparrow} with respect to λ . The magnetic field shifts up the spin-down electron level. As a result, in this scenario, one would expect J_{\downarrow} to reduce as λ is increased. Fig. 12 depicts 3D plots of J_{\uparrow} and J_{\downarrow} with λ and $\mu_B B$.

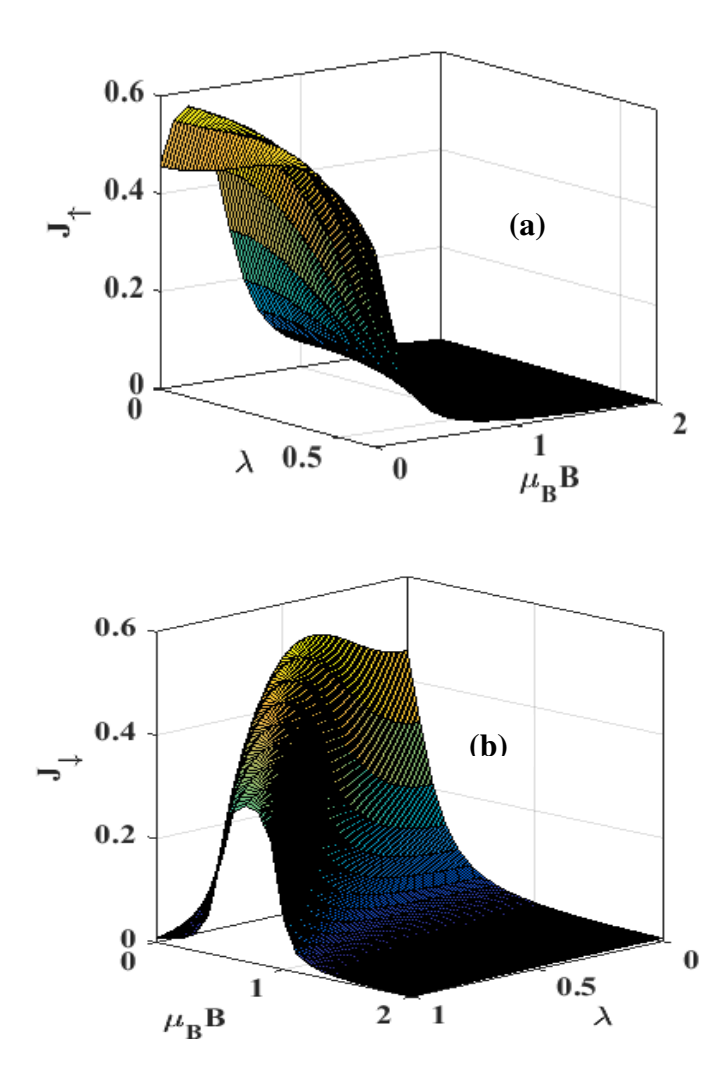


Fig. 12 Three dimensional plots of Spin-polarized current densities for $eV_b = 0.5$ as a function of both λ and $\mu_B B$.

Figs. 13 and 14 show how the differential conductance (*G*) varies with V_b . The inset in Fig. 13(a) depicts the variation for $\lambda = \gamma = B = 0$, whereas the main figure shows the behaviour for $\lambda = 0.6$ and $\gamma = 0.02$ for a few $\mu_B B$ values. For $\lambda \neq 0$, one can see that even for B = 0, the

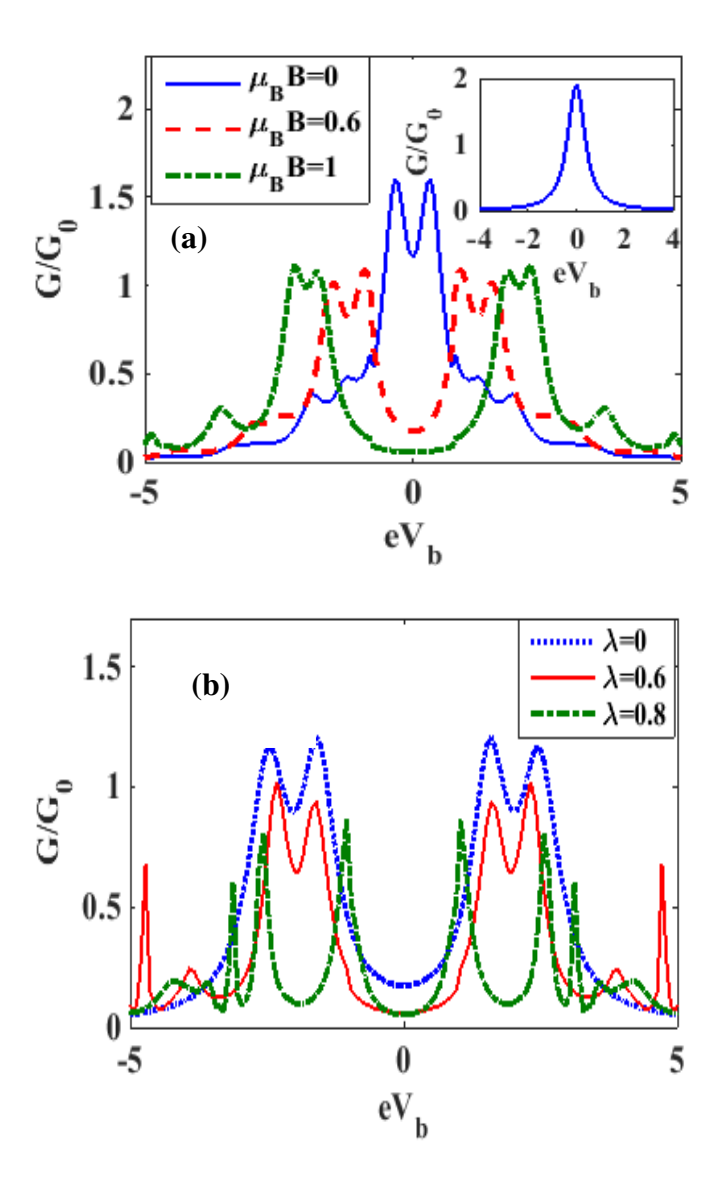


Fig. 13 G/G_0 Vs. eV_b : (a) for different B values with $\lambda=0.6$. (Inset: $\lambda=\gamma=B=0$); (b) for different values of λ with $\mu_B B=0.5$, $\gamma=0$.

there is a splitting in the peak. As $\mu_B B$ increases, splitting occurs in each peak. Also the distance between the two double peak structures increases. Because of the el-ph interaction, a few side peaks arise at higher values of V_b . As previously said, each peak signals the probability of an excitation. As a result, as $\mu_B B$ increases, the states accessible for participation in conduction process also increases in a certain range of V_b . Fig. 13(b) depicts the behaviour of G with V_b for various λ -values in the case when

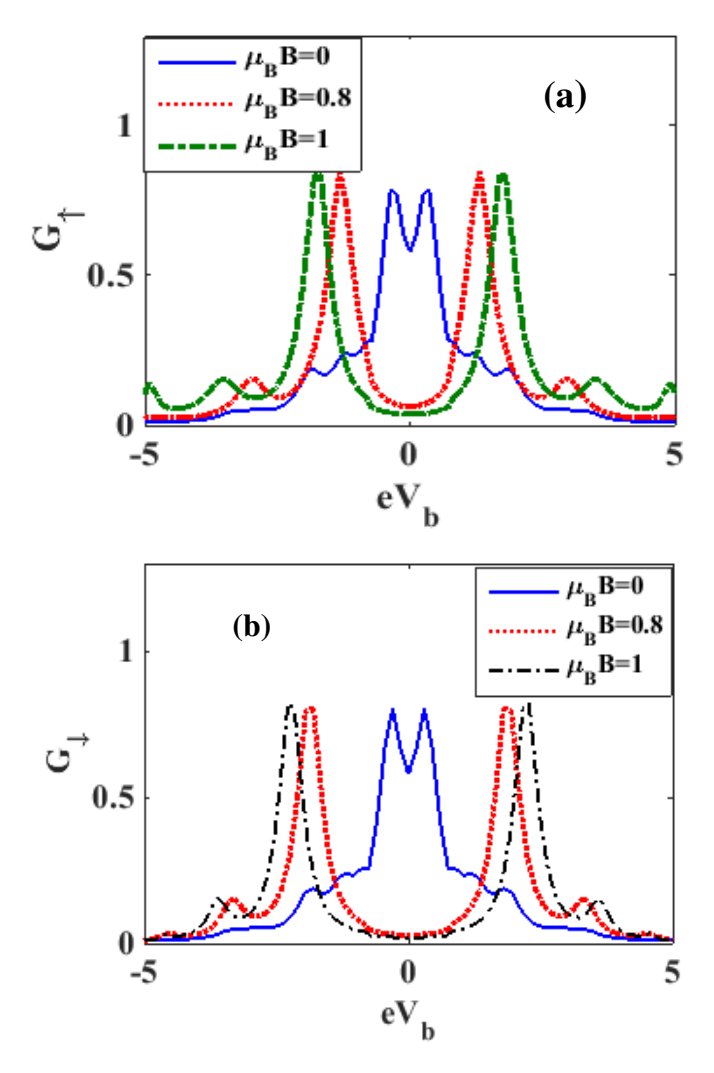


Fig.14 G_{\uparrow} and G_{\downarrow} vs. eV_b for a few B vaues at $\lambda = 0.6$, $\gamma = 0.02$.

there is no dissipation. As expected, G is found to decrease as λ increases. Figs. 14(a-b) show the changes a magnetic field brings about in the graph of spin-polarised differential conductances (G_{\uparrow} and G_{\downarrow}) versus V_b .

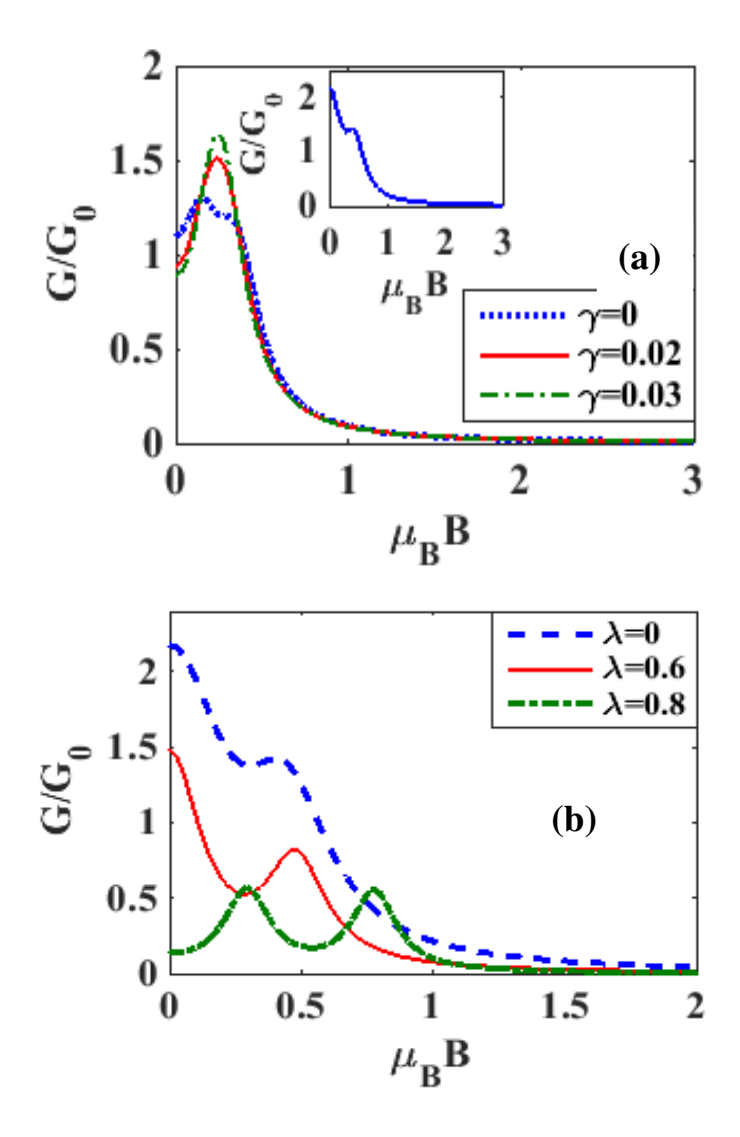


Fig. 15 G/G_0 Vs. $\mu_B B$: (a) for a few values of γ with $\lambda=0.5$ and $eV_b=0.5$ (inset G/G_0 vs $\mu_B B$ for $\lambda=\gamma=0$ and $eV_b=0.5$); (b) for a few values of λ with $\gamma=0$ and $eV_b=0.5$.

In Fig. 15, we study the direct effect of the magnetic field on G. Fig.

15(a) shows the behaviour for different γ values with $\lambda=0.5$. The inset in the figure shows that for $\lambda=\gamma=0$, G reduces as B increases, which is expected as the magnetic field has a localizing effect. However, G also exhibits a small shoulder in a specific window of the magnetic field. In the case of $\gamma\neq 0$, G generally decreases and the decrease becomes more rapid as $\mu_B B$ increases. It is interesting to mention that the shoulder appearing

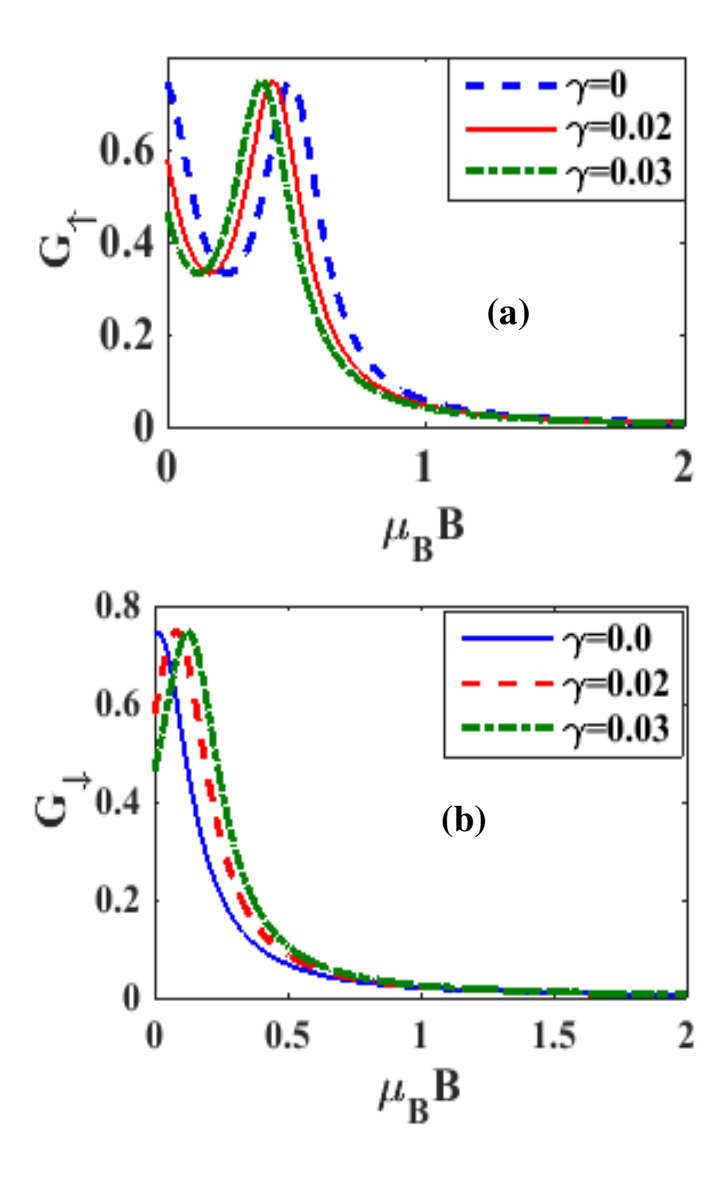


Fig.16 G_{\uparrow} and G_{\downarrow} Vs. $\mu_B B$ for a few values of γ at $\lambda = 0.6$ and $eV_b = 0.5$.

in the absence of el-ph interaction changes into a peak for $\lambda \neq 0$ and the height of the peak grows as γ is increased. In Fig 15(b), we plot G versus $\mu_B B$ for $\lambda = 0.0$, 0.0.6 and 0.8 and $\gamma = 0$. As λ increases, we find that the shoulder changes into a peak structure. G produces two peaks for $\lambda = 0.8$. We show in Figs. 16 (a-b) the behaviour of G_{\uparrow} and G_{\downarrow} with respect to $\mu_B B$ for a few values of γ . One can explain the behavior using Figs. 7 and 8. We investigate the el-ph coupling effect on G_{\uparrow} and G_{\downarrow} in Figs. 17(a-b). The observed behaviour can be understood in view of Fig. 11.

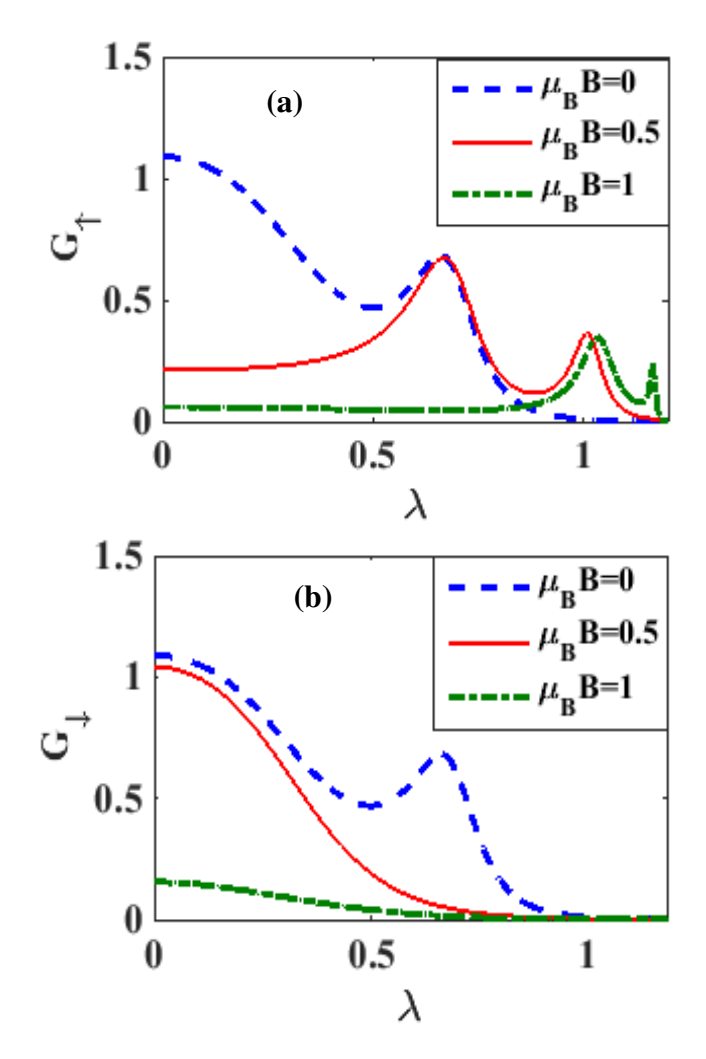


Fig. 17 G_{\uparrow} and G_{\downarrow} Vs. λ for a few values of $\mu_B B$ at $eV_b=0.5$, $\gamma=0.02$

In Fig. 18(a), we study the behaviour of the spin polarisation parameter $P_{\sigma,-\sigma}$ with V_b for a few values of B values for non-zero λ and γ . At low values of $\mu_B B$, $P_{\sigma,-\sigma}$ first grows with V_b , reaches a maximum and then decreases to zero. At higher values of $\mu_B B$ too, $P_{\sigma,-\sigma}$ first increases with V_b but finally bends over and reaches a saturation value that is dependent of $\mu_B B$. Fig. 18(b) reveals that as λ increases, $P_{\sigma,-\sigma}$ diminishes at small V_b though beyond a certain V_b , $P_{\sigma,-\sigma}$ grows with λ . This gives rise to a crossing behaviour.

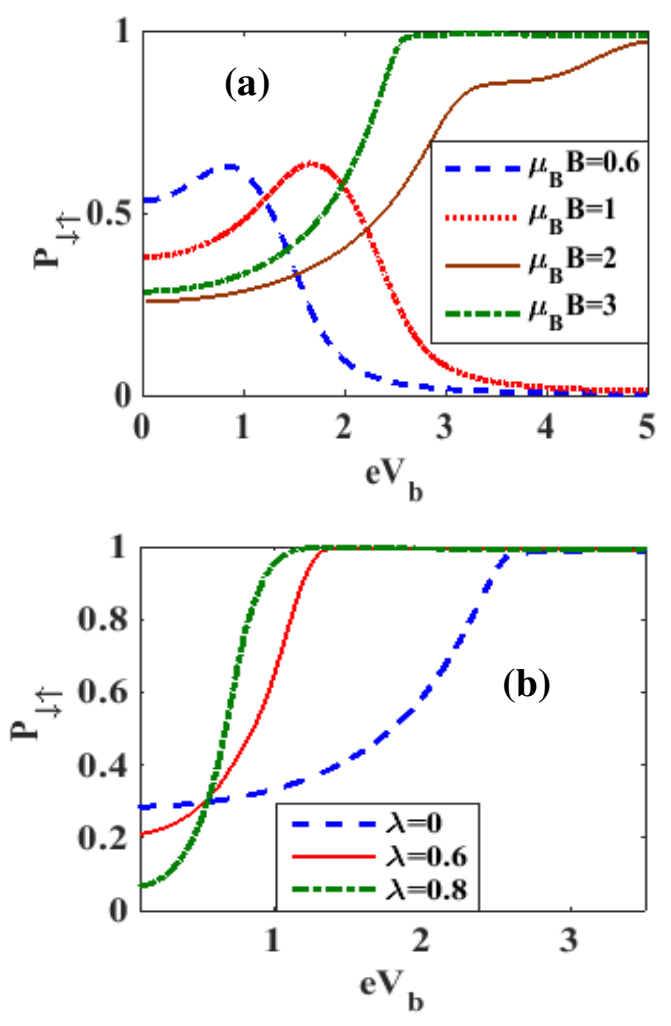


Fig. 18 $P_{\sigma,-\sigma}$ vs. eV_b : (a) for a few values of $\mu_B B$ with $\lambda = 0.5$ & $\gamma = 0.02$; (b) for a few values of λ with $\mu_B B = 3$ & $\gamma = 0.02$.

Fig. 19 shows the behaviour of $P_{\sigma,-\sigma}$ with respect to $\mu_B B$. In the case of $\lambda=0=\gamma$, as $\mu_B B$ increases, $P_{\sigma,-\sigma}$ first rises with $\mu_B B$, assumes a maximum value and then reduces to constant value. For $\lambda\neq 0$, $P_{\sigma,-\sigma}$ behaves in the same way initially and exhibits a maximum but as $\mu_B B$ increases further, $P_{\sigma,-\sigma}$ eventually falls to zero. Fig. 19(b) depicts the behaviour of $P_{\sigma,-\sigma}$ with $\mu_B B$ for various values of γ . The qualitative behaviour in this case turns out to be essentially similar to that seen in the

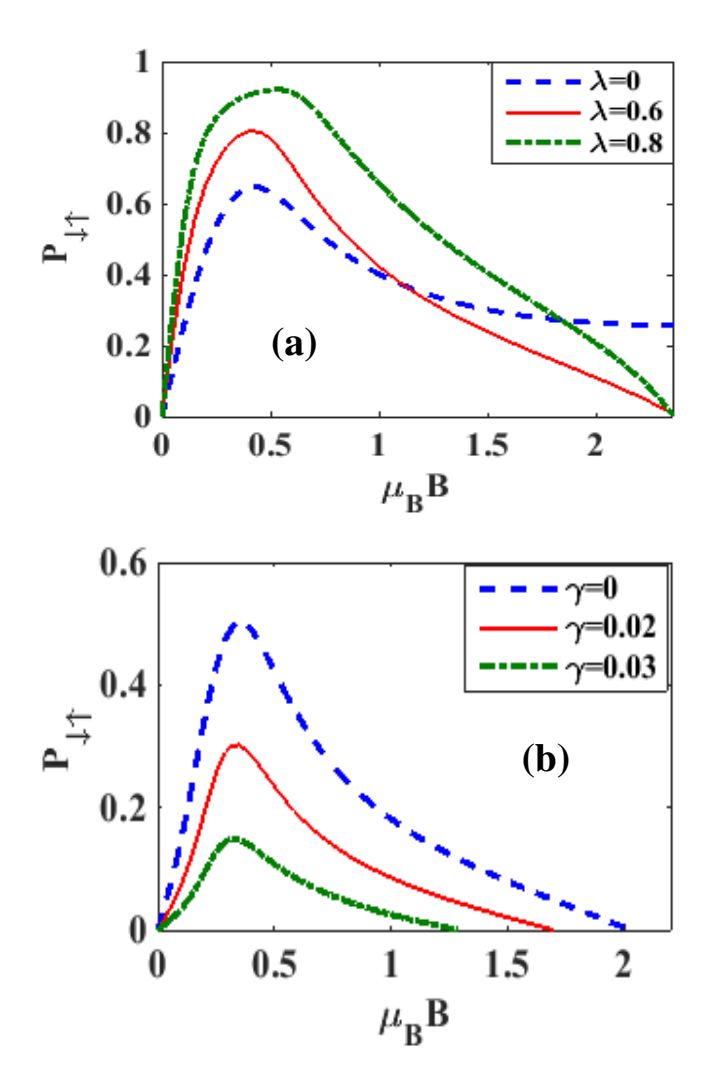


Fig. 19 $P_{\sigma,-\sigma}$ Vs. $\mu_B B$: (a) for a few values of λ with $\gamma = 0$ and $eV_b = 0.5$; (b) for a few values of γ with $\lambda = 0.5$ and $eV_b = 0.5$.

 $P_{\sigma,-\sigma} - \mu_B B$ - graphs for $\lambda \neq 0$. Also, $P_{\sigma,-\sigma}$ decreases as damping increases.

Fig. 20 displays the behavior of J/J_0 as a function of the mid-voltage eV_m for some $\mu_B B$ values with $\lambda = 1$ and U = 5. In the inset, we show the variation of J/J_0 for U = 0, B = 0, $eV_b = 3.6$ and $\lambda = 0$ and 1 as obtained by Chen et al. [18]. It is clear that at $\lambda = 0$, J/J_0 has a asymmetric plateau-like structure and the el-ph coupling reduces J/J_0 , and induces a wavy structure in the plateau and J/J_0 becomes symmetric around V_m . The main figure shows that for $U \neq 0$, J/J_0 has a peak structure which shifts to the positive mid-voltage side as B increases. Furthermore, J/J_0 is now zero for negative V_m .

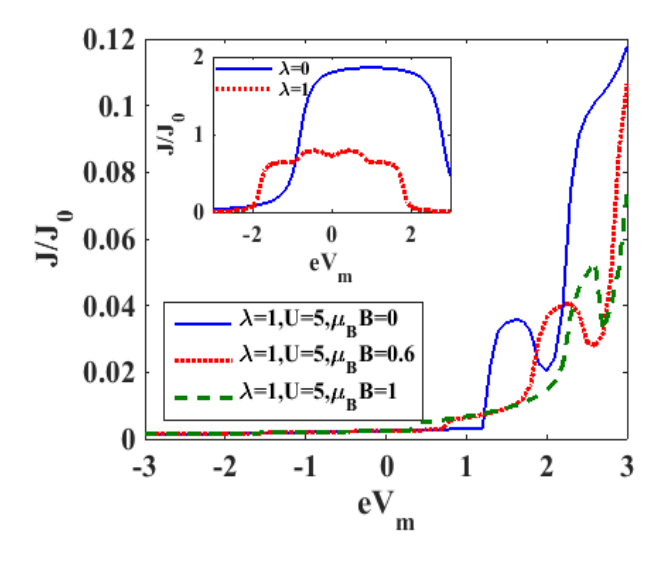


Fig. 20 J/J_0 vs eV_m at U=5, $eV_b=3.6$ for different B values. (**Inset:** J/J_0 vs eV_m at U=0, $eV_b=3.6$ and $\mu_BB=0$).

We plot G/G_0 vs. V_m with U=5 in the absence of a magnetic field in Fig. 21(a). We also display the results for U=0, and $\lambda=0$ and 1 as obtained by Chen et al. [18] to see how el-el interaction affects the results. For $\lambda=0$, G exhibits two peaks appearing asymmetrically around $V_m=0$. The peaks get shorter and sharper at $\lambda=1$ and symmetric with $V_m=0$. A

few symmetric side-peaks can also be seen. When U increases to U=5, peak-heights reduce and the peaks move to right hand side of $eV_m=0$. Furthermore, G reduces to zero for negative V_m and also for small positive values of V_m . Fig. 21(b) shows the plot of G/G_0 with V_m for $\lambda=1$, U=5, and two values of B. We see a lot of peaks at $\mu_B B=0.6$. Peak structures change when $\mu_B B$ approaches 1.

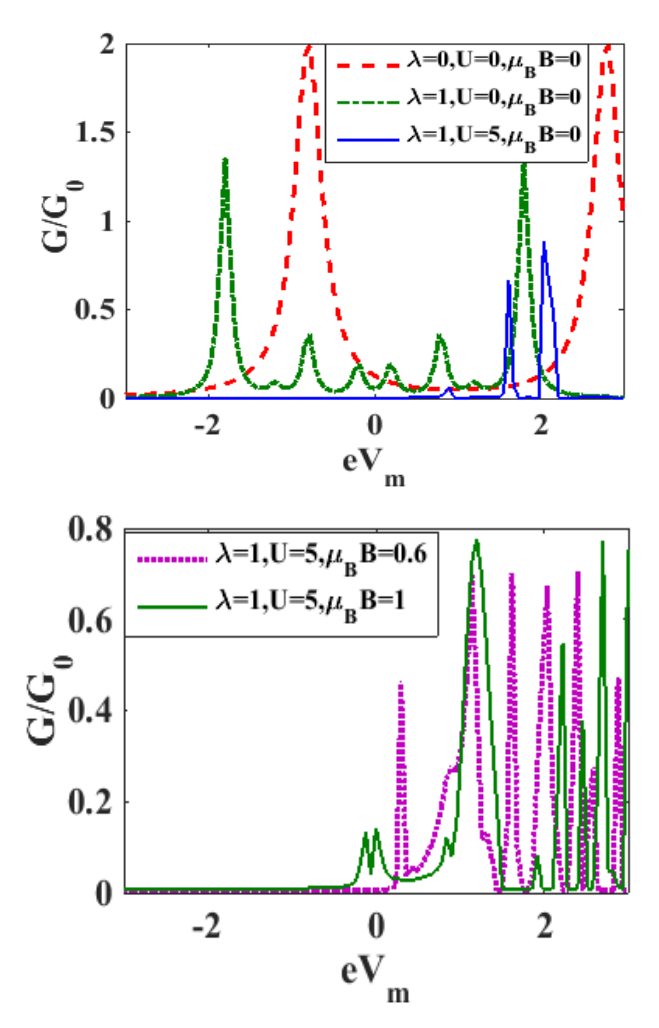


Fig.21 G/G_0 Vs. eV_m : (a) for $\mu_B B = 0$, $eV_b = 3.6$, U = 0 and 5, $\lambda = 0$ and 1; (b) for different values of $\mu_B B$ at U = 5, $eV_b = 3.6$.

Fig. 22 shows the contour diagram of J in the (V_b-V_m) - plane for a few sets

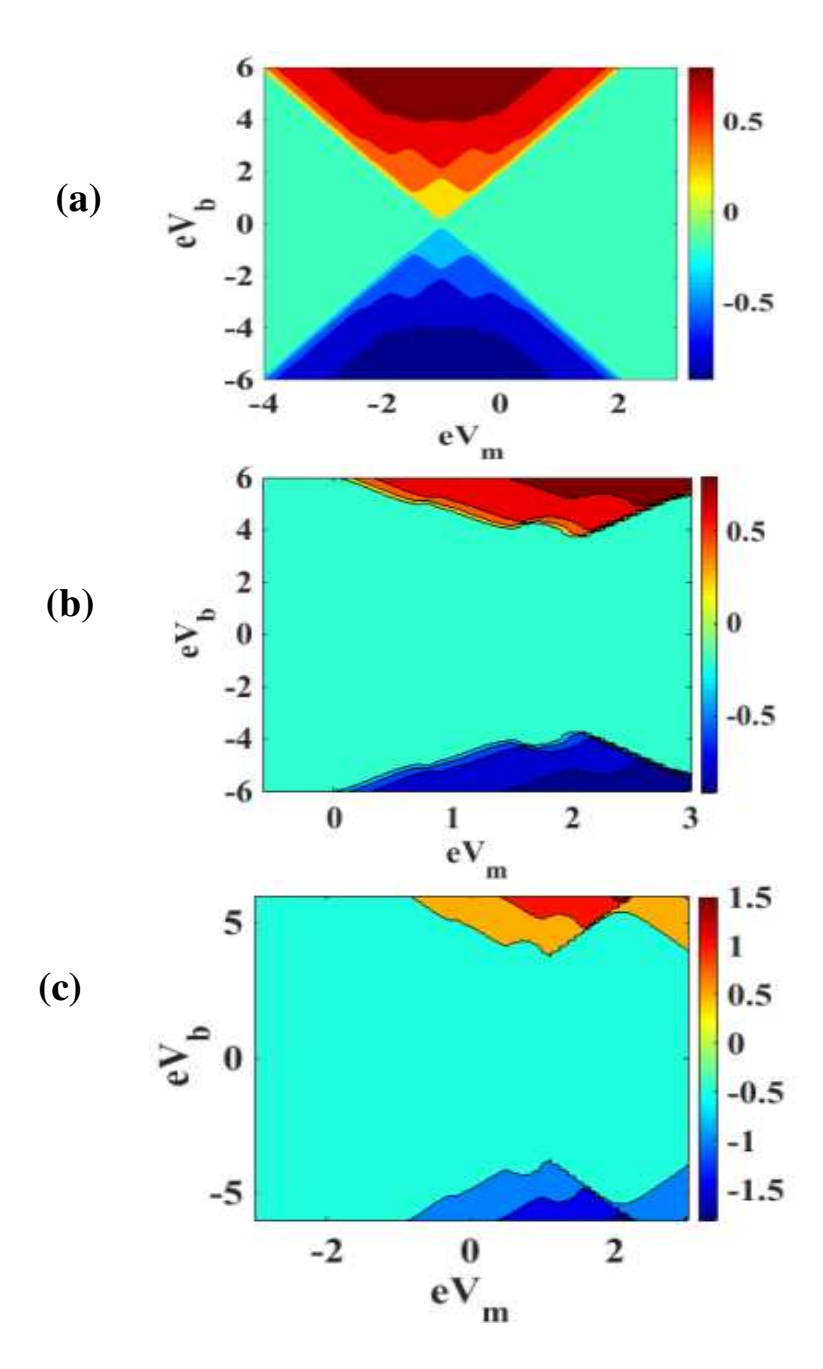


Fig. 22 Map of J in the V_b - V_m - space : (a) for $\lambda=1$, $\mu_B B=1$ and U=0 ;(b) for $\lambda=1$, B=0 and U=5 ;(c) for $\lambda=1$, $\mu_B B=1$ and U=5 .

of parameter values such as: $\lambda = 1$, $\mu_B B = 1$, U = 0; $\lambda = 1$, $\mu_B B = 0$, U = 5 and $\lambda = 1$, $\mu_B B = 1$, U = 5. It is useful to make a comparison of Fig.

22 (a) with the similar figure in [18]. This shows that the magnetic moves J to the left on the V_m - axis bringing in symmetry in J around $V_m = 0$. It can also

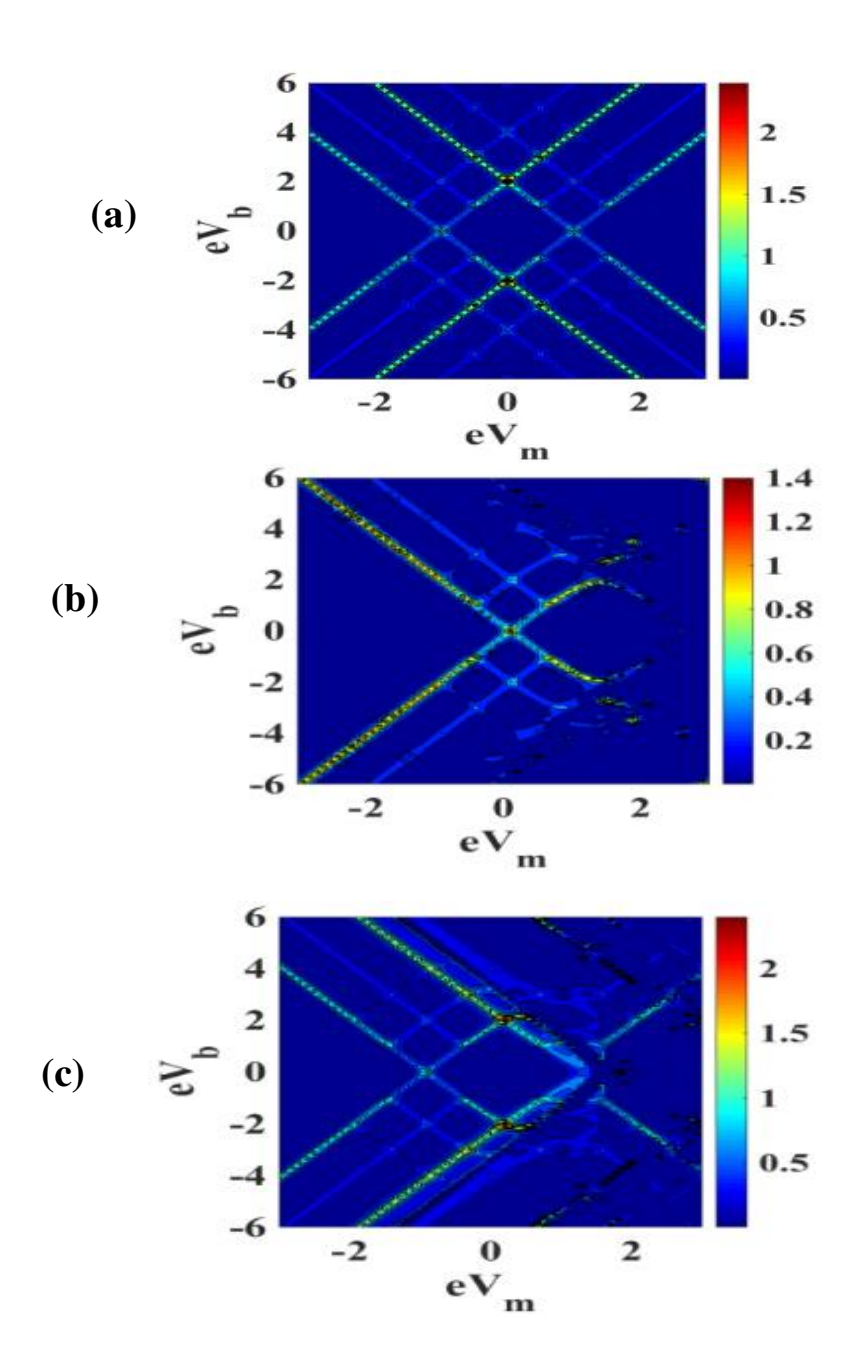


Fig 23 Map of G in (V_b-V_m) -space for: (a) $\lambda=1$, $\mu_BB=1$ and =0; (b) $\lambda=1$, B=0 and U=5.; (c) $\lambda=1$, $\mu_BB=1$ and U=5.

be noticed that plateaus appear corresponding to different values of J. Fig. 22(b) shows that J decreases for $U \neq 0$. Furthermore, J is non-zero only for positive V_m . The J-map for non-zero $\mu_B B$ and λ is shown in Fig. 22 (c). As expected, now the plateau heights come down and the J-map shifts to the right on the V_m axis.

Fig. 23 shows the contour plot of G in the $(V_b - V_m)$ – plane for a few sets of parameters: $\lambda = 1$, $\mu_B B = 1$, U = 0; $\lambda = 1$, B = 0, U = 5 and $\lambda = 1$, $\mu_B B = 1$, U = 5. When Fig. 23 (a) is compared to the similar map in [18], it becomes clear that magnetic field splits each peak in the G –map into two. The role of Coulomb correlation on the contour plot of G is depicted in Fig. 23 (b). The el-el interaction clearly reduces the differential conductance. This map also shows some chaotic behaviour for $V_m > 0$. The origin of this complicated behaviour is, however, not clear. Figure 23(c) presents the effect of both e-e interaction and the magnetic field along with the el-ph interaction. Fig. 22(c) contains more general information than Figs. 22(a) and 22(b).

2.7 Conclusion

In this chapter, we have presented our work on the effect of el-ph interaction, onsite Coulomb correlation, magnetic field, and damping on transport properties of an SMT system. The system has been modeled by the Anderson-Holstein-Caldeira-Leggett Hamiltonian. The dissipative effect is caused by the linear coupling between the lattice mode the QD and substrate phonons according to the Caldeira-Leggett model and has been approximately addressed by a canonical transformation. This reduces the QD phonon frequency, which is precisely the effect of dissipation. The

Holstein el-ph Hamiltonian has been dealt with by the Lang-Firsov method and averaging with respect to the zero-phonon state. We have used the Keldysh Green function method to calculate the spectral function A, current density J, differential conductance G, and spin polarization parameter $P_{\sigma,-\sigma}$ and the effect of el-ph coupling, magnetic field, and dissipation on the transport properties have been investigated.

The spin degeneracy of the QD energy levels is removed by the magnetic field $\mu_B B$. As a result, the electron levels of QD are split, and consequently SD functions develop peaks. Both the el-ph coupling and magnetic field reduce J_{\downarrow} . However, J_{\uparrow} increases with $\mu_B B$ up to a critical $\mu_B B$ and then drops to zero. J_{\uparrow} versus λ shows a similar behaviour.

The spin-split conductances G_{\uparrow} and G_{\downarrow} have been shown to decrease as B is increased. As a function of λ , however, the behaviour of G_{\uparrow} and G_{\downarrow} is opposite. It is also observed that el-ph interaction induces G_{\uparrow} to develop peaks while it suppress them in G_{\downarrow} .

At small $\mu_B B$, $P_{\sigma,-\sigma}$, as a function of V_b , exhibits a peak and then falls off to zero whereas at large $\mu_B B$, $P_{\sigma,-\sigma}$ initially increases with V_b and eventually saturates. Furthermore, as $\mu_B B$ increases, $P_{\sigma,-\sigma}$ decreases and finally drops to zero. It has been shown that the phononic dissipation considered in this chapter enhances J_{\uparrow} , J_{\downarrow} and $P_{\sigma,-\sigma}$. We have also shown that the number of peaks in the graph of G versus V_m , increases with $\mu_B B$ due to spin-splitting. The present work suggests that the SMT device considered here can have potential applications in spin-filtering device.

2.8 References

- 1 Costi. T. A. Magnetotransport through a strongly interacting quantum dot. *Phys. Rev.* B **64**, 241310(R) (2001).
- 2 Bing. D and Lei. X. L. Kondo-type transport through a quantum dot under magnetic fields. *Phys. Rev.* B **63**, 235306(2001).
- 3 Caldeira. A. O & Leggett. A. J. Quantum tunneling in dissipative system. Ann. Phys. **149**, 374 (1983).
- 4 Cornaglia. P. S & Grempel. D. R. Strongly correlated regimes in a double quantum dot device. *Phys. Rev. B* **71**, 245326–6(2005).
- 5 Hui. P. Spin-polarized current diode effect of a quantum dot in a rotating magnetic field. *Phys. scr.* **78**, 065703(2008).
- 6 Weiss. U, Quantum Dissipative systems (University of Stuttgart, 1999).
- 7 Lang. I. G & Firsov. Yu. A. Kinetic theory of semiconductors with low mobility. Sov. Phys. JETP 16, 1301 (1962).
- 8 Jauho. A. P, Wingreen. N. S & Meir. Y. Time-dependent transport in interacting and noninteracting resonant-tunneling systems. *Phys. Rev. B* **50**, 5528 (1994).
- 9 Meir. Y, Wingreen. N. S and Lee. P. A. Transport through a strongly interacting electron system: Theory of periodic conductance oscillations. *Phys. Rev.* Lett. **66**, 3048 (1991).
- 10 Swirkowicz. R *et al.*, Nonequilibrium Kondo effect in quantum dots. *Phys. Rev.* B **68**, 195318 (2003).
- 11 Keldysh. L. V. Diagram technique for nonequilibrium processes. *Sov. Phys. JETP* **20**, 1018 (1965).

- 12 Narasimha Raju. Ch. and Ashok. C. Quantum dissipative effects on non-equilibrium transport through a single-molecular transistor: The Anderson-Holstein-Caldeira-Leggett model. Scientific Reports. 6, 18511 (2016).
- **13** Khedri. A Costi. T.A, Meden V. Exponential and power-law renormalization in phonon-assisted tunneling, *Phys. Rev.B* **96**, 195155 (2017).
- **14** Khedri. A Costi. T.A, Meden V. Influence of phonon-assisted tunneling on the linear thermoelectric transport through molecular quantum dots, *Phys. Rev.B* **96**, 195156 (2017).
- **15** Khedri. A Costi. T.A, Meden V. Nonequilibrium thermoelectric transport through vibrating molecular quantum dots, *Phys. Rev.B* **98**, 195138 (2018).
- **16** Keldysh. L. V. Diagram technique for nonequilibrium processes. *Sov. Phys. JETP* **20**, 1018–1026 (1965).
- 17 Luffe. M. C., Koch, J. & von Oppen, F. Theory of vibrational absorption sidebands in the Coulomb-blocked regime of singlemolecular transistors. Phys. Rev. B 77, 125306–7 (2008).
- **18** Chen. Z. Z, Lü. R, Zhu B. F. Effects of electron-phonon interaction on nonequilibrium transport through a single-molecule transistor. *Phys, Rev. B* **71**, 165324 (2005).

Chapter 3

Quantum transport in a single molecular transistor at finite temperature

3.1 Introduction

In recent years, several researchers [1-3] have investigated experimentally the temperature dependent transport in SMT. Theoretical research, on the other hand, has been scarce [4]. In this work, our aim is to to study the effect of temperature on transport properties in an SMT device. We examine the same SMT system as introduced in Chapter 1. As before, we model the system by AHCL Hamiltonian and study the non-equilibrium quantum transport using Keldysh Green function approach.

3.2 The Model

The SMT device to be studied in this chapter is shown schematically in Fig. 1. The system is modelled by the Hamiltonian

$$H = H_{S,D} + H_{QD} + H_h + H_{QD-ph} + H_{QD-ep} + H_B + H_M$$

$$= \sum_{k\alpha} \varepsilon_k n_{k\alpha} + \sum_{\sigma} \varepsilon_d n_{d\sigma} + U n_{d,\uparrow} n_{d,\downarrow} + \sum_{\sigma,k\alpha \in S,D} V_k (c_{k\alpha}^{\dagger} c_{d\sigma} + h.c)$$

$$+ \hbar \omega_0 b^{\dagger} b + \lambda \hbar \omega_0 (b^{\dagger} + b) \sum_{\sigma} n_{d\sigma} + \sum_{j=1}^{N} \left[\frac{p_j^2}{2m_j} + \frac{1}{2} m_j \omega_j^2 x_j^2 \right]$$

$$+ \sum_{i=1}^{N} \beta_j x_j x_0.$$
(3.1)

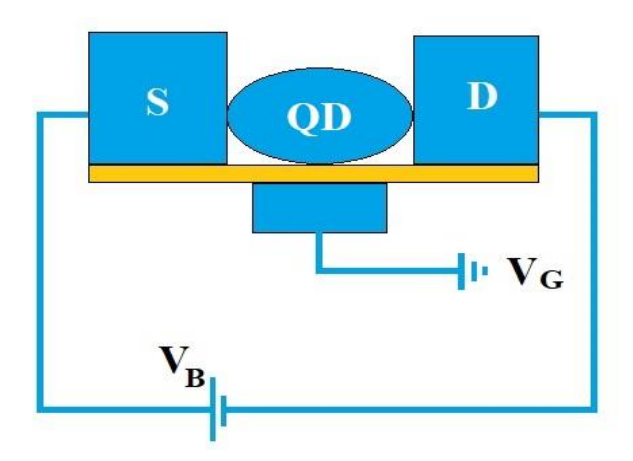


Fig.1 Schematic diagram of an SMT device

As in Chapter 2, we first use a simple canonical transformation to partially decouple the QD phonon and the bath oscillators and then deal with the el-ph coupling using the Lang-firsov transformation. The transformed Hamiltonian of the SMT system then reads

$$\widetilde{H} = \sum_{k\sigma} \varepsilon_k \, n_{k\sigma} + \sum_{\sigma} \widetilde{\varepsilon}_d \, n_{d\sigma} + \widetilde{U} n_{d,\uparrow} n_{d,-\downarrow} + \hbar \omega_0 b^{\dagger} b + \sum_{k,\sigma} (V_k c_{k\sigma}^{\dagger} \widetilde{c}_{d\sigma} + h.c)$$
(3.2)

where the system parameters get renormalized as

$$\tilde{\varepsilon}_d = \varepsilon_d - eV_G - \lambda^2 \hbar \omega_0, \tag{3.3}$$

$$\widetilde{U} = U - 2\hbar\omega_0\lambda^2,\tag{3.4}$$

$$\widetilde{V}_k = V_k \hat{\chi} = V_k e^{\lambda (b - b^{\dagger})} . \tag{3.5}$$

3.2 Current density and Spectral density function:

As shown in Chapter 2, the tunneling current [5-7] flowing through QD is given by

$$J = \frac{e}{2h} \int (\{f_S(\omega)\Gamma_S - f_D(\omega)\Gamma_D\}A(\omega) + (\Gamma_S - \Gamma_D)G^{<}(\omega)) d\omega, \quad (3.6)$$

where

$$\Gamma_{S,D}(\varepsilon_k) = 2\pi \varrho_{S,D}(\varepsilon_k) \bar{\tilde{V}}_k V_k^*, \tag{3.7}$$

 $\overline{\tilde{V}}_k$ referring to the phonon-average of \tilde{V}_k and $\rho_{S(D)}$, the density of states in S(D), $f_{S(D)}(\omega)$ refers to the FD distribution in S (D) which has the following expression

$$f_{S,D}(\omega) = \frac{1}{[\exp[(\mu_{S,D} - \omega)/k_B T] + 1]}$$
, (3.8)

 $\mu_{S,D}$ being the chemical potential of S(D) and related to V_B and V_m as:

$$eV_b = (\mu_S - \mu_D), \ eV_m = \frac{(\mu_S + \mu_D)}{2},$$
 (3.9)

 $A(\omega)$ is the SD function which is related to Green's functions as follows:

$$A(\omega) = i[G_{dd}^{r}(\omega) - G_{dd}^{a}(\omega)] = i[G_{dd}^{>}(\omega) - G_{dd}^{<}(\omega)], \quad (3.10)$$

where $G_{dd}^{r(a)}(\omega)$ represents the energy-dependent retarded (advanced) Green function and $G_{dd}^{<(>)}(\omega)$ is the (greater) Green function corresponding to the QD electron. All the afore-mentioned quantities including the Green functions have been introduced in Chapter 2. These Green functions can be derived using EOM as we have shown in Chapter 2. We calculate the mean occupancy on QD using the equation

$$n_{d\sigma} = \int d\omega \frac{\left[(f_s \Gamma_s + f_D \Gamma_D) A(\omega) \right]}{2\pi \Gamma}.$$
 (3.11)

For mathematical simplicity, we consider symmetric coupling of QD with leads. Then we may write:

$$\Gamma(\omega) = \frac{\left[\Gamma_{S}(\omega) + \Gamma_{D}(\omega)\right]}{2}.$$
 (3.12)

where we approximate $\Gamma_{S(D)}$ by its n-phonon average. Thus we have

$$\Gamma_{S(D)} = 2\pi\rho(0)|V_k|^2 e^{\left[-\lambda^2 (f_{ph}+1/2)\right]},$$
 (3.13)

where

$$f_{ph} = \frac{1}{[e^{(\hbar \tilde{\omega}_0/k_B T)} - 1]}$$
 (3.14)

denotes the phonon distribution at a specific temperature. The spectral function of SMT is obtained as

$$A(\omega) = \sum_{n=-\infty}^{\infty} i L_n(z) \left[\tilde{G}^{>}(\omega - n\widetilde{\omega}_0) - \tilde{G}^{<}(\omega + n\widetilde{\omega}_0) \right]$$

$$= \sum_{n=-\infty}^{\infty} L_n(z) \left[\frac{2\tilde{\Gamma}}{\left(\omega + n\widetilde{\omega}_0 - \tilde{\varepsilon}_d - \widetilde{U}(n_{d,-\sigma})\right)^2 + \tilde{\Gamma}^2} \right], \quad (3.15)$$

where n denotes the number of phonons,

$$\tilde{\Gamma} = \Gamma e^{-\lambda^2 (2f_{ph} + 1)},\tag{3.16}$$

and

$$L_{\pm n} = e^{\left[-\lambda^2 (2f_{ph} + 1) + \frac{n\tilde{\omega}_0}{2k_B T}\right]} I_n \left(2\lambda^2 \left[f_{ph} (1 + f_{ph})\right]^{1/2}\right), \quad (3.17)$$

where I_n is the Modified Bessel function and $L_{\pm n}$ are the spectral weights of the +nth and -nth phonon side bands as indicated in [8]. $A(\omega)$ is calculated and consequently J is determined.

3.3 **Differential conductance** (G)

G is defined as: $G = dI/dV_b$. Straight-forward calculation gives

$$G = \frac{e^2 \Gamma}{2h} \sum_{n=-\infty}^{\infty} L_{\pm n} \int_{-\infty}^{\infty} d\omega F_n(\omega) A(\omega - n\widetilde{\omega}_0), \qquad (3.18)$$

where

$$F_{n}(\omega) = \frac{1}{2k_{B}T} [f_{S}(\omega)\{1 - f_{S}(\omega)\} + f_{D}(\omega)\{1 - f_{D}(\omega)\}]$$

$$\times \left[1 + \frac{1}{2} \left(e^{-\frac{n\widetilde{\omega}_{0}}{k_{B}T}} - 1\right) [f_{S}(\omega - n\widetilde{\omega}_{0}) + f_{D}(\omega - n\widetilde{\omega}_{0})]\right]$$

$$+ \frac{1}{4k_{B}T} \left(e^{-\frac{n\widetilde{\omega}_{0}}{k_{B}T}} - 1\right) [f_{S}(\omega) - f_{D}(\omega)]$$

$$\times \left[f_{S}(\omega - n\widetilde{\omega}_{0})\{1 - f_{S}(\omega - n\widetilde{\omega}_{0})\} - f_{D}(\omega - n\widetilde{\omega}_{0})\right]$$

$$\times \left\{1 - f_{D}(\omega - n\widetilde{\omega}_{0})\}\right]. \tag{3.19}$$

3.4 Results and Discussions

We set the phonon energy $\hbar\omega_0$ as the scale of energy in our numerical computation and for the SMT parameters, we set the following values: $\varepsilon_d=0$, $eV_g=0$, $\Gamma=0.2$, $eV_m=0.5$, U=3 (unless otherwise specified). To understand the effect of temperature on the transport properties of the SMT device, we calculate the SD function A, Current density J and the differential conductance G at different values of T. Fig. 2 depicts the behavior of the SD function $A(\omega)$ with energy ω at $\lambda=0.6$,

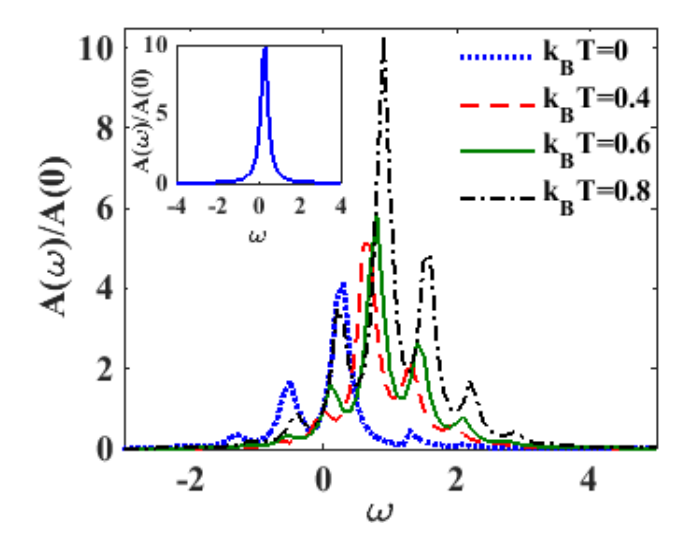


Fig. 2 $A(\omega)/A(0)$ vs. ω for different values of k_BT .

 $eV_m=0.5$, $eV_b=2.5$. The results for $\lambda=0$ and $k_BT=0$ are shown in the inset which clearly shows the Lorentzian peak at $\omega=0$. The main graph in Fig. 2 shows the behavior of $A(\omega)$ with respect to ω for several T values with $\lambda\neq0$. The figure demonstrates that when the el-ph interaction is activated at T=0, the polaronic effect renormalizes the SMT parameters, causing the central peak in $A(\omega)$ to redshift and side peaks to emerge at $\omega\mp n\widetilde{\omega}_0$ in it. The emergence of sidebands represents the excitation of phonons. An electron can tunnel into or out of QD by

emitting or absorbing a phonon, which appears as side bands in A. The probability of occurrence of higher-order phonon processes is smaller and therefore the side-band heights fall with increasing energy. At finite temperature, a more fascinating situation emerges. At $T \neq 0$, the central peak sharpens, becomes higher and goes through a blue shift. Also, as T increases, the side bands diminish in the region: $\omega < 0$ and grow in the region: $\omega > 0$.

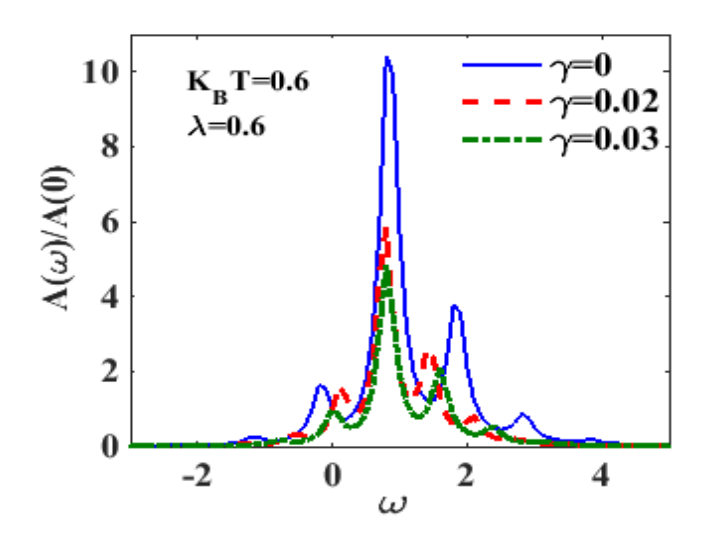


Fig. 3 $A(\omega)/A(0)$ vs. ω for a few γ values .

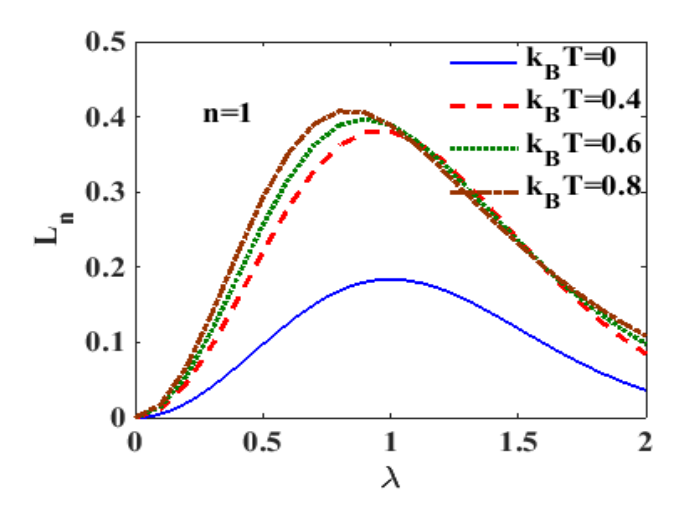


Fig. 4 L_n vs. λ for a few T values with $\gamma = 0.02$.

Fig. 3 depicts the behavior of $A(\omega)$ with ω at $k_BT=0.6$ for $\lambda=0.6$ and several γ values. As dissipation increases, the height of the peak in $A(\omega)$ decreases and its width broadens. So we conclude that the dissipation reduces the occupancy of the phonon side-bands as stated in [9, 10].

In [8], nature of the spectral weight (L_n) has been demonstrated at T = 0K for various n. Fig. 4 presents the behaviour of L_n (n = 1) with λ for a few T values. L_n grows in height with rising T until some critical value, after which the T- dependence of L_n appears to be insignificant. As a function λ , L_n first increases, reaches a peak at some λ , and then drops in a smooth way. We have observed (though we have not shown here) that for higher values of n, though the qualitative behavior remains the same, the quantitative value of L_n decreases quite significantly.

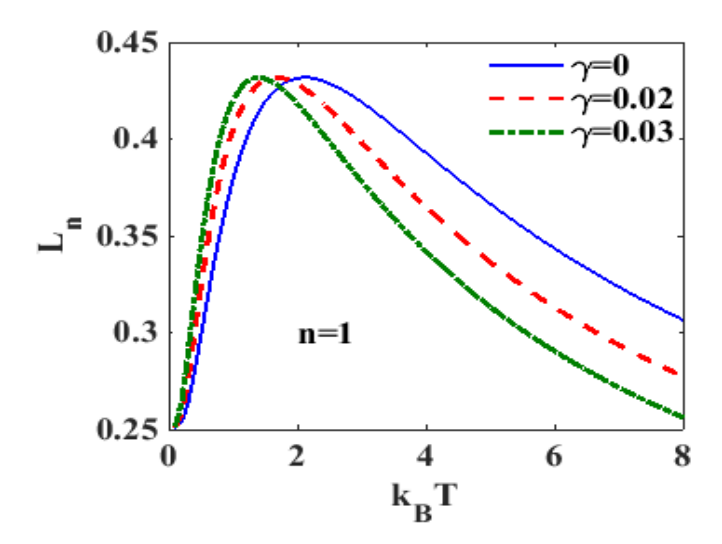


Fig. 5 L_n vs. k_BT for a few γ values with $\lambda = 0.6$.

We plot L_1 versus T for various γ in Fig.5 to see the effect of damping effect at n = 1. It is evident that as T increases, L_1 grows rapidly and

reaches a peak value at some T, and finally declines with a further rise in T. One can also see that up to a certain T, dissipation enhances L_1 , albeit marginally and above a certain T, dissipation reduces L_1 .

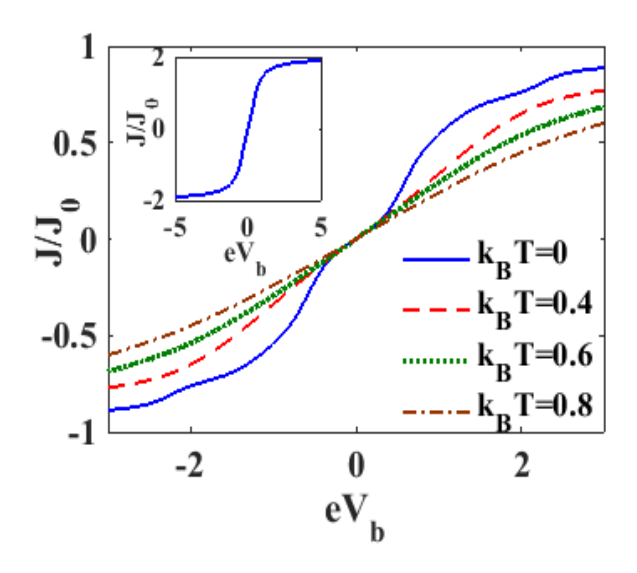


Fig. 6 J/J_0 vs. eV_b for different values of k_BT .

The behavior of current density J with bias voltage V_B for a specific value of λ is plotted at different values of T in Fig. 6. The inset which gives the behaviour for $\lambda = T = \gamma = 0$, suggests that J linearly increases with V_B and finally saturates. According to main graph, as T increases, J decreases. We present in Fig.7 the plot of J versus V_B for various λ values. The el-ph interaction reduces the current density at a finite temperature due to the polaronic effect. The reduction is, however, marginal for the el-ph coupling range studied in this work. To understand how dissipation influences behaviour of J with respect to V_B at a finite temperature, we plot J versus V_B for various γ values with $\lambda = 0.6$ and $k_B T = 0.6$ in Fig.8. J increases just marginally with increasing γ .

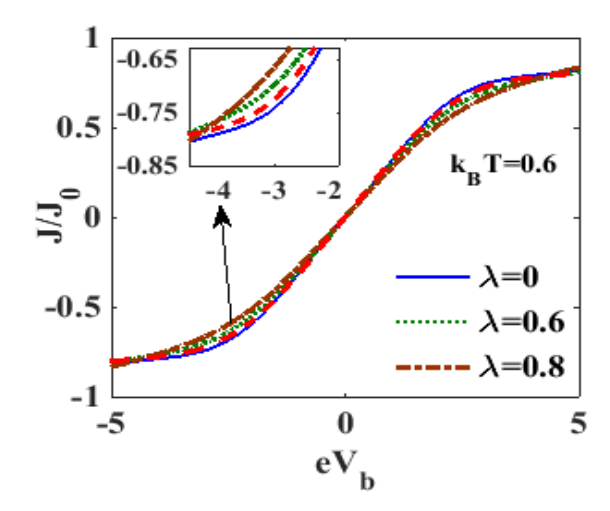


Fig.7 J/J_0 vs. eV_b for different values of λ .

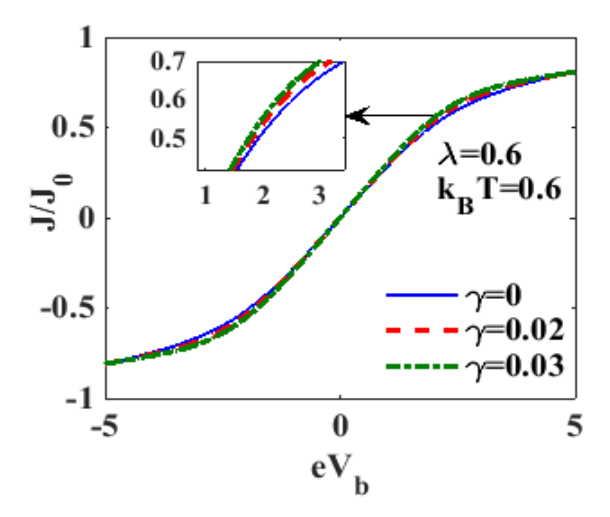


Fig. 8 J/J_0 vs eV_b for different values of γ .

Fig. 9 presents the plot for J versus λ . The el-ph interaction reduces the current density and at some critical λ , the current density reaches to zero. The graph also indicates that when T increases, J reduces. Fig. 10 depicts directly how J varies with T for various values of the el-ph interaction strength λ . As one would normally expect, J is found to decrease with increasing T and λ . This is consistent with Figs. 6 and 7.

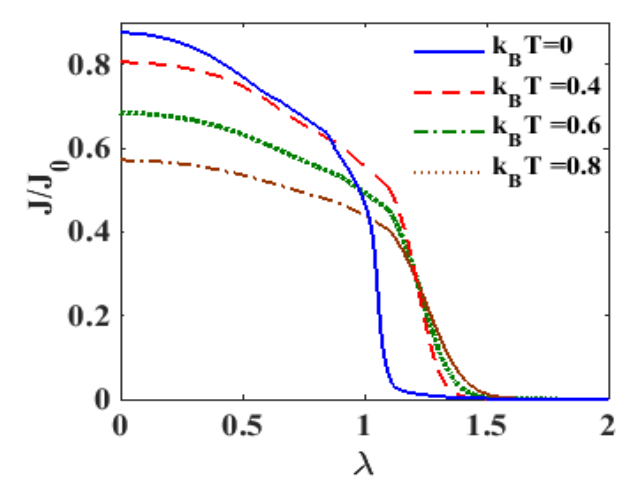


Fig.9 J/J_0 vs λ for different values of k_BT .

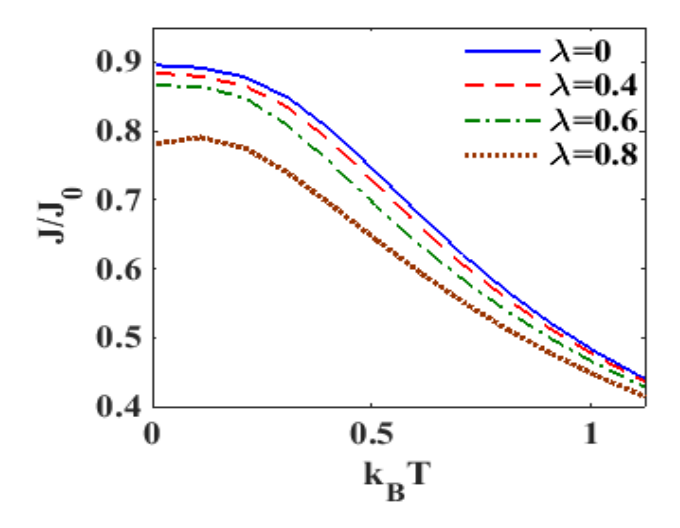


Fig.10 J/J_0 vs k_BT for a few λ values.

Fig. 11 presents the behaviour of G with V_B at various T values. The plot at T=0K for $\lambda=0$ and $\gamma=0$ is shown in the inset. Obviously, for $=\gamma=T=0$, G has a central symmetric peak. The main graph reveals that because of the el-ph coupling, the central peak splits resulting in two symmetric peaks and a few side bands are produced. Temperature appears to reduce G in general.

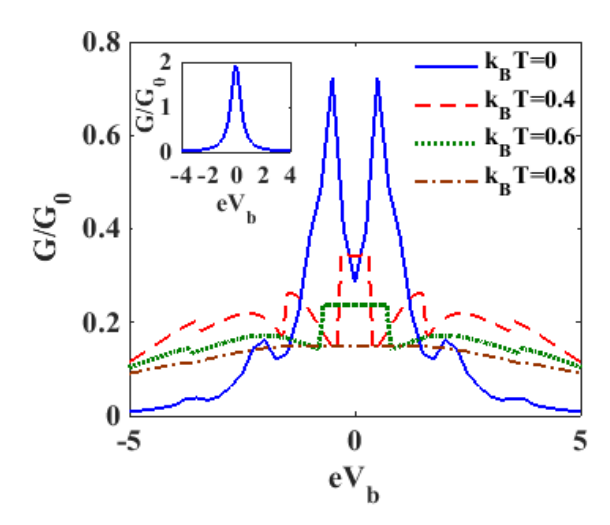


Fig. 11 G/G_0 vs eV_b for different values of k_BT

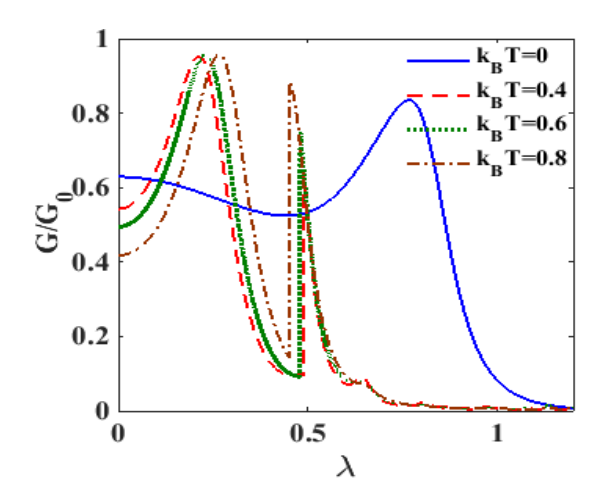


Fig. 12 G/G_0 vs. λ for different values of k_BT .

The behaviour of G with λ is displayed in Fig. 12 at various T values. As can be seen from the figure, at T=0K, as λ is increased from zero, G first decreases and develops a minimum and then exhibits a peak and eventually falls off to zero. It is worth noting that when the T is made finite, the behavior of G changes qualitatively. To be more explicit, G displays a double-peak structure, one at (say) λ_1 and the other at (say) λ_2 , where $\lambda_2 > \lambda_1$. The peak at λ_1 is significantly broader than the peak at λ_2 .

Also, as T increases, λ_1 also increases while λ_2 decreases. Furthermore, as T increases, the second peak decreases in height, whereas the first peak appears to remain unchanged. At small λ , G reduces with increasing temperature.

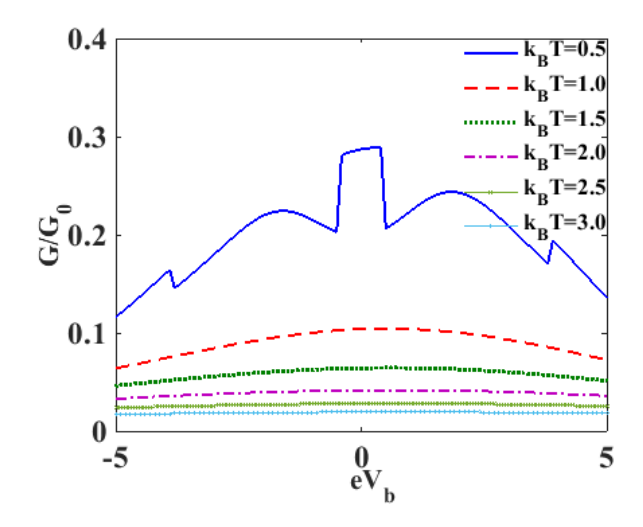


Fig. 13 G/G_0 vs. eV_b for different values of k_BT .

Fig. 13 shows the plot of G versus V_B for various T values. We observe that with increase in T, G shows a decreasing nature. However, as T increases, the side bands vanish altogether, and we observe only a single broad maximum in the $G - eV_b$ curves. With further increase in T, the nature of the curves becomes quite flat and hardly depends on V_b .

Fig. 14 shows the behavior of G with V_B at T=0 for a few λ values. The figure displays a peak at $V_b=0$ for $\lambda=0$. For non-zero λ , the $V_B=0$ -peak splits into two peaks, resulting in a minimum at $V_B=0$. With increase in λ , the heights of the peaks diminish and the distance between them increases. Also the minimum $V_b=0$ becomes broader and comes down. One can observe that for $\lambda=0.8$, G continues to remain zero at low V_b around $V_b=0$.

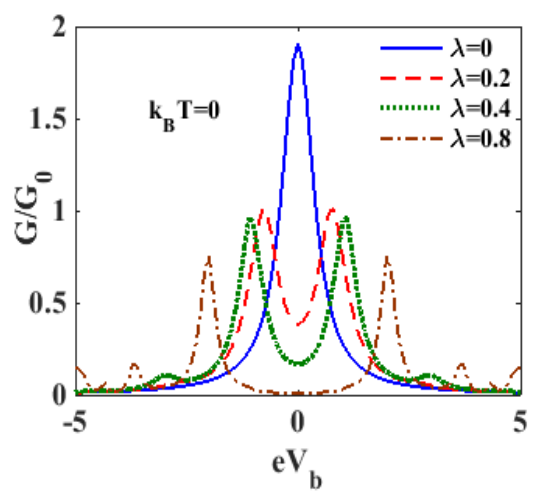


Fig. 14 G/G_0 vs. eV_b for a few λ values.

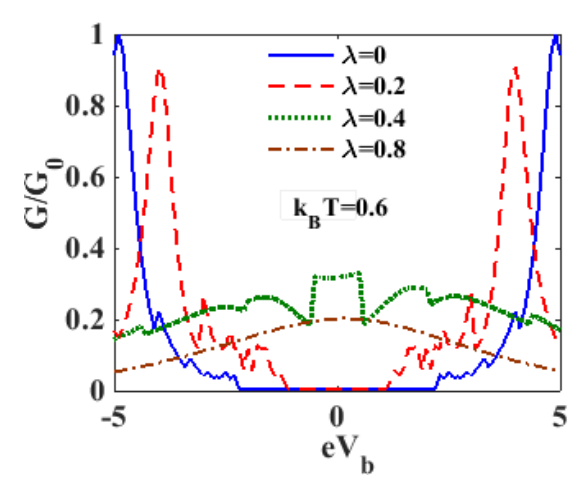


Fig. 15 G/G_0 vs. eV_b for different values of λ .

Fig. 15 displays the variation of G with V_b at a finite temperature ($k_BT=0.6$). Now the $\lambda=0$ -peak of G is also split and G has the value zero over a wider window of V_b on both sides of $V_b=0$. At low λ , as we increase λ , the peaks get shorter and closer, and the range of V_b -values for which G remains zero, reduces. However, as λ exceeds a certain value, double-peak pattern ceases to exist and single broad maximum with the maximum at $V_b=0$, appears. As λ is further increased, an interesting structure with a fat maximum around $V_b=0$ is observed.

We demonstrate in Fig. 16, the nature of variation of G with V_m for $\lambda \neq 0$ and $U \neq 0$, for several values of T. Evidently, G and its peak diminish with increase in T. It is found that when the temperature rises, the peaks move to the positive side. At $T \neq 0$, peaks, in general, decreases. As a result, as temperature rises, the differential conductance decreases.

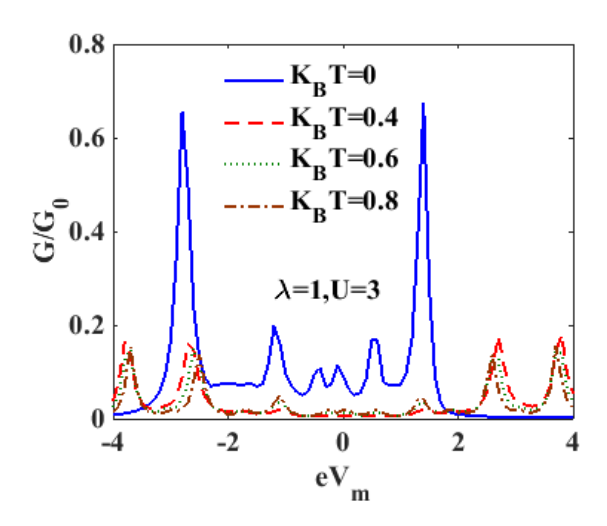


Fig. 16 G/G_0 vs eV_m for a few T values.

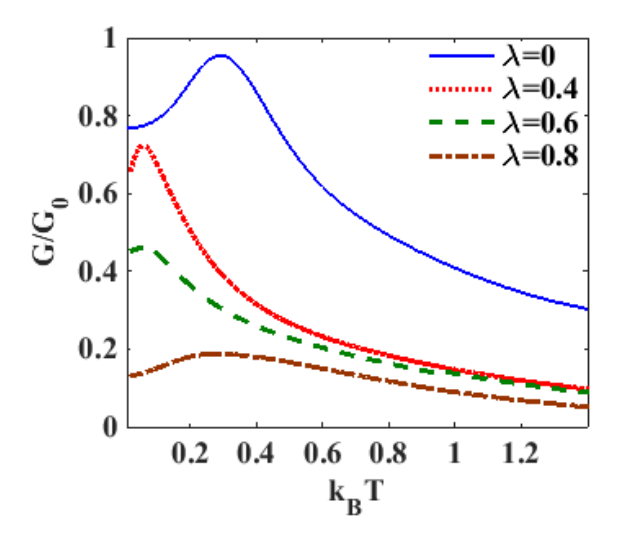


Fig. 17 G/G_0 vs k_BT for a few λ values.

To find the effect of T on G more clearly, we present our results of G directly with respect to T in Fig. 17 for various λ values. At $\lambda = 0.4$, we see that as a function of T, G first rises and exhibits a peak and finally drops continuously with T. As λ increases, the peak becomes broader in width and moves in the direction in which T increases. A careful examination of the nature of variation of G with T and X suggests that the behaviour is dependent on the range of T or X.

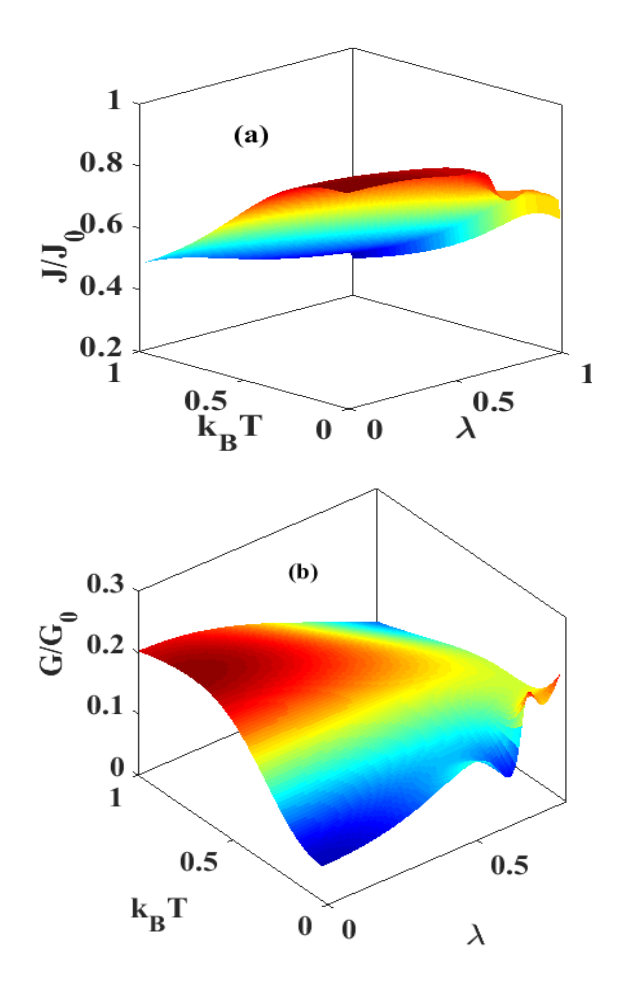


Fig. 18 3D graphs for (a) J/J_0 vs. k_BT and λ ; (b) G/G_0 vs k_BT and λ (at $eV_b=2.5$).

Fig. 18 displays the 3D diagrams of J and G as a function of T and λ , while Figs. 19 and 20 present the contour plots of J and G as a function

of V_b and V_m respectively at different values of T. Figs. 19 and 20 show that though the boundary area of the J-curves decrease with increasing T, that of the G-curves appear to broaden with temperature.

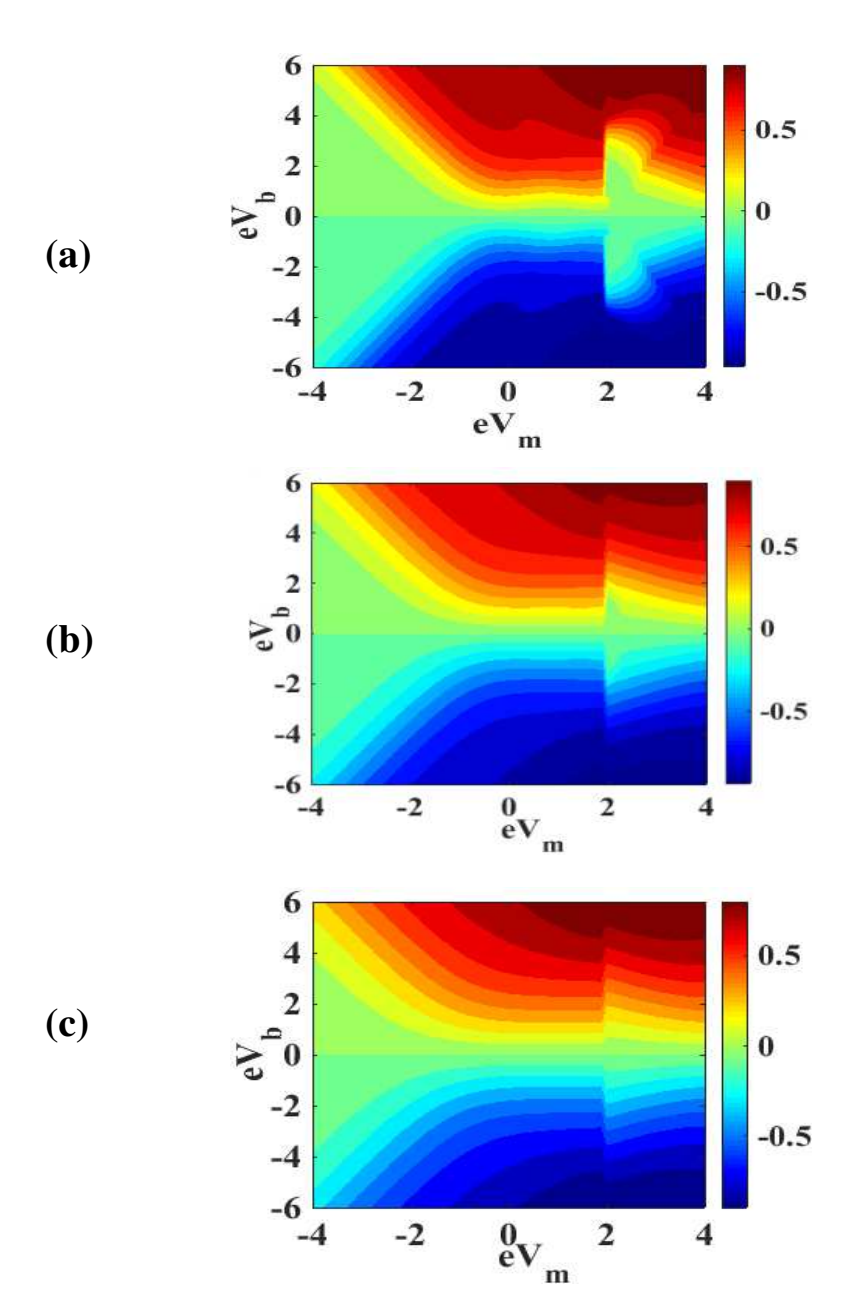


Fig. 19 Contour plot J in $(V_b - V_m)$ – plane with $\lambda = 0.6$ and U = 3 for (a) $k_B T = 0.4$; (b) $k_B T = 0.6$; (c) $k_B T = 0.8$.

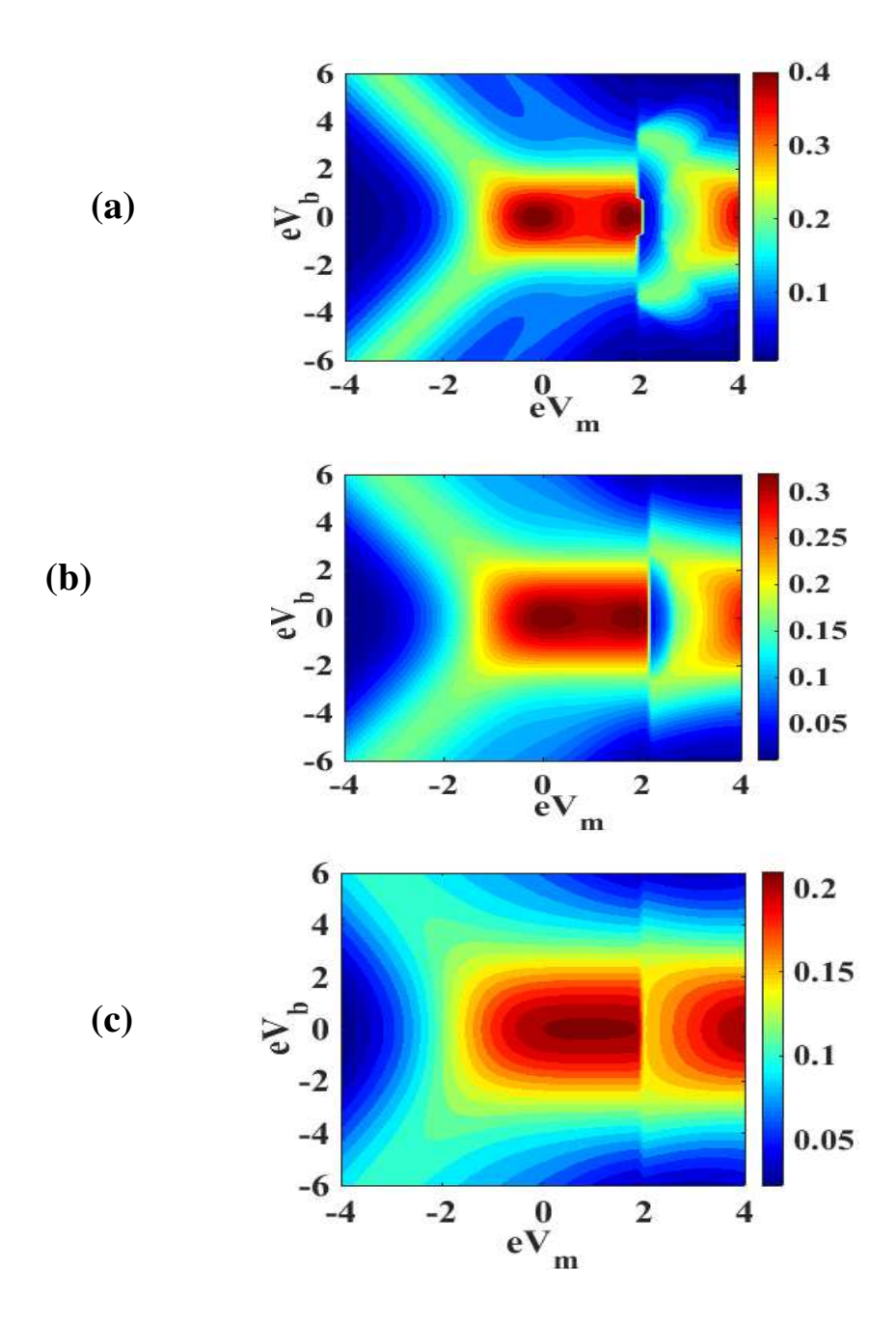


Fig. 20 Contour plot of G in $(V_b - V_m)$ – plane with $\lambda = 0.6$ and U = 3 for (a) $k_B T = 0.4$; (b) $k_B T = 0.6$; (c) $k_B T = 0.8$.

3.5 Conclusion

In this chapter, we have investigated the quantum dissipative effect on the electronic transport properties of an SMT device at finite temperature in the presence of el-el and el-ph interaction. The interaction of the QD phonon with the phonons of the substrate, which functions as a heat reservoir, causes the dissipative effect. The QD phonon interacts with the phonons of the substrate, according to the Caldeira-Leggett model. This interaction produces quantum dissipation, which has been approximately addressed by a canonical transformation. This led to the renormalization of the frequency of the QD phonon. The el-ph interaction term has been separated using the conventional Lang-Firsov transformation followed by an averaging with respect to the zero-phonon state. Finally, the transport parameters have been calculated using the Keldysh technique and the equation of motion method. The impact of temperature, damping rate, and el-ph interaction on the spectral function, current density, and differential conductance has been explored. The quantum dissipative effects on the spectral weight have also investigated at finite temperature. It has been discovered that as the damping rate increases, the spectral weight also increases. It is found that the damping rate enhances the current density at finite temperature but not as much as it does at zero temperatures. Also the current density decreases with increasing el-ph interaction and temperature, and the differential conductance follows the same behaviour. In the presence of an external magnetic field or spin-orbit interactions, this system can be utilised as a spin filter.

3.6 References

- 1. Alvar, R. G., Lejia, W., Enrique, D. B. & Christian, A. N. Electrostatic control over temperature-dependent tunneling across a single-molecule junction. Nature. Comm 7, 11595 (2016).
- Alvar, R. G., Lejia, W., Simranjeet, S., Enrique, D. B. & Christian, A. N. Temperature dependent charge transport across tunnel junctions of single-molecules and self-assembled monolayers: a comparative study. Dalton Trans. 45, 17153 (2016).
- 3. Kamenetska, M., Widawsky, J. R., Dell'Angela, M., Frei, M., & Latha, V. Temperature dependent tunneling conductance of single molecule junctions. J. Chem. Phys. **146**, 092311 (2017).
- 4. Lundin, U., & McKenzie, R. H. Temperature dependence of polaronic transport through single molecules and quantum dots. Phys. Rev B **66**, 075303 (2002).
- Keldysh. L. V. Diagram technique for non-equilibrium processes. Sov. Phys. JETP 20, 1018 (1965); A. P. Jauho, N. S. Wingreen. & Y. Meir. Time-dependent transport in interacting and non-interacting resonant tunneling systems. Phys. Rev. B 50, 5528 (1994).
- 6. Meir. Y, Wingreen. N. S, Lee. P. A. Transport through a strongly interacting electron system: Theory of periodic conductance oscillations *Phys. Rev. Lett.* **66**, 3048 (1991);
- 7. Swirkowicz. R *et al.* Non-equilibrium Kondo effect in quantum dots. *Phys. Rev. B* **68**, 195318 (2003).
- 8. Chen. Z. Z, Lü. R, Zhu. B. F. Effects of electron-phonon interaction on non-equilibrium transport through a single-molecule transistor. *Phys, Rev. B* **71**, 165324 (2005).

- 9. Narasimha Raju. Ch and Chatterjee. A. Quantum dissipative effects on non-equilibrium transport through a single molecular transistor: The Anderson-Holstein-Caldeira-Leggett model. *Sci. Rep.* **6**, 18511 (2016).
- **10.** Kalla. M, Narasimha Raju. Ch, Chatterjee. A. Magneto-transport properties of a single molecular transistor in the presence of electron-electron and electron-phonon interactions and quantum dissipation. *Sci. Rep.* **9**, 16510 (2019).

Chapter 4

Tunneling conductance of electron spin across a metal-semiconductor junction with Rashba and Dresselhaus spin-orbit interactions

4.1 Introduction

The Rashba and Dresselhaus spin-orbit interactions (SOI), which have a significant influence on the properties of nano-structures, have paved the way for a new research frontier in semiconductor nanotechnology called Spintronics [1-3]. This area was initiated by Datta and Das through their pioneering work on the spin-field-effect transistor [4, 5]. Since then, a significant number of studies on the impact of spin-orbit interaction on the energy spectrum and impurity states in low-dimensional systems have been reported in the literature [6-19]. The SOI effect on persistent current in quantum rings has recently been explored [20, 21]. However, the fundamental interest in spintronics lies on the transport of electron spins and in this context, a reliable source of spin-polarized electron generator is required [22-24]. Spin polarisation can be accomplished using a variety of sources, such as magnetic semiconductors [25, 26], ferromagnetic-metal interfaces [27], ferromagnetic-superconducting interfaces [28, 29], graphene-based spin filters [30-32], and so on. However, spin filters based on hetero-structures [33-35] have some advantages. For example, since

high-quality heterostructures can be easily manufactured using the modern fabrication techniques, it is easier to have high-quality spin-filters through this approach. Spin polarizability in semiconductor devices can be achieved by utilising the zero-field spin splitting caused by Rashba SOI (RSOI) and Dresselhaus SOI (DSOI) [36-38].

Koga et al. [39] have conducted the first theoretical investigation on the role of SOI in spin-filtering applications. Khodas et al. [40] have developed an alternative approach for producing spin currents. They have used the spin-orbit interaction (SOI) effect to cause electron polarisation in nonmagnetic semiconductor heterostructures. Dargys [41-43] have explored the phenomenon of electron reflection by an infinite barrier in a two-dimensional device. Using Clifford (geometric) algebra, they have discovered that under certain conditions for the angle of incidence, SOI results in double refraction [44] for the incident electrons. Recently, we have extended the works of Khodas et al. and Dargys to investigate the refraction and reflection of electrons over a metal/semiconductor junction where the semiconductor material is a semi-infinite two-dimensional electron gas (2DEG) with non-zero RSOI and DSOI. Following Srisongmuang et al. [45, 46], we have calculated the zero-temperature current density and differential conductance. The most important finding of this work is that the inclusion of DSOI makes the spin-filtering effect much stronger. In this chapter we shall present the results of this work.

4.2 The Model

We consider an infinite two-dimensional (2D) system in the x - y plane, where a metallic 2D lead fills the region x < 0 and a 2D

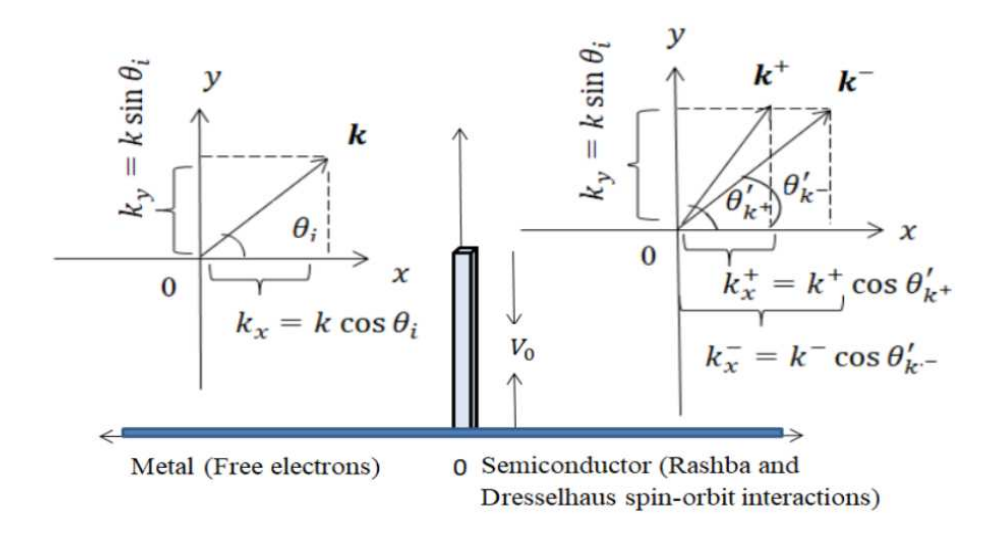


Fig. 1 Schematic sketch of the system

semiconductor system with RSOI and DSOI occupies the region x > 0. At x = 0, the two materials are separated by an interface. The system is schematically described in Fig. 1. The system Hamiltonian H can be represented as

$$H = H_{\rm I} + H_{\rm II} \tag{4.1}$$

where $H_{\rm I}$, the free-electron Hamiltonian in the metallic region with the eigenfunction $\psi_{\rm I}$ and energy ε_k , is given by

$$H_{\rm I} = \frac{p_x^2}{2m} + \frac{p_y^2}{2m}$$
, $for - \infty \le x < 0$, (4.2)

and H_{II} is the Hamiltonian for an electron in the semiconductor area with both RSOI and DSOI in the presence of a perpendicular electric field and

a barrier V_0 , with the appropriate eigenfunction ψ_{II} and energy E. The Thomas term (H_T) of the Dirac theory that provides in general the spin-orbit interaction is given by

$$H_T = -\frac{e\hbar \, \sigma. (\mathbf{E} \times \mathbf{p})}{4m^2c^2} \ . \tag{4.3}$$

When an electric field of strength E is applied in the z direction, i.e., $E = E \hat{z}$, the system inversion symmetry is broken at the surface, and the ensuing SOI or H_T corresponds to RSOI. We denote this interaction Hamiltonian by H_R which can be written as

$$H_R = -\frac{e\hbar\sigma \mathbf{E}.\left(\hat{\mathbf{z}}\times\mathbf{p}\right)}{4m^2c^2} = -\frac{\alpha}{\hbar}\left(\sigma_y p_x - \sigma_x p_y\right). \tag{4.4}$$

where

$$\alpha = \frac{e\hbar^2 E}{4m^2 c^2} \tag{5}$$

denotes the RSOI strength. DSOI occurs in heterostructures with bulk inversion asymmetry and is described by the Hamiltonian H_D :

$$H_D = \frac{\beta}{\hbar} (\sigma_x p_x - \sigma_y p_y). \tag{4.6}$$

 $H_{\rm II}$ is given by:

$$H_{II} = \frac{p_x^2}{2m} + \frac{p_y^2}{2m} + H_R + H_D + V_0 \quad for - \infty \le x < 0 \quad . \tag{4.7}$$

4.3 Formulation

The Schrodinger equations for regions I and II are given by

$$H_{\rm I}\psi_{\rm I} = \varepsilon_k \psi_{\rm I} \tag{4.8}$$

$$H_{\mathrm{II}}\psi_{\mathrm{II}} = E\psi_{\mathrm{II}} \ . \tag{4.9}$$

The energy eigenvalue in region I is given by:

$$\varepsilon_k = \frac{\hbar^2 (k_x^2 + k_y^2)}{2m} = \frac{\hbar^2 k^2}{2m}$$
 (4.10)

and the corresponding wave function is given as

$$\psi_{\mathrm{I}} = \frac{1}{\sqrt{2}} \begin{bmatrix} 1\\1 \end{bmatrix} e^{i(k_{x}x + k_{y}y)} + \begin{bmatrix} b_{\uparrow}\\b_{\downarrow} \end{bmatrix} e^{-i(k_{x}x - k_{y}y)} , \qquad (4.11)$$

where the first term presents the incoming wave with equal probability amplitudes of up-spin and down-spin electrons, and the second term represents to the reflected wave with b_{\uparrow} and b_{\downarrow} referring to the spin-up and spin-down probability amplitudes Because the system is translationally symmetric along the y axis, the y-th components of the wave vector for up-spin and down-spin electrons are equal. However, in the x-direction, they can differ. The wave function of the electron in region II can be written as

$$\psi_{II} = A_{II}e^{i(k_x x + k_y y)} + B_{II}e^{-i(k_x x - k_y y)}$$
, (4.12)

which on substituting in Eq. (9) leads to the following matrix equation:

$$\begin{bmatrix} \varepsilon_{k} & f(k_{x}, k_{y}) \\ f^{*}(k_{x}, k_{y}) & \varepsilon_{k} \end{bmatrix} \begin{bmatrix} A_{\text{II}}^{(1)} \\ A_{\text{II}}^{(2)} \end{bmatrix} = (E - V_{0}) \begin{bmatrix} A_{\text{II}}^{(1)} \\ A_{\text{II}}^{(2)} \end{bmatrix} = E' \begin{bmatrix} A_{\text{II}}^{(1)} \\ A_{\text{II}}^{(2)} \end{bmatrix}$$
(4.13)

where

$$f(k_x, k_y) = -(\alpha k_y + \beta k_x) - i(\alpha k_x + \beta k_y), \tag{4.14}$$

We obtain a similar equation for $(B_{II}^{(1)}, B_{II}^{(2)})$. We now define

$$\gamma_k = \alpha k_v + \beta k_x = (\alpha \sin \theta_k' + \beta \cos \theta_k')k, \qquad (4.15)$$

$$\delta_k = \alpha k_x + \beta k_y = (\alpha \cos \theta_k' + \beta \sin \theta_k')k \quad , \tag{4.16}$$

so that we can write

$$\gamma_k^2 + \delta_k^2 = k^2 [\alpha^2 + \beta^2 + 4\alpha\beta \sin\theta_k' \cos\theta_k'] . \tag{4.17}$$

Defining

$$\phi_k = \tan^{-1}\left(\frac{\delta_k}{\gamma_k}\right) = \tan^{-1}\left(\frac{\alpha\cos\theta_k' + \beta\sin\theta_k'}{\alpha\sin\theta_k' + \beta\cos\theta_k'}\right),\tag{4.18}$$

we can write

$$\gamma_k \pm i \,\delta_k = \sqrt{(\gamma_k^2 + \delta_k^2)} \,e^{\pm i\phi_k} \quad , \tag{4.19}$$

and finally, we obtain two solutions for the energy of the electron in the region *II* as:

$$E_k = \varepsilon_k + V_0 \pm k\lambda(\theta_k') \quad , \tag{4.20}$$

where

$$\lambda(\theta_k') = \frac{1}{k} (\gamma_k^2 + \delta_k^2)^{1/2} = \sqrt{\alpha^2 + \beta^2 + 4\alpha\beta \sin \theta_k' \cos \theta_k'} \quad . \tag{4.21}$$

Substituting

$$\varepsilon_k = \frac{\hbar^2 k^2}{2m} \quad , \tag{4.22}$$

in Eq. (20), we get a quadratic equation in k:

$$k^{2} \pm \frac{2m}{\hbar^{2}} \lambda(\theta'_{k})k - \frac{2m}{\hbar^{2}} (E_{k} - V) = 0.$$
 (4.23)

Solving the above equation, we get two solutions for k, one positive and the other negative. We choose the positive solution:

$$k = -\frac{m\lambda(\theta_k')}{\hbar^2} + \sqrt{\left(\frac{m\lambda(\theta_k')}{\hbar^2}\right)^2 + \frac{2m(E_k - V_0)}{\hbar^2}}.$$
 (4.24)

Eq. (20) demonstrates that for a given k, E_k has two values depending on whether the positive or negative sign in Eq. (20) is used. The wave vector corresponding to the positive sign is represented as k^+ whereas the wave vector corresponding to the negative sign is denoted as k^- . Thus we can write

$$k^{\pm} = -\frac{m\lambda(\theta'_{k^{\pm}})}{\hbar^{2}} + \sqrt{\left(\frac{m\lambda(\theta'_{k^{\pm}})}{\hbar^{2}}\right)^{2} + \frac{2m(E_{k^{\pm}} - V_{0})}{\hbar^{2}}}.$$
 (4.25)

Each k in the preceding equations for the semiconductor area can be replaced by k^{\pm} and these two wave vectors form two spin-split refracted waves with wave vectors k^{+} and k^{-} . As there is no reflection in the semiconductor region, we have:

$$B_{\rm II}^{(1)} = B_{\rm II}^{(2)} = 0$$
 , (4.26)

and as a result, we get

$$\psi_{II}(x,y) = \left[A_{II}^{(1)} \begin{bmatrix} 1 \\ -e^{-i\phi_{k^{+}}} \end{bmatrix} e^{ik_{x}^{+}x} + A_{II}^{(2)} \begin{bmatrix} e^{i\phi_{k^{-}}} \\ 1 \end{bmatrix} e^{ik_{x}^{-}x} \right] e^{ik_{y}y}. \quad (4.27)$$

Using the boundary conditions:

$$\psi_{\mathrm{I}}(0,y) = \psi_{\mathrm{II}}(0,y) \; ; \; \left[\frac{\partial \psi_{\mathrm{I}}(x,y)}{\partial x}\right]_{x=0} = \left[\frac{\partial \psi_{\mathrm{II}}(x,y)}{\partial x}\right]_{x=0}, \quad (4.28)$$

and taking the wave vector at the boundary and defining

$$tan\theta = \frac{k_y}{k_x} \tag{4.29}$$

we get

$$\sin \theta_{k^{\pm}}' = \frac{\sin \theta}{n_{k^{\pm}}} \tag{4.30}$$

where the refractive indices for the two refracted waves are n_{k+} and n_{k-} . The projection of the wave vector on to the boundary between the two media (i.e., at x=0) should be conserved and so we have

$$k_i \sin \theta_i = k^{\pm} \sin \theta'_{k^{\pm}}$$

$$\Rightarrow n_{k^{\pm}} = \left(\frac{k^{\pm}}{k_{i}}\right) = \frac{\sin \theta_{i}}{\sin \theta'_{k^{\pm}}}$$

$$\Rightarrow \theta'_{k^{\pm}} = \sin^{-1}\left\{\left(\frac{k_{i}}{k^{\pm}}\right)\sin \theta_{i}\right\}. \tag{4.31}$$

The wave vector corresponding to the metallic region is denoted by k_i in the above equations. Solving Eqs. (20), (21), (25) and (31) self-consistently, we obtain k^{\pm} and the related energies from (20). As the incident beam gets divided into two refracted beams in region II, there will be two critical angles, one for each refracted wave. As a result, we have

$$n_{k^{\pm}} = \sin \theta_{c}^{\pm} = \frac{k^{\pm} \lambda \left(\frac{\pi}{2}\right)}{k_{i}}$$

$$= \mp \left(\frac{m}{2\varepsilon_{k}}\right)^{\frac{1}{2}} \frac{\lambda \left(\frac{\pi}{2}\right)}{\hbar} + \frac{\left\{\left(m\lambda \left(\frac{\pi}{2}\right)\right)^{2} + 2m\left(E_{k^{\pm}}\left(\frac{\pi}{2}\right) - V_{0}\right)\right\}^{\frac{1}{2}}}{\sqrt{\frac{2m\varepsilon_{k}}{\hbar^{2}}}}. (4.32)$$

Using the boundary conditions for ψ_I and ψ_{II} , we obtain

$$A_{\rm II}^{(1)} = \frac{\sqrt{2}}{(1 + k_x^+/k_x)} \frac{\left(e^{-i\phi_{k^+}} - 1\right)}{\left(e^{-i\phi_{k^+}} + e^{-i\phi_{k^-}}\right)} , \qquad (4.33)$$

$$A_{\rm II}^{(2)} = \frac{\sqrt{2}}{(1 + k_x^-/k_x)} \frac{\left(e^{-i\phi_{k^-}} - 1\right)}{\left(e^{-i\phi_{k^+}} + e^{-i\phi_{k^-}}\right)} , \qquad (4.34)$$

$$b_{\uparrow} = \frac{\sqrt{2}}{(1 + k_x^+/k_x)} \frac{\left(1 - e^{i\phi_{k^-}}\right)}{\left(1 + e^{-i(\phi_{k^+} - \phi_{k^-})}\right)}$$

$$+\frac{\sqrt{2}}{(1+k_x^{-}/k_x)}\frac{\left(1+e^{i\phi_{k^{+}}}\right)}{\left(1+e^{i(\phi_{k^{+}}-\phi_{k^{-}})}\right)}-\frac{1}{\sqrt{2}},\qquad(4.35)$$

$$b_{\downarrow} = \frac{\sqrt{2}}{(1 + k_x^+/k_x)} \frac{\left(1 - e^{-i\phi_{k^-}}\right)}{\left(1 + e^{i(\phi_{k^+} - \phi_{k^-})}\right)}$$

$$+\frac{\sqrt{2}}{(1+k_x^{-}/k_x)}\frac{\left(1+e^{-i\phi_{k^{+}}}\right)}{\left(1+e^{-i(\phi_{k^{+}}-\phi_{k^{-}})}\right)}-\frac{1}{\sqrt{2}},\qquad(4.36)$$

Using Eqs. (33-36), one can write the reflection and refraction coefficients as

$$R_{\uparrow,\downarrow} = 2|b_{\uparrow,\downarrow}|^2,\tag{4.37}$$

$$T_{\uparrow,\downarrow} = 2(k_x^{+,-}/k_x) |A_{\rm II}^{(1,2)}|^2$$
, (4.38)

where the pre-factor 2 corresponds to two spin orientations for the unpolarized incident electron. The current densities at zero temperature are are given by the following expressions [40]:

$$J_{\uparrow}^{Refr}(V) = J_o \int_0^{eV} dE \int_{-\pi/2}^{\pi/2} d\theta_i \cos \theta_i \sqrt{1 + \left(\frac{E}{E_F}\right)} (T_{\uparrow}), \quad (4.39a)$$

$$J_{\downarrow}^{Refr}(V) = J_o \int_0^{eV} dE \int_{-\pi/2}^{\pi/2} d\theta_i \cos \theta_i \sqrt{1 + \left(\frac{E}{E_F}\right)} (T_{\downarrow}), \qquad (4.39b)$$

$$J_{\uparrow}^{Refl}(V) = J_o \int_0^{eV} dE \int_{-\pi/2}^{\pi/2} d\theta_i \cos \theta_i \sqrt{1 + \left(\frac{E}{E_F}\right)} (R_{\uparrow}), \quad (4.39c)$$

$$J_{\downarrow}^{Refl}(V) = J_o \int_0^{eV} dE \int_{-\pi/2}^{\pi/2} d\theta_i \cos \theta_i \sqrt{1 + \left(\frac{E}{E_F}\right)} (R_{\downarrow}) . \quad (4.39d)$$

The differential conductance

$$G = \left[\frac{dJ(V)}{dV} \right] \tag{4.40}$$

in the semiconductor region is obtained as [40]:

$$G_{\uparrow,\downarrow}(V) = G_o \int_{-\pi/2}^{\pi/2} d\theta_i \cos \theta_i \sqrt{1 + \left(\frac{eV}{E_F}\right)} \left(T_{\uparrow,\downarrow}\right), \tag{4.41}$$

with

$$J_0 = \frac{eAk_F}{2\pi h} \quad , \tag{4.42}$$

and

$$G_o = \frac{e^2 A k_F}{2\pi h} \quad , \tag{4.43}$$

where A represents the area of the metallic region, θ_m gives the maximum possible incident angle, E_f denotes the Fermi energy, and eV is the applied voltage. Finally, we define the spin polarization current as:

$$P_j = \frac{J_{\uparrow} - J_{\downarrow}}{J_{\uparrow} + J_{\downarrow}}.\tag{4.44}$$

For the reflected current densities, P_j is denoted as P_j^{Refl} , while for the refracted ones, P_j is denoted as P_j^{Refr} .

Before moving on to the numerical results, we would like to discuss the competition between the two interactions, RSOI and DSOI.

Let us consider the following transformation:

$$U = \frac{\sigma_z(\sigma_x + \sigma_y)}{2} \tag{4.45}$$

Under this transformation, σ_x transforms to

$$U\sigma_x U^{\dagger} = -\sigma_y , \qquad (4.46)$$

and σ_y transforms to

$$U\sigma_{\nu}U^{\dagger} = -\sigma_{\nu} \tag{4.47}$$

and σ_z to $-\sigma_z$. Thus under this transformation, the RSOI Hamiltonian changes to the DSOI Hamiltonian and vice versa. When RSOI is replaced by DSOI, the spin-current

$$J_s^z = \frac{\sigma_z \dot{x} + \dot{x} \sigma_z}{2} \tag{4.48}$$

reverses direction and becomes $-J_s^z$. As a result, RSOI and DSOI polarise the spins in different directions. When α and β both are present in the system, the scattering of up and down-spin electrons along, say, the x-direction will be different for RSOI and DSOI, and the wave functions will acquire phases depending on the strengths of RSOI and DSOI. Because the scattering phases for up and down-spin electrons differ, different transmission coefficients will emerge from the interference of the scattered waves for electrons with opposite spins.

4.4 Numerical Results and Discussion

In our numerical computation, We consider that the incident electron energy E is 20meV and the potential height V_o is 12meV. Fig.1 shows the behavior of the refracted angle $(\theta'_{k^{\pm}})$ as a function of the incident angle (θ_i) . We chose $\alpha = 5meV - nm$ and $\beta = 5meV - nm$. The angle of refraction is zero for normal incidence ($\theta_i = 0$). Furthermore, as expected, in the absence of SOIs in region II, the angle of refraction equals the angle of incidence. According to Khodas et al., in the presence of RSOI in region II, the electron with energy $E'_k(\theta'_{k+})$ increases with increasing α while the electron with energy $E'_k(\theta'_{k-})$ reduces with increasing α resulting in a split in the path of the spin-up and spin-down electrons In the presence of both RSOI and DSOI, we determine the angle of refraction of spin-up and spin-down electrons. In Fig. 2 (a), we show that in the presence of DSOI, the angle of refraction of both spin-up and spin-down electrons decreases, the spin-down electrons, however, experiencing significantly larger decrease. Thus, the increase in the spin polarizability is more in the presence of both SOIs as compared to that in the presence of RSOI alone. This spin polarizability looks similar to the double refraction seen in some optical materials. As suggested by Khodas et al. [40], we see from Fig. 2 (a) that there exists a critical angle of incidence at which the up-spin electrons undergoes a total internal reflection while no such total internal reflection is possible for the down-spin electrons. In contrast, down-spin electrons do not undergo total internal reflection. We find that DSOI enhances the critical angle of incidence for the total internal reflection of up-spin electrons. Fig.2 (b) shows the variation of the angle of refraction of the spin-up and the spin-down electrons as a function of the angle of refraction for two different incident energies for certain values of RSOI and DSOI coefficients. We observe that as the incident energy is

increased, the angle of refraction of spin-up electrons increases while that of spin-down electrons decreases.

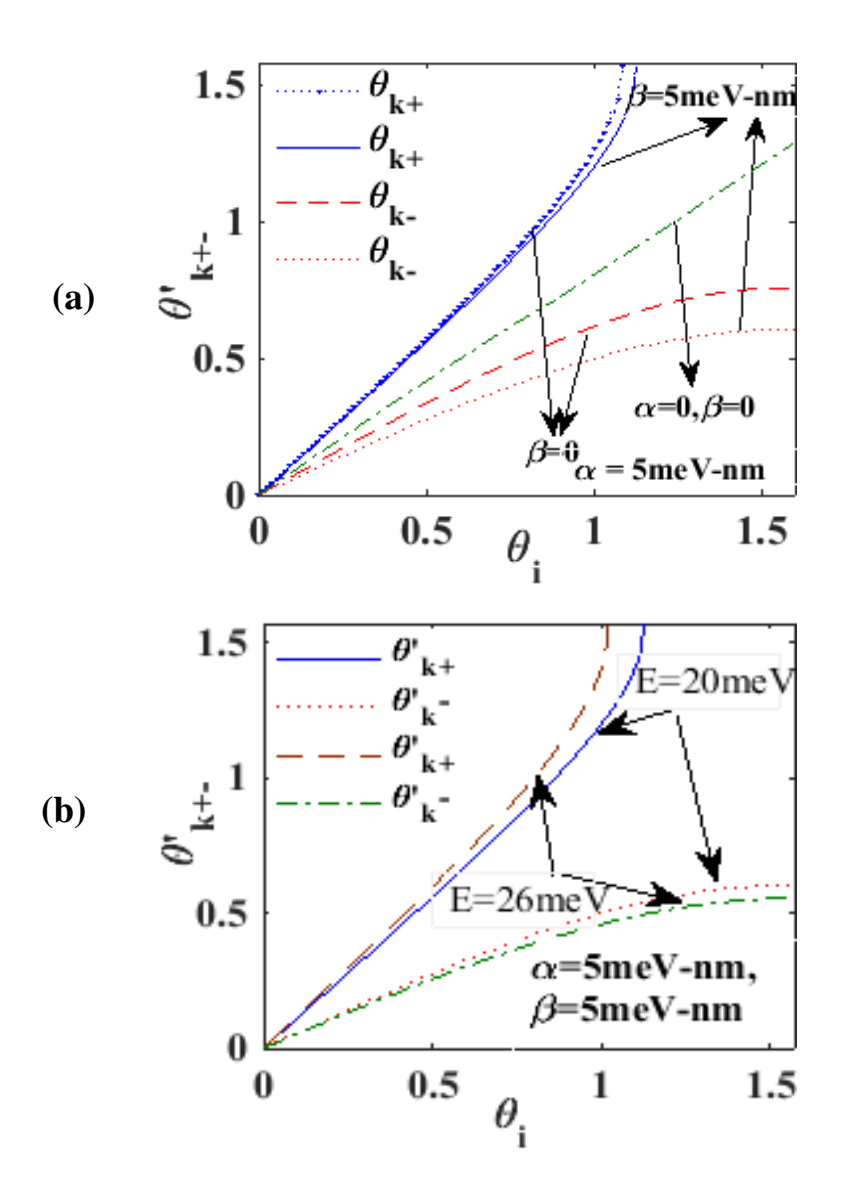


Fig. 2 $\theta'_{k^{\pm}}$ Vs. θ_{i} for different values of: (a) α , β ; (b) E.

Fig. 3 depicts the variation of θ'_{k^+} and θ'_{k^-} with RSOI for various DSOI values. The figure clearly shows that in the absence of DSOI, θ'_{k^+} first

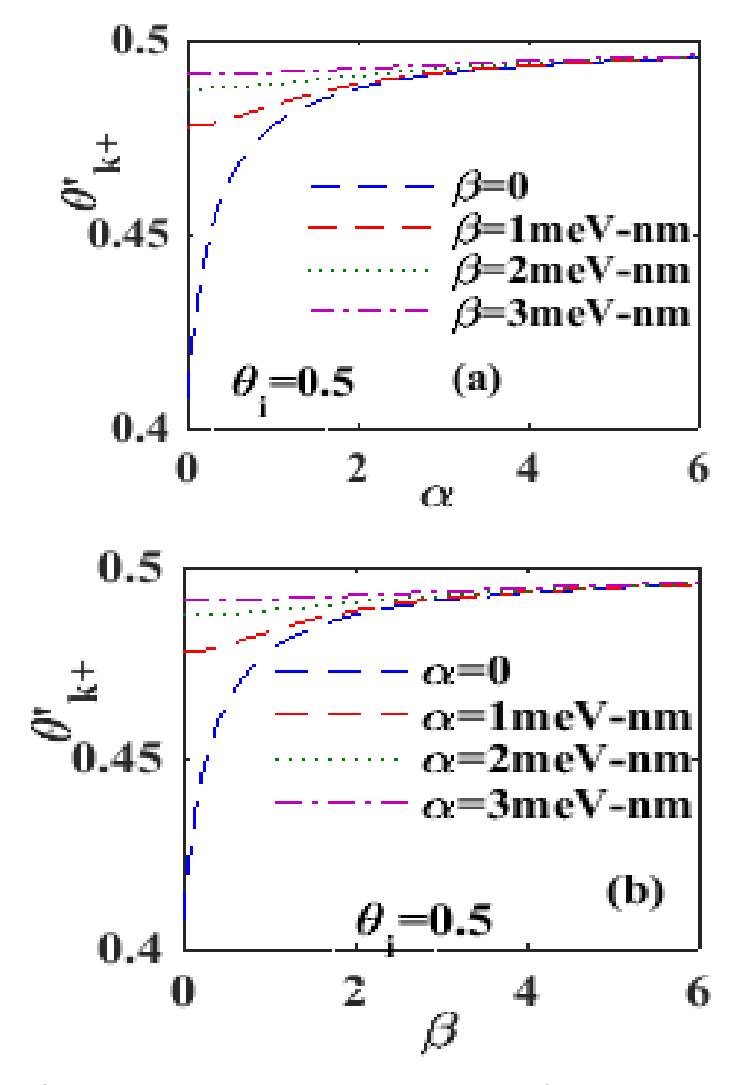


Fig. 3 (a) θ'_{k^+} vs. α for different values of β at $\theta_i = 0.5$; (b) θ'_{k^+} vs. β for different values of α at $\theta_i = 0.5$.

exhibits a substantial monotonic growth with α , but eventually saturates to a constant value at higher levels of α . In the presence of DSOI, θ'_{k^+} is shown to be high even at $\alpha=0$, but it increases slowly with β and eventually saturates to the same constant value as observed at $\beta=0$. One can observe that as β increases, the saturation of θ'_{k^+} becomes faster.

However, the behavior of θ'_{k} - with respect to α is virtually opposite to that of θ'_{k} + i.e., it reduces with α and eventually saturates to a constant.

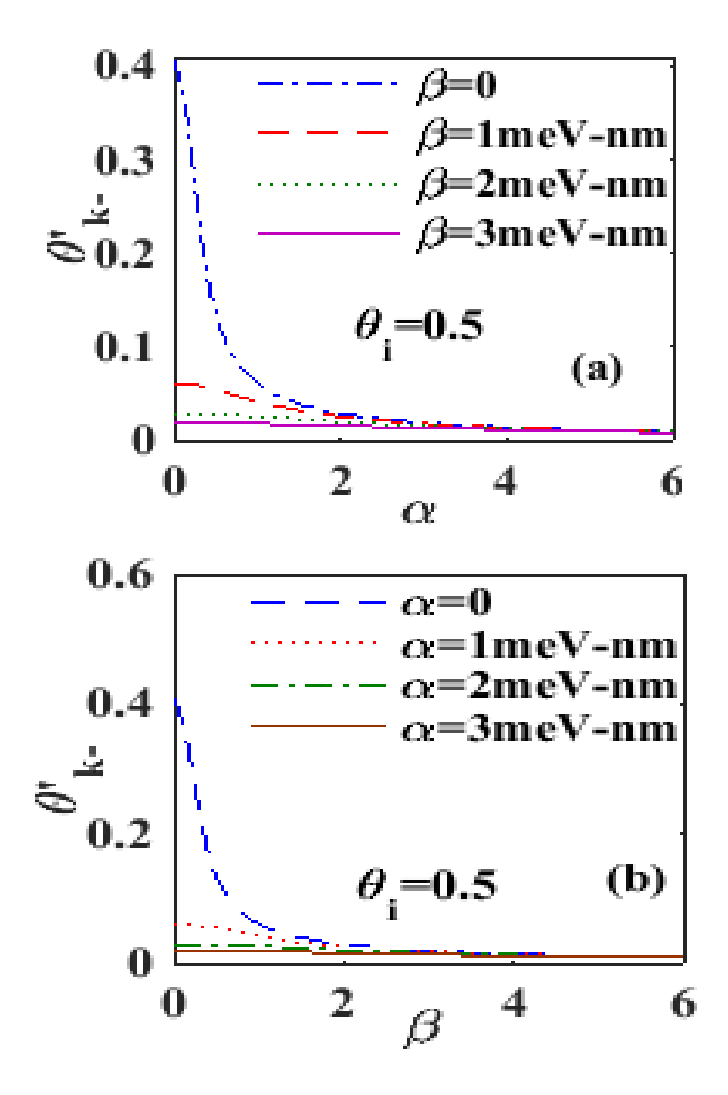


Fig. 4 (a) θ'_{k^-} vs. α for different values of β at $\theta_i = 0.5$; (b) θ'_{k^-} vs. β for different values of α at $\theta_i = 0.5$.

Fig. 4 gives the behavior of θ'_{k^+} and θ'_{k^-} with respect to β . A comparison of Figs. 3 and 4 reveals that the behavior of θ'_{k^+} and θ'_{k^-} with respect to α and β is similar. This is obvious from Eq. (5), which is

symmetric in α and β . Fig. 4 gives the behavior of θ'_{k^+} and θ'_{k^-} with respect to β . A comparison of Figs. 3 and 4 reveals that the behavior of θ'_{k^+} and θ'_{k^-} with respect to α and β is similar. This is obvious from Eq. (5), which is symmetric in α and β .

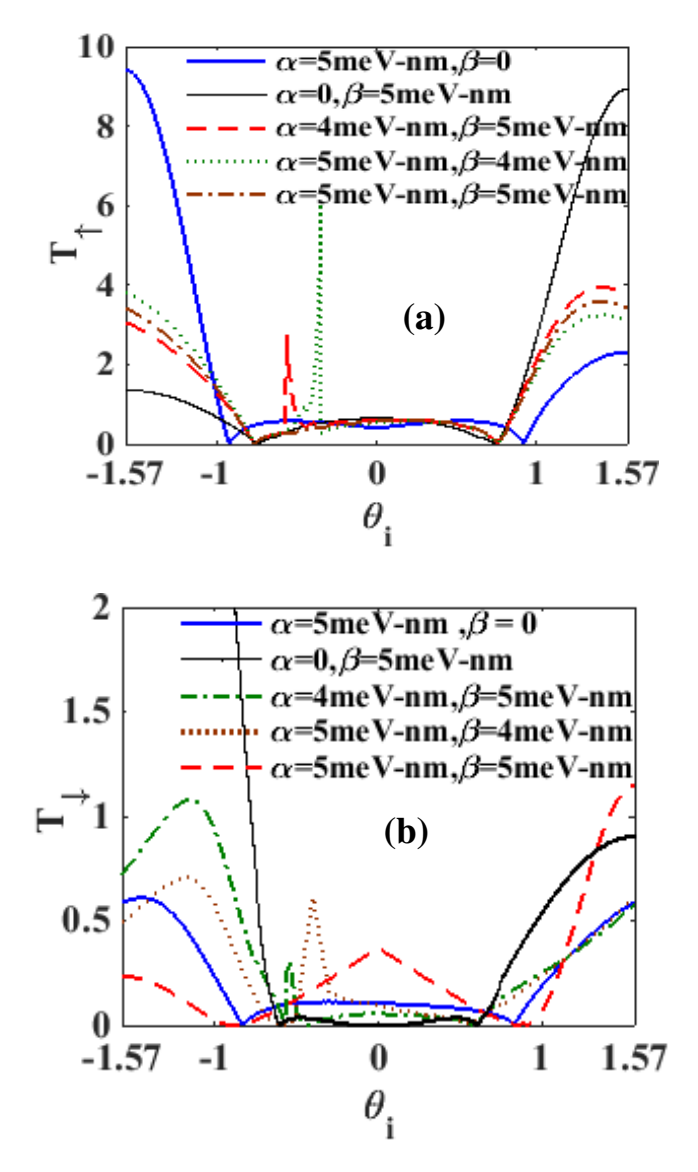


Fig. 5 (a) T_{\uparrow} Vs. θ_i ; (b) T_{\downarrow} Vs. θ_i for different cases as: $(1)\alpha \neq 0, \beta = 0$ $(2)\alpha = 0, \beta \neq 0$ $(3)\alpha < \beta(4)\alpha > \beta(5)\alpha = \beta$.

In Fig. 5, we show the plot of refraction coefficients $(T_{\uparrow}, T_{\downarrow})$ for up-spin

and down-spin electrons with respect to the incident angle for various combinations of α and β . We can easily see that T_{\uparrow} and T_{\downarrow} are asymmetric over the range: $-\frac{\pi}{2}$ to $\frac{\pi}{2}$ and T_{\uparrow} is generally greater than T_{\downarrow} . In the presence of only RSOI, T_{\uparrow} is larger in the –ve side than in the +ve side. On both sides of $\theta_i=0,\ T_{\uparrow}$ continues to remain small but finite up to a certain value of $|\theta_i|$ and then reduces to zero and shows a dip structure thereafter. After the dip structure, T₁ increases very rapidly on the negative side, while on the positive side, it shows a rather slow increase and a down-turn after a certain value of θ_i . Even on the negative side, there appears to be an indication of the down-turn effect. When only DSOI is present, T_{\uparrow} behaves in a similar but opposite way to that in the presence of only RSOI. There is no much structural difference for other combinations of RSOI and DSOI coefficients. When RSOI is less than DSOI, the value of T_{\uparrow} is lower in the –ve side than the –ve side and the opposite behaviour is observed when RSOI is greater than DSOI. When RSOI and DSOI are equal, T_{\uparrow} is higher in the -ve side and lower in the +ve side. T_{\downarrow} is more significant in the presence of only DSOI than in the presence of the only RSOI, and T_{\downarrow} is greater in the –ve side than in the +ve side. The dip-like structure observable in the case of T_{\downarrow} at certain values of θ_i is comparable to the structures observed for T_{\uparrow} . For other combinations of RSOI and DSOI, T_{\downarrow} behaves in an opposite to T_{\uparrow} .

We plot the variation of reflection coefficient (R_{\uparrow}) for spin-up and spindown electrons with respect to α and β in Figs. 6. Fig. 6 (a) shows that for $\beta = 0$, R_{\uparrow} rises monotonically but slowly with α . For a non-zero but small value of β (say $\beta = 0.1$), as α is increased, R_{\uparrow} initially increases and reaches a maximum, and then passes through a broad minimum with a further increase in α . As β increases, the maximum in R_{\uparrow} becomes broader and shifts towards larger values of α . As β becomes larger than a specific value, R_{\uparrow} increases monotonically with α and eventually saturates. Fig. 6 (b) shows the variation of R_{\uparrow} with β for various values of α . For $\alpha=0$, R_{\uparrow} shows an infinitesimally small decrease as β increases. For non-zero α , as β increases, R_{\uparrow} initially increases, reaches a broad maximum and then decreases as β increases further.

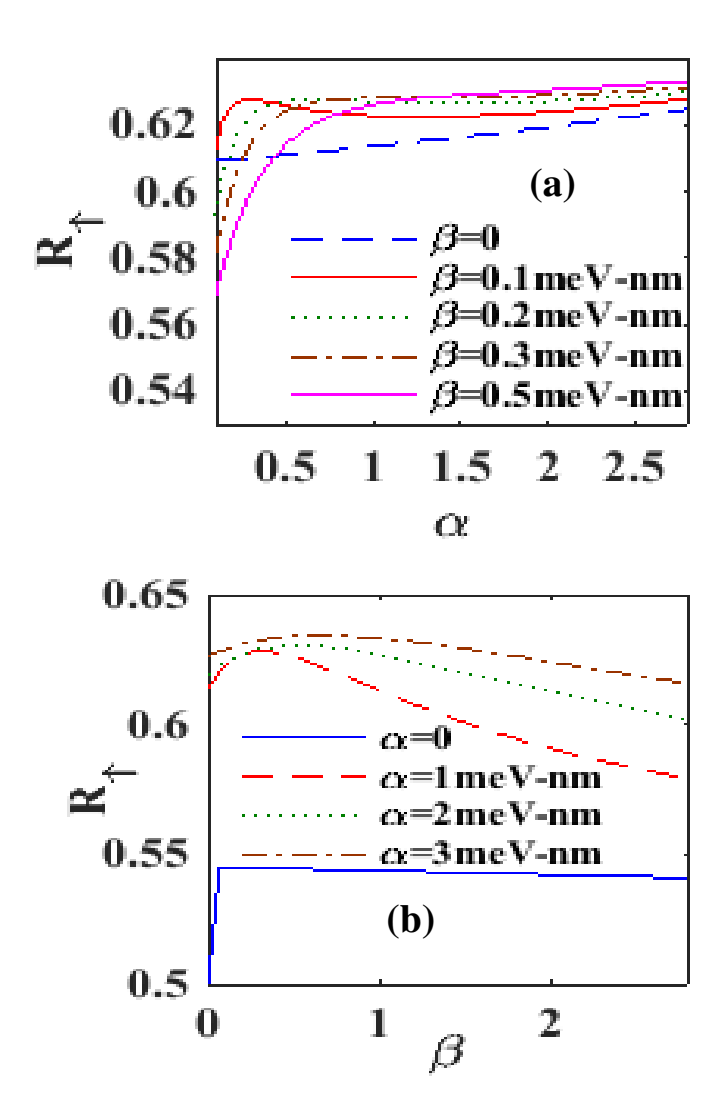


Fig. 6 (a) R_{\uparrow} vs. α for different values of β ; (b) R_{\uparrow} vs. β for different values of α .

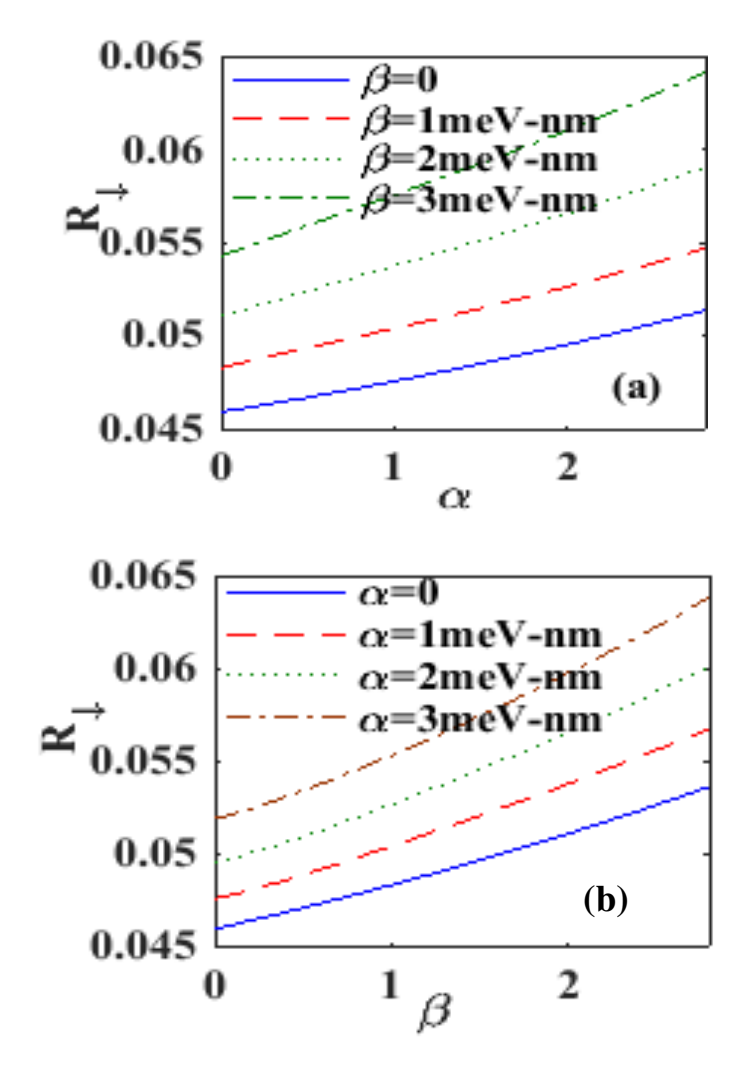


Fig. 7 (a) R_{\downarrow} vs. α for different values of β ; (b) R_{\downarrow} vs. β for different values of α .

Fig. 7 represents the behaviour of R_{\downarrow} as a function of α and β . Fig. 7 (a) shows that R_{\downarrow} rises monotonically with both α and β . It may be noted from Fig. 7 (a) and (b) that R_{\downarrow} behaves symmetrically with respect to α and β .

The variation of T_{\uparrow} with respect to α and β are shown in Fig. 8 (a) and 8 (b). As shown in these figures, the behaviour of T_{\uparrow} is similar to that of R_{\uparrow} , except for a small difference in T_{\uparrow} vs. β behaviour at low β .

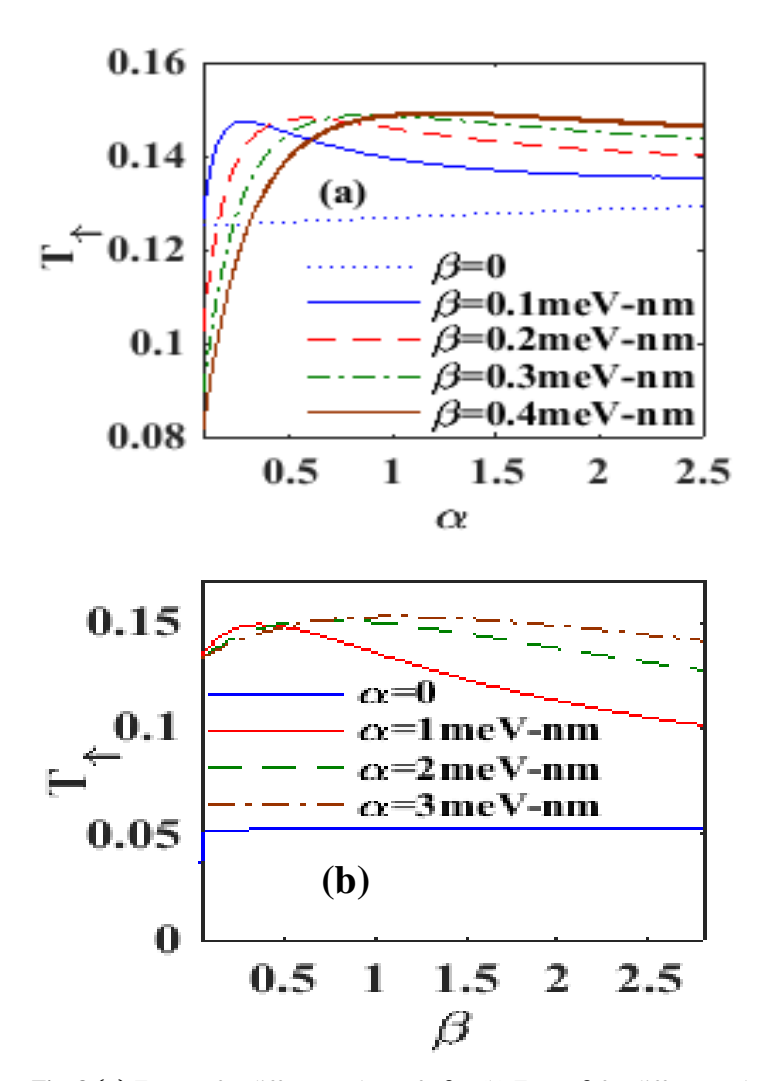


Fig. 8 (a) T_{\uparrow} vs. α for different values of β ; (b) T_{\uparrow} Vs β for different values of α .

Fig. 9 depicts the variation of T_{\downarrow} with α and β . Fig. 9(a) shows that for $\beta = 0$, T_{\downarrow} drops monotonically with increasing α almost linearly. For non-zero but small β , T_{\downarrow} first decreases rapidly as α increases from zero, then acquires a shallow minimum-like structure, and finally decreases

again. As β becomes a little lartger, the minimum disappears and T_{\downarrow} decreases with increasing α in a non-linear manner. The variation of T_{\downarrow} with β for different values of α is shown in Fig. 9 (b). For $\alpha=0$, T_{\downarrow}

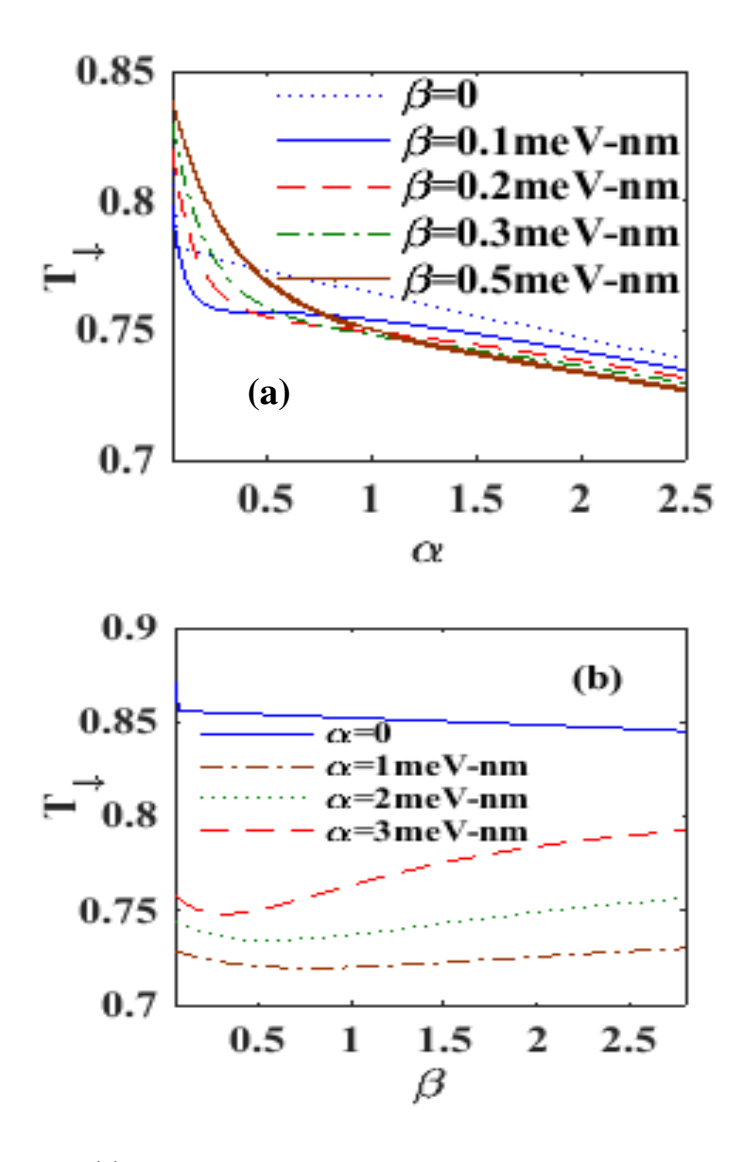


Fig. 9 (a) T_{\downarrow} Vs. α for different values of β ; (b) T_{\downarrow} Vs β for different values of α .

exhibits a slow monotonic linear decrease with increasing β . For non-zero α , T_{\downarrow} initially decreases as β increases from zero, develops a shallow

minimum-like structure and again increases. As α becomes larger, the minimum flattens more and more. We notice that T_{\downarrow} decreases with increasing α in a non-linear way.

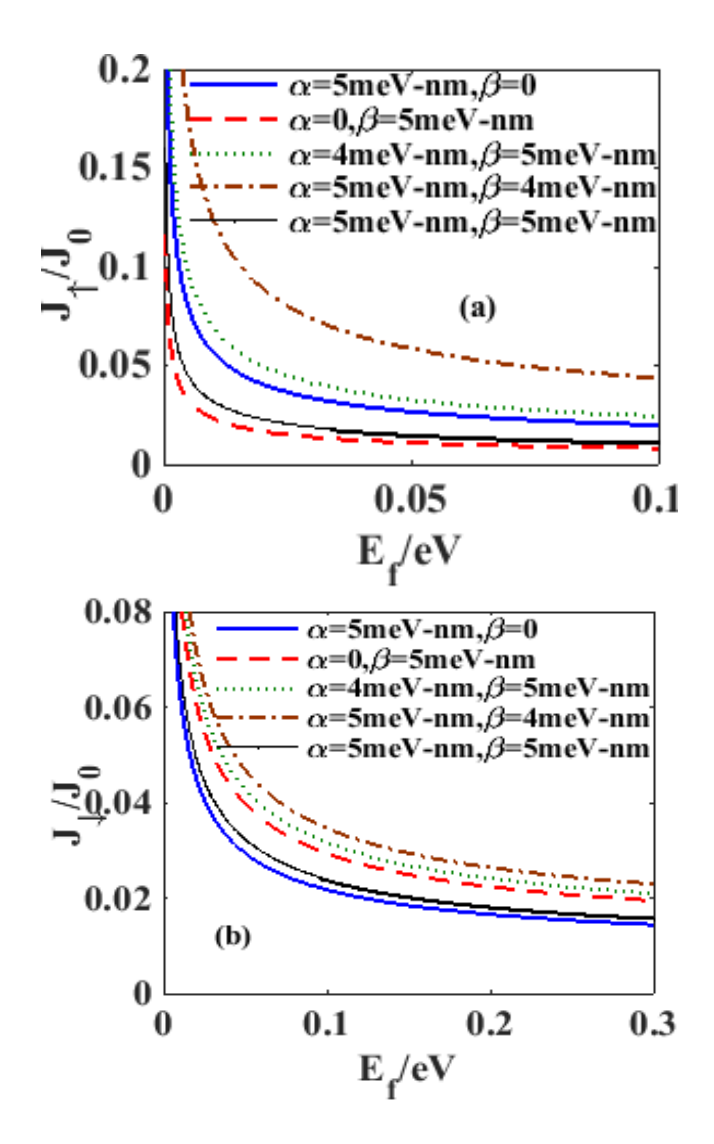


Fig. 10 (a) J_{\uparrow} Vs. E_f (b) J_{\downarrow} vs E_f for different cases as: $(1)\alpha \neq 0, \beta = 0$ $(2)\alpha = 0, \beta \neq 0$ $(3)\alpha < \beta(4)\alpha > \beta(5)\alpha = \beta$.

Fig. 10 gives the behavior of spin-polarized current densities $(J_{\uparrow} \ and \ J_{\downarrow})$ with Fermi energy E_f for various values of α , β (with $eV = 25 \ meV$). In

general, at small E_f , both J_{\uparrow} and J_{\downarrow} decrease rapidly with E_f , but as E_f is increased further, the rate of decrease in J_{\uparrow} and J_{\downarrow} becomes very slow and J_{\uparrow} and J_{\downarrow} appear to reach saturation. For certain combinations of α , β , the saturation in J_{\uparrow} happens quite fast though for a few other combinations the saturation is not so fast and also the saturation value is large. Fig. 10(b) shows that the saturation in J_{\downarrow} is slower in the case when either RSOI or DSOI is present than in the case when both are present.

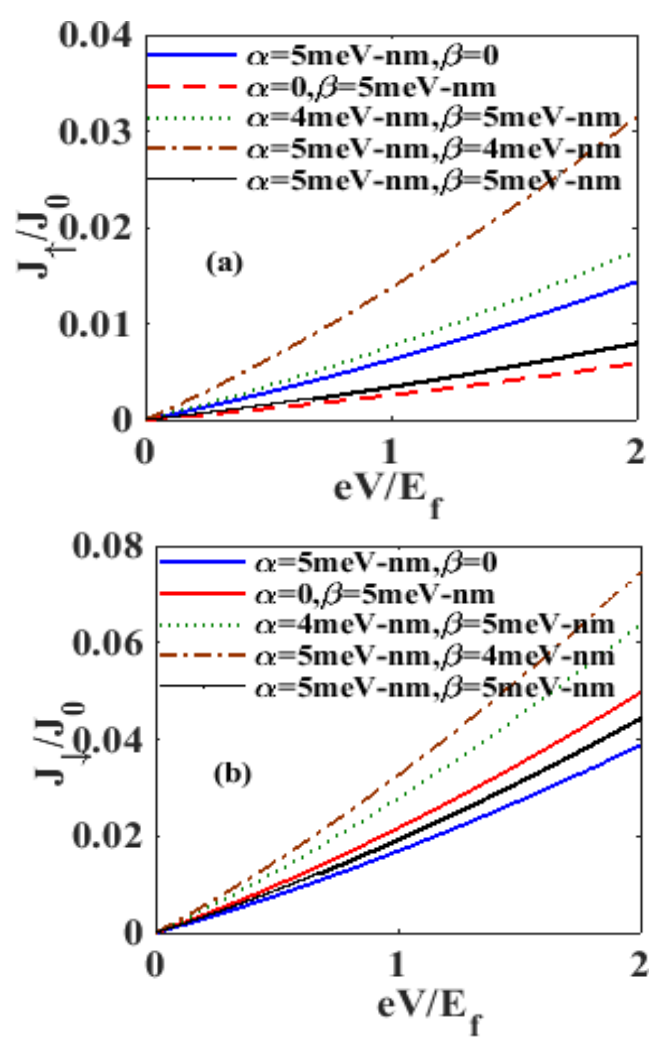


Fig. 11 (a) J_{\uparrow} vs. V (b) J_{\downarrow} vs. V for different cases as: $(1)\alpha \neq 0, \beta = 0$ $(2)\alpha = 0, \beta \neq 0$ $(3)\alpha < \beta$ $(4)\alpha > \beta$ $(5)\alpha = \beta$.

Fig. 11 (a) shows the variation of spin-polarized current density (J_{\uparrow}) with respect to the applied voltage for a few combinations of RSOI and DSOI coefficients with $E_f = 15 meV$. The figure suggests that J_{\uparrow} increases with the applied voltage monotonically and also reveals that J_{\uparrow} in the presence of RSOI alone, is much greater than J_{\uparrow} in the presence of DSOI alone. In

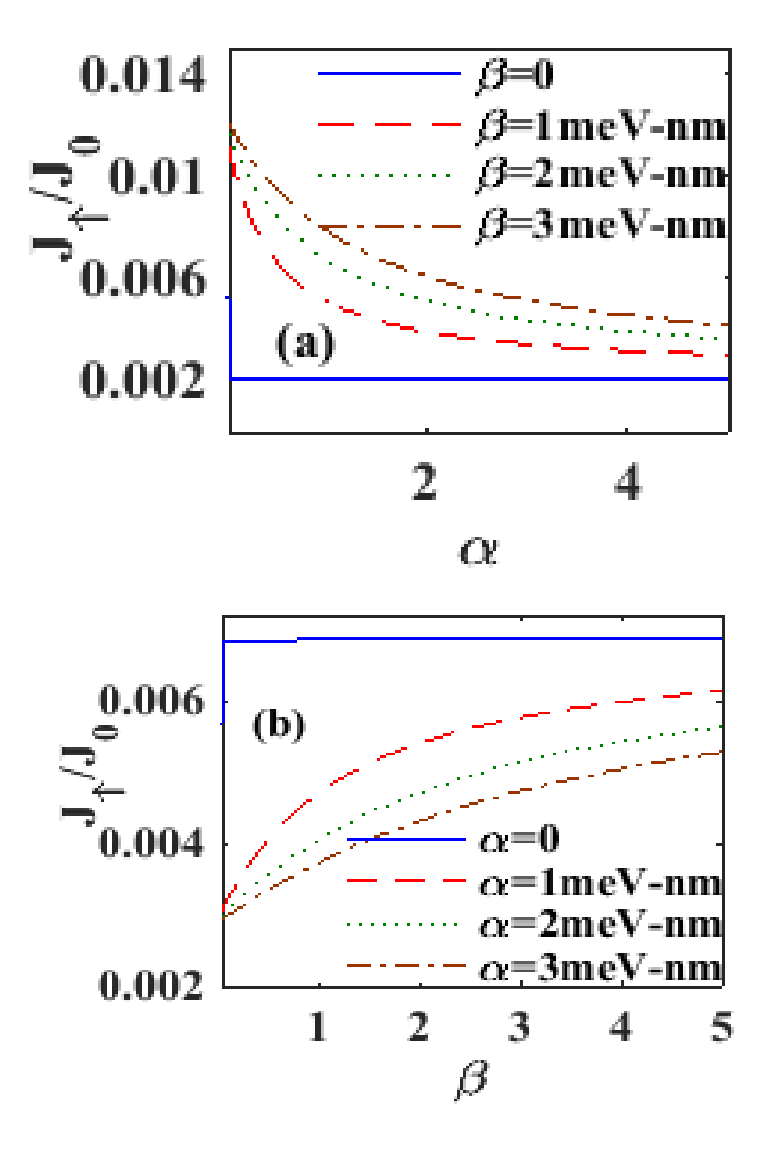


Fig. 12 (a) J_{\uparrow} vs. α for different values of β ; (b) J_{\uparrow} vs. β for different values of α .

the presence of RSOI, as DSOI is switched on, J_{\uparrow} initially increases with the voltage as β increases, though beyond a critical value of β , J_{\uparrow} decreases with the increase in the voltage. The behaviour of J_{\downarrow} with the voltage is shown in Fig. 11 (b) which is qualitatively similar to that of J_{\uparrow} .

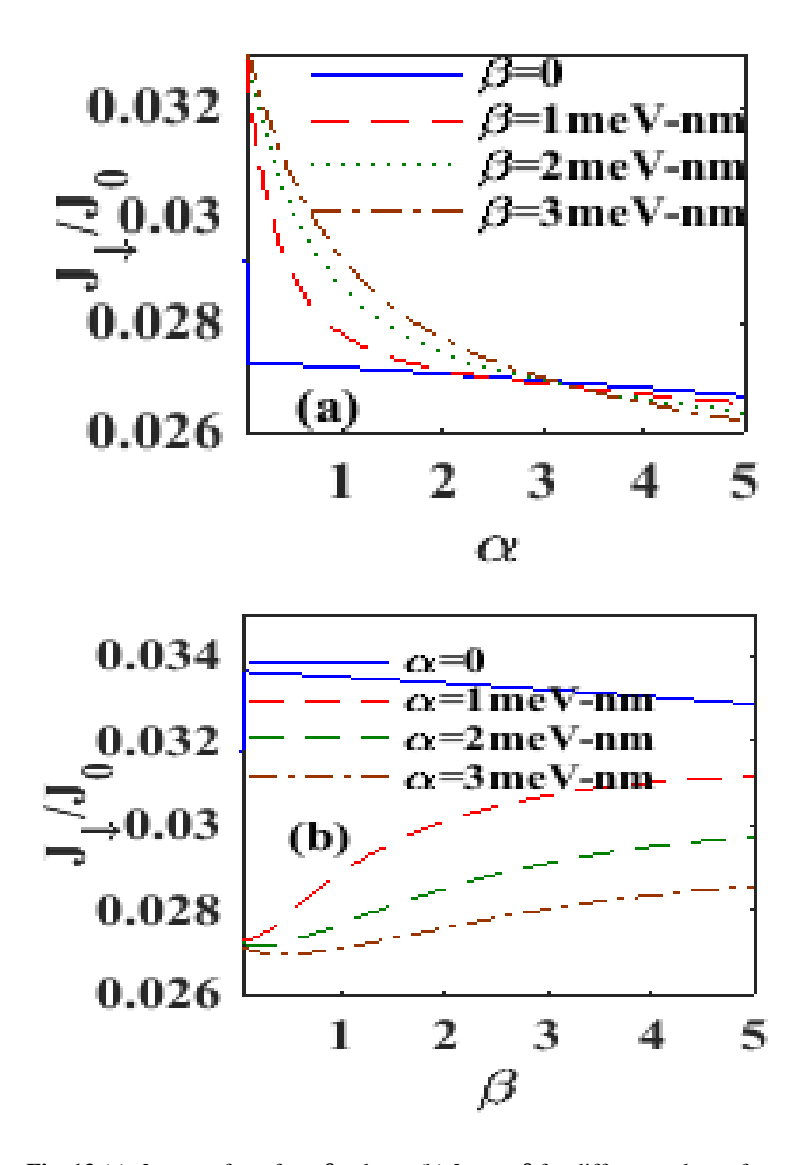


Fig. 13 (a) J_{\downarrow} vs. α for a few β value; (b) J_{\downarrow} vs. β for different values of α .

Figs. 12(a) and 12(b) show the plots of J_{\uparrow} with respect to of α and β respectively. One can see that RSOI reduces J_{\uparrow} while DSOI enhances it.

Fig. 13 shows that the variations of J_{\downarrow} with respect to α and β are very similar to those of J_{\uparrow} , although the magnitude of J_{\downarrow} is significantly larger than that of J_{\uparrow} .

The variation of the spin-up differential conductance G_{\uparrow} as a function of the SOI strengths is shown in Fig. 14. The inset of Fig.4 (a) shows that in the absence of DSOI, G_{\uparrow} increases with increasing α almost linearly. For non-zero, however, G_{\uparrow} remains zero up to a certain value of α , beyond

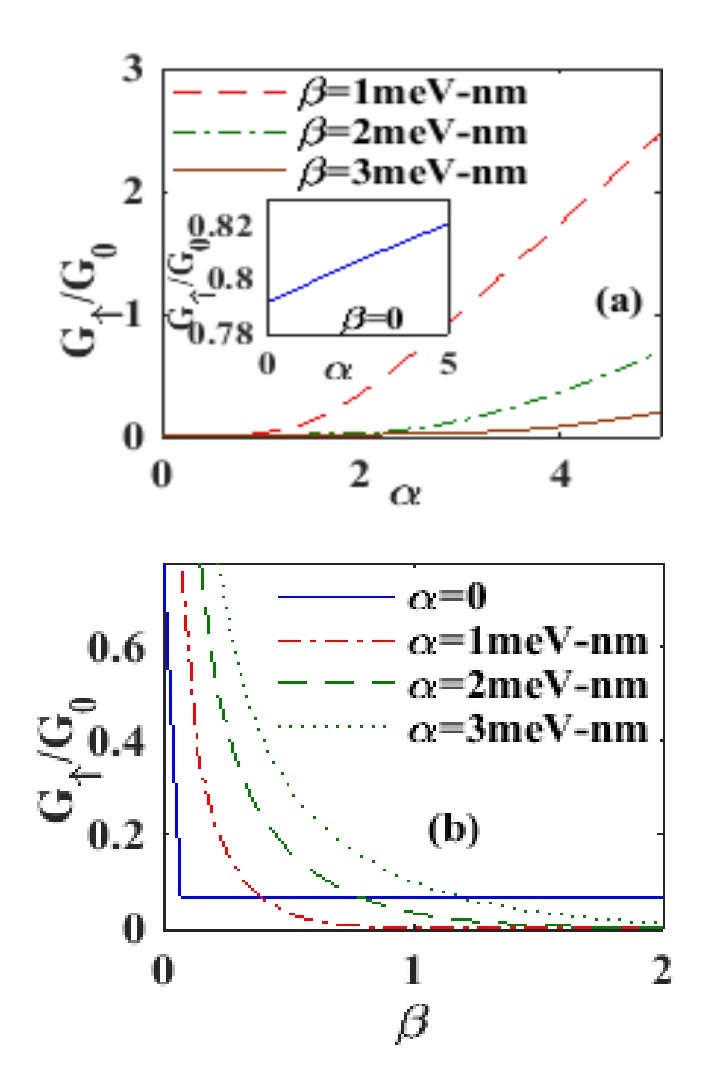


Fig. 14 (a) G_{\uparrow} vs. α for different values of β ; (b) G_{\uparrow} vs. β for different values of α .

which it monotonically grows with α . Fig. 14 (b) shows that in the absence of RSOI, G_{\uparrow} is virtually independent of β , while for non-zero values of α , G_{\uparrow} is extraordinarily large at small values of β , and as β increases, G_{\uparrow} rapidly falls off to zero.

Fig. 15 shows the behavior of G_{\downarrow} with regard to SOIs. As shown in Fig. 15 (a), for $\beta = 0$, G_{\downarrow} is very large up to a particular value of α , after

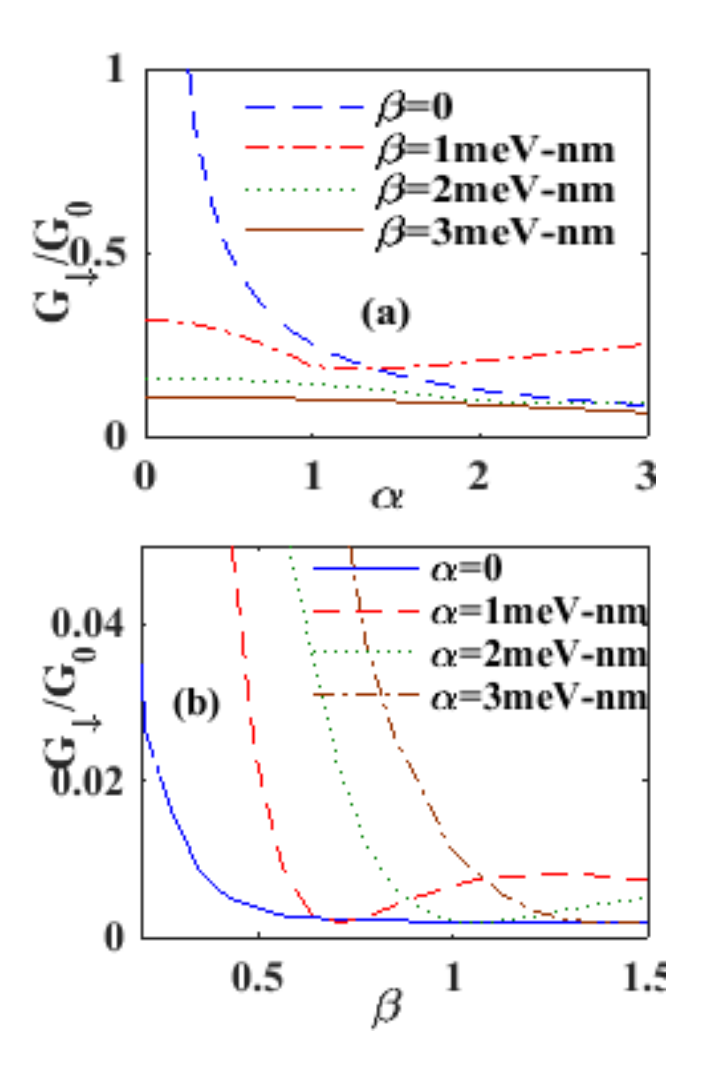


Fig. 15 (a) G_{\downarrow} vs. α for different values of β ; (b) G_{\downarrow} vs. β for different values of α .

which it rapidly drops to some constant value. For non-zero but small values of β (such as $\beta=1$), G_{\downarrow} is generally small at small α . It however shows a decreasing behaviour with increasing α , and then exhibits a dip-like structure and finally shows a slow linear increase with α . As β is increased further, G_{\downarrow} gets even smaller and drops extremely slowly with α . For large β , G_{\downarrow} becomes essentially independent of α . According to

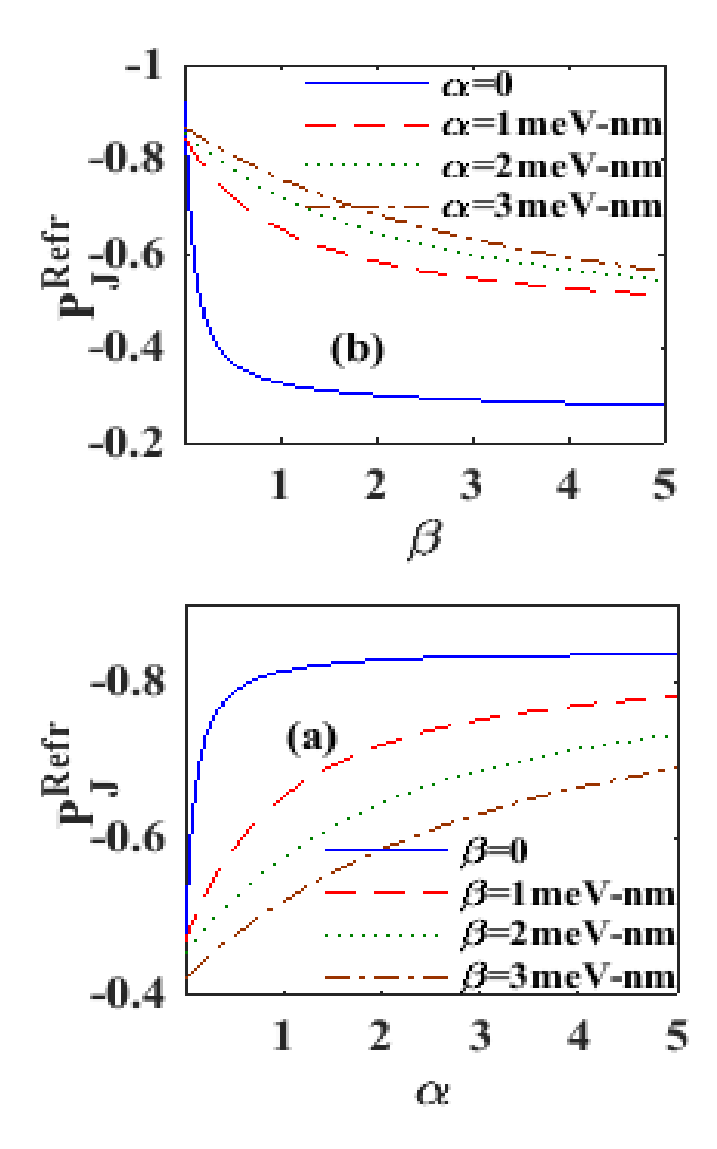


Fig. 16 (a) P_j^{Refr} vs. α for different values of β ; (b) P_j^{Refr} vs. β for different values of α .

Fig. 15(b), as a function of β , G_{\downarrow} decreases quite rapidly to a constant value for $\alpha = 0$. However, for nonzero values of α , G_{\downarrow} is very large below a specific value of β (which varies with α), above which, however, it rapidly decreases and produces a shallow minimum. The minimum shifts to the right and becomes shallower as α is increased.

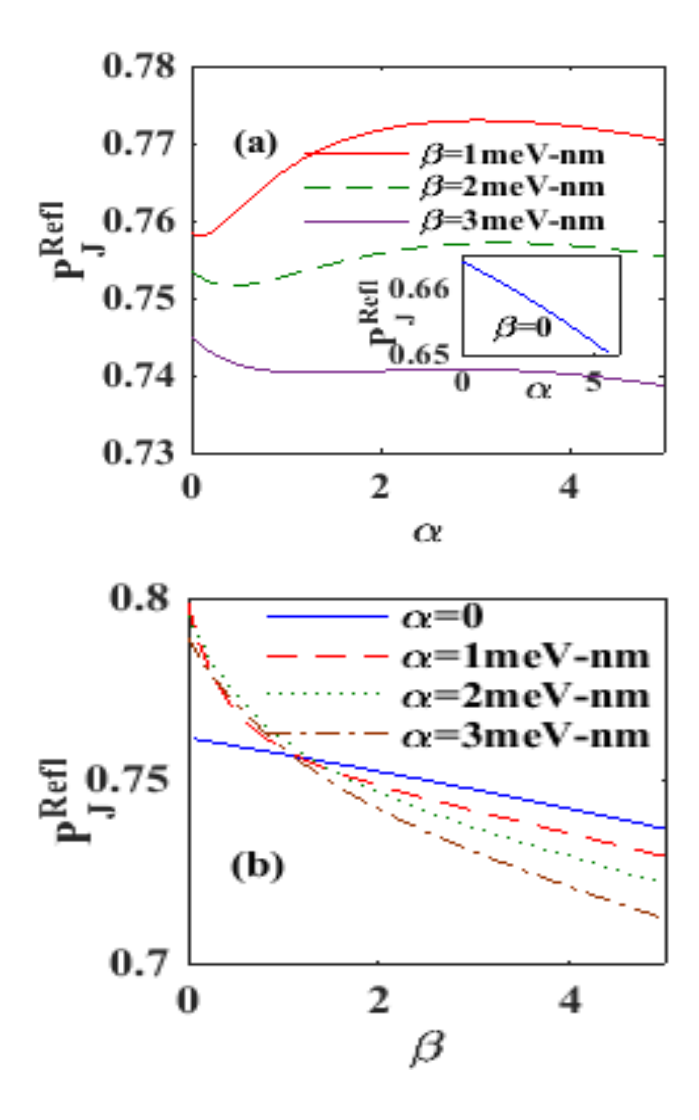


Fig. 17 (a) P_j^{Refl} vs. α for different values of β ; (b) P_j^{Refl} vs. β for different values of α .

The variation of spin polarisation current with α and β in the semiconductor region (P_j^{Refr}) is showed in Fig.16. Fig. 16(a) reveals that P_j^{Refr} is negative and its magnitude increases with α and saturates as α becomes large. The magnitude of P_j^{Refr} diminishes as a function of β and appears to saturate to some constant value at some large β . The same conclusion can be drawn from Fig. 16(b).

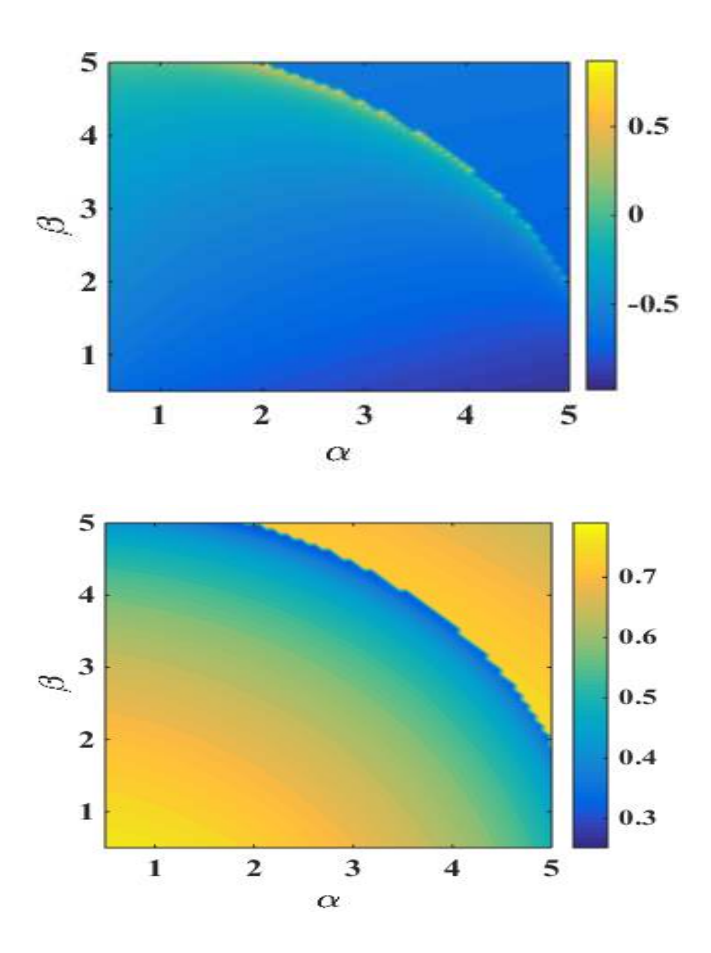


Fig. 18 Contour plots of (a) P_j^{Refr} in $\alpha - \beta$ space (b) P_j^{Refl} in $\alpha - \beta$ space.

The behavior of spin polarisation current (P_j^{Refl}) in the metallic region as a function of α and β is plotted in Fig. 17. The figures clearly show that

 P_j^{Refl} is positive. According to the inset of Fig. 17(a), in the absence of DSOI, P_j^{Refl} reduces with α . For non-zero β , P_j^{Refl} depends on α in a more complicated way. As α increases, P_j^{Refl} initially decreases, develops a shallow minimum (which becomes even shallower as increases α), and then develops a broad hump. Fg.17 (b) demonstrates that P_j^{Refl} reduces with increasing β and exhibits a crossing behavior.

Fig. 18 shows the contour plots of P_j^{Refr} and P_j^{Refl} . We see that P_j^{Refr} is negative while P_j^{Refl} is positive. This is consistent with the findings in Figs. 16 and 17. According to Fig. 18(a), the values of P_j^{Refr} are larger for higher values of α and for lower values of β . Thus, DSOI reduces P_j^{Refr} while RSOI increases it. As a result, RSOI and DSOI have competing effects on P_j^{Refr} . Consequently, spin polarisation current is greater when the only α is large than when both α and β are large. As shown in Fig. 18 (b), both RSOI and DSOI diminish the spin polarisation current in the metallic region.

4.5 Conclusions

The spin polarisation effects caused by electron refraction and reflection across a barrier separating a metal and a semiconductor have been investigated in the presence of both RSOI and DSOI. The refraction and reflection coefficients have been calculated, and experimentally measurable quantities such as up and down-spin current densities, the corresponding differential conductances, and the spin-polarization current have been obtained. The effects of incident angle, incident energy, applied voltage, and SOI strengths have been investigated. DSOI reduces the angle

of refraction of spin-up and spin-down electrons, with the spin-down electrons going through a significantly greater reduction. When both SOIs are present, the spin polarisability increases significantly, improving the spin-filtering effect as compared to the case when RSOI is present alone. It has been demonstrated that increasing the incident energy increases the angle of refraction of spin-up electrons while it decreases the angle of refraction of spin-down electrons. As a result, the incident energy can be employed to tune the spin-filtering effect J_{\uparrow} and J_{\downarrow} are likewise shown to decrease with Fermi energy and increase with applied voltage. Furthermore, RSOI decreases J_{\uparrow} while DSOI increases it. The behavior of J_{\downarrow} with respect to α and β is found to be comparable to that of J_{\downarrow} although the magnitude of J_{\downarrow} is significantly bigger than that of J_{\uparrow} .

When both RSOI and DSOI are present, the spin polarisation current P_j^{refr} in the semiconductor material is found to be negative, and its magnitude increases with α and decreases with β . The spin polarisation current P_j^{refl} in the metallic region turns out to be positive, and its magnitude increases with α and decreases with β . The current work could be used in spin filtering and spin polarising devices.

References

- 1. Bernardes. E, Schliemann. J, Lee. M, Egues. J. C, Loss. D. Spin-orbit interaction in symmetric wells with two subbands. *Phys. Rev. Lett.* **99**, 076603, (2007).
- **2.** Brüning. J, Geyler. V, Pankrashkin. K, Russ. On the discrete spectrum of spin-orbit Hamiltonians with singular interactions. *J. Math. Phys.* **14**, 423, (2007).

- **3.** Li. S. S, Xia. J. B. Spin-orbit splitting of a hydrogenic donor impurity in GaAs/GaAlAs quantum wells. *Appl. Phys. Lett.* **92**, 022102, (2008).
- **4.** Datta. S, Das. B. Ground state and binding energies of (D0), (D–) centres and resultant dipole moment of a (D–) centre in a GaAs quantum dot with Gaussian confinement. *Appl. Phys. Lett*, **56**, 665 (1990).
- **5.** Xiao. Y. C, Zhu. R, Deng. W. J. Ballistic transport in extended Datta–Das spin field effect transistors. *Solid State Commun.* **151**, 1214, (2011).
- 6. Pietilainen. P, Chakraborty. T, Phys. Rev. B, 73, 155315 (2006).
- 7. Boda. A, Chatterjee. A. Ground state and binding energies of (D0), (D-) centres and resultant dipole moment of a (D-) centre in a GaAs quantum dot with Gaussian confinement. *Physica E* **45**, 36, (2012).
- 8. Kumar. D. S, Mukhopadhyay. S, Chatterjee. A. Effect of Rashba interaction and Coulomb correlation on the ground state energy of a GaAs quantum dot with parabolic confinement. *Physica. E* **47**, 270 (2013).
- 9. Kumar. D. S, Boda. A, Mukhopadhyay. S, Chatterjee. A. Effect of Rashba spin-orbit interaction on the ground state energy of a D^0 centre in a GaAs quantum dot with Gaussian confinement. Superlattices and Microstructures 88,174 (2015).
- 10. Kumar. D. S, Mukhopadhyay. S, Chatterjee. A. Magnetization and susceptibility of a parabolic InAs quantum dot with electron–electron and spin–orbit interactions in the presence of a magnetic field at finite temperature. *J. Mag. Mag. Mat.* **418**, 169 (2016).
- 11. Boda. A, Boyacioglu. B, Erkaslan. U and Chatterjee. A. Effect of Rashba spin—orbit coupling on the electronic, thermodynamic, magnetic and transport properties of GaAs, InAs and InSb quantum dots with Gaussian confinement. *Physica B* **498**, 43 (2016).
- 12. Saini. P, Boda. A, Chatterjee. A. Effect of Rashba and Dresselhaus spin-orbit interactions on a D0 impurity in a two-dimensional Gaussian GaAs quantum dot in the presence of an external magnetic field. *J. Mag. Mag. Mat.* **485**, 407 (2019).
- 13. Schliemann. J, Lee. M, Egues. J. C, Loss. D. Nonballistic Spin-Field-Effect Transistor. *Phys. Rev. Lett.* **90**, 146801 (2003).

- 14. Schliemann. J, Loss. D. Anisotropic transport in a two-dimensional electron gas in the presence of spin-orbit coupling. *Phys. Rev.* B <u>68</u>, 165311 (2003).
- 15. Meng. T, Klinovaja. J, Loss. D. Renormalization of anticrossings in interacting quantum wires with Rashba and Dresselhaus spin-orbit couplings. *Phys. Rev.* B **89**, 205133 (2014).
- 16. Biswas. T, Gosh. T. K. Zitterbewegung of electrons in quantum wells and dots in the presence of an in-plane magnetic field. *Jour of Phys. Cond. Matt* **24**, 185304 (2012).
- 17. Sinitsyn. N. A, Hankiewicz. E. M, Teizer. W, and Sinova. J. Spin Hall and spin-diagonal conductivity in the presence of Rashba and Dresselhaus spin-orbit coupling. *Phys. Rev.* B **70**, 081312(R) (2004).
- 18. Badalyan. S. M, Abiague. A. M, Vignale. G, and Fabian. J. Anisotropic plasmons in a two-dimensional electron gas with spin-orbit interaction. *Phys. Rev.* B **79**, 205305(2009).
- 19. Matos-Abiague. A, Fabian. J. Anisotropic tunneling magnetoresistance and tunneling anisotropic magnetoresistance: Spin-orbit coupling in magnetic tunnel junctions. *Phys. Rev.* B **79**, 155303 (2009).
- 20. Monisha. P. J, Sankar. I.V, Sil. S and Chatterjee. A. Persistent current in a correlated quantum ring with electron-phonon interaction in the presence of Rashba interaction and Aharonov-Bohm flux. *Sci. Rep.* **6**, 20056 (2016).
- 21. Chatterjee. A, Smolkina. M. O, Popov. I. Y. Persistent current in a chain of two Holstein-Hubbard rings in the presence of Rashba spin-orbit interactions *Nanosystems: Physics, Chemistry, Mathematics* **10**, 50 (2019).
- 22. Prinz. G. A. Magnetoelectronics. *Science* **282**, 1660, (1998).
- 23. Heckel. B. R, Cramer. C. E, Cook. T.S, Adelberger. E. G, Schlamminger. S, Schmidt. U. New CP-violation and preferred-frame tests with polarized electrons. *Phys. Rev. Lett.* **97**, 021603, (2006).
- 24. Johnson. P. D. Spin-polarized photoemission. *Reports Prog. Phys.* **60**, 1217, (1997).
- **25.** Egues. J. C. Spin-Dependent Perpendicular Magnetotransport through a Tunable ZnSe / Zn 1 x Mn x Se Heterostructure: A Possible Spin Filter. *Phys. Rev. Lett.* **80**, 4578, (1998).

- **26.** Chang. K, Peeters. F. M. Spin polarized tunneling through diluted magnetic semiconductor barriers. *Solid State Commun.* **120**, 181, (2001).
- **27.** Schäpers. T, Nitta. J, Heersche. H. B, Takayanagi. H. Interference ferromagnet/semiconductor/ferromagnet spin field-effect transistor. *Phys. Rev. B.* **64**, 125314, (2001).
- 28. Li. H, Yang. X, Chen. W. Spin-polarization transport in ferromagnetic semiconductor/ferromagnetic -wave superconductor junctions. *Solid State Commun.* **150**, 772, (2010).
- 29. Högl. P, Matos-Abiague. A, Žutić. I, Fabian. J. Magnetoanisotropic Andreev reflection in ferromagnet-superconductor junctions. *Phys. Rev. Lett.* **115**, 116601, (2015).
- **30.** Aghel. F, Safaiee. R, Golshan. M. M. Dynamical spin polarization in single-layer graphene. *Phys. E Low-Dimensional Syst. Nanostructures.* **54**, 133, (2013).
- **31.** Shiraishi. M, Ohishi. M, Nouchi. R, Mitoma. N, Nozaki. T, Shinjo. T, Suzuki. Y. Robustness of Spin Polarization in Graphene-Based Spin Valves. *Adv. Funct. Mater.* **19**, 3711, (2009).
- **32.** Dyrdał, Barnaś. J. Current-induced spin polarization and spin-orbit torque in graphene. *Phys. Rev. B.* **92**, 165404, (2015).
- **33.** Papp. G, Peeters. F. M. Spin filtering in a magnetic–electric barrier structure. *Appl. Phys. Lett.* **78**, 2184, (2001).
- 34. Vali. R, Mirzanian. S. M. Effect of Rashba spin—orbit coupling on the spin polarized transport in diluted magnetic semiconductor barrier structures. *Solid State Commun.* **149**, 2032, (2009).
- 35. Ramaglia. V. M, Bercioux. D, Cataudella. V, De Filippis. G, Perroni. C. A. Spin polarization of electrons with Rashba double-refraction. *J. Phys. Condens. Matter.* **16**, 9143, (2004).
- 36. Dragoman. D. Optical analogues of nanostructures with Rashba–Dresselhaus interactions. *J. Opt.* **16**, 015710, (2014).
- 37. Yokoyama. T, Tanaka. Y, Inoue. J. Charge transport in two-dimensional electron gas/insulator/superconductor junctions with Rashba spin-orbit coupling. *Phys. Rev. B.* **74**, 035318, (2006).

- **38.** Egues. J. C, Gould. C, Richter. G, and Molenkamp. L. W. Spin-Dependent Perpendicular Magnetotransport through a Tunable ZnSe / Zn 1 x Mn x Se Heterostructure: A Possible Spin Filter. *Phys. Rev* B **64**, 195319 (2001).
- 39. Koga. T, Nitta. J, Takayanagi. H, Datta. S. Spin-filter device based on the Rashba effect using a nonmagnetic resonant tunneling diode. *Phys. Rev. Lett.* **88**, 126601, (2002).
- 40. Khodas. M, Shekhter. A, Finkel'stein. A. M. Spin polarization of electrons by nonmagnetic heterostructures: the basics of spin optics. *Phys. Rev. Lett.* **92**, 086602, (2004).
- **41.** Dargys. A. Double reflection of electron spin in 2D semiconductors. *Superlattices Microstruct.* **48**, 221, (2010).
- **42.** Dargys. A. Boundary conditions and transmission reflection of electron spin in a quantum well. *Semicond. Sci. Technol.* **27**, 045009, (2012).
- **43.** Dargys. A. Control of two-dimensional electron spin by an abrupt change of physical parameters of a quantum well. Lith. *J. Phys.* **51**, 53, (2011).
- **44.** Shao. P, Deng. W. Electronic double refraction due to the Rashba effect: Analytical and numerical results. *Front. Phys. China.* **2**, 44, (2007).
- 45. Srisongmuang. B, Pairor. P, Berciu. M. Tunneling conductance of a two-dimensional electron gas with Rashba spin-orbit coupling. *Phys. Rev. B.* **78**, 155317, (2008).
- 46. Ramaglia. V. M, Bercioux. D, Cataudella. V, De Filippis. G, Perroni. C. A., Ventriglia. F. Conductance of a large point contact with Rashba effect. *Eur. Phys. J. B Condens. Matter.* **36**, 365, (2003).

Chapter 6

Conclusions

In this thesis, we have investigated quantum transport SMT incorporating the effects of el-ph interaction Coulomb correlation and phononic dissipation and have also studied the Tunneling Conductance of electron spin across a metal-semiconductor junction where the semiconductor material contains Rashba and Dresselhaus spin-orbit interactions. In Chapters 2 and 3, we have studied the transport in the SMT system and in Chapter 4, we have studied the transport across a metal-semiconductor junction.

The SMT device we have explored in our work consists of a central quantum dot connected to two metallic electrodes, one being the Source (S) and the other the Drain (D). The central QD has been assumed to have a single phonon mode which interacts with the QD electrons. We have modelled this interaction using the Holstein Hamiltonian. The S-QD-D system is placed on an insulator substrate that works as a heat-bath. The heat-bath phonons and the QD phonon interact via Caldeira-Leggett coupling causing a quantum dissipative effect on the current in SMT. The entire dissipative SMT system has been modelled by the Anderson-Holstein-Caldeira-Leggett-Model.

In Chapter 2, we have considered the aforementioned SMT system in magnetic field at zero temperature. The coupling between the QD phonon and the bath phonons has been treated approximately using a unitary transformation that takes care of the dissipative effect of this coupling. The dissipation essentially reduces the QD phonon frequency and hence the energy. The Lang-Firsov unitary transformation has been used to separate the el-ph interaction from the system Hamiltonian. As a consequence, the device parameters are renormalized. The spectral density A, the tunnelling current J, and the differential conductance G have been calculated by employing the Keldysh non-equilibrium Green function approach. The spin polarisation parameter $P_{\sigma,-\sigma}$ has been estimated.

The spin degeneracy of the electronic state in QD is lifted by the magnetic field and this leads to splitting in the electron energy in QD and peaks in the spectral density. A_{\downarrow} is shifted to the +ve energy region by the magnetic field and A_{\uparrow} to the –ve energy region. J_{\downarrow} is reduced by both the magnetic field and el-ph coupling, as expected, but J_{\uparrow} increases with the increase in the magnetic field up to a critical value of B and then reduces to zero. J_{\uparrow} exhibits a similar pattern with respect to the el-ph coupling constant λ . The G-plots also indicate peak splitting due to the magnetic field B. This gives rise to additional energy levels accessible due to the splitting of spin degeneracy. G_{\uparrow} and G_{\downarrow} are found to reduce with increasing B. At zero magnetic field, G_{\uparrow} as well as G_{\downarrow} exhibits a peak at a particular value of λ and then both reduce to zero. With increasing B, the number of peaks G_{\uparrow} increases and the peaks become sharper. In the case of G_{\downarrow} however, the peak is suppressed by the magnetic field. At low magnetic field, $P_{\sigma,-\sigma}$, as a function of V_b , initially increases and reaches a maximum at a acertain value of V_b after which it starts decreasing and eventually reduces to zero. At higher magnetic fields, $P_{\sigma,-\sigma}$ increases with V_b and finally reaches saturation. We observe that as a function of the

magnetic field, $P_{\sigma,-\sigma}$ initially increases with B, attains a maximum and then reduces with further increase in B and eventually becomes zero. We have demonstrated that increasing the damping rate raises the spin polarised current densities, differential conductance, and spin polarisation parameter.

The behaviour of J and G with V_m had been studied before without taking into account the effect of el-el coupling and magnetic field. We have shown in this work that for $B \neq 0$, and $U \neq 0$, J vs V_m and G vs V_m curves undergo a shift towards positive side of V_m . Also in the case of G vs V_m curves, the number of peaks increases with G. The results of the present work suggest that the spin-polarization parameter can be tuned by a magnetic field and so an SMT device can find potential applications as a spin filter.

In Chapter 3, quantum transport in the same SMT system as above has been studied at finite temperature in the absence of a magnetic field using the same method. It is observed that dissipation increases the tunnelling current at finite temperatures but not as much as at zero temperature. As temperature increases, the current decreases and a similar behaviour is observed for the differential conductance.

In Chapter 4, we have studied the spin polarisation effects caused by electron reflection and refraction across a barrier separating a metal and a semiconductor that contains Rashba and Dresselhaus spin-orbit interaction (SOI) effects. The reflection and refraction coefficients have been calculated as a function of incident angle, incident energy, and SOI strengths. Furthermore, the effects of applied voltage, Fermi energy and SOIs have been studied on experimentally measurable quantities like up and down spin-current densities and the corresponding differential conductances. Finally the effect of SOIs on spin-polarization current has

been studied. It is found that DSOI reduces the angle of refraction of spinup and spin-down electrons, the reduction being much larger for the spindown electrons. Thus, when both SOIs are present, the spin polarizability increases substantially giving rise to a much larger spin-filtering effect compared to that in the presence RSOI alone. It is shown that the increase in the incident energy increases the angle of refraction of spin-up electrons while it reduces that of the spin-down electrons. Thus the incident energy can also be used to tune the spin-filtering effect. It is also observed that J_{\uparrow} and J_{\downarrow} decrease with Fermi energy and increase with the applied voltage. The spin polarization current P_j^{refr} in the semiconductor material is found to be negative in the presence of both RSOI and DSOI and their magnitudes increase with α and decrease with β while the spin polarization current P_j^{refl} in the metallic region is positive and it slightly increases with α and decreases with β . The present work has potential applications in spin filtering and spin polarizing devices.

Transport properties of a single molecular transistor and also across a metal-semiconductor interface

by Manasa Kalla

Indira Gandhi Memorial Library UNIVERSITY OF HYDERABAD Central University P.O.

HYDERABAD-500 046.

Submission date: 16-Mar-2022 05:42PM (UTC+0530)

Submission ID: 1785568931

File name: Manasakalla.pdf (2.14M)

Word count: 14767 Character count: 70404

Transport properties of a single molecular transistor and also across a metal-semiconductor interface

ORIGINALITY REPORT

SIMILARITY INDEX

INTERNET SOURCES

STUDENT PAPERS

PRIMARY SOURCES

Manasa Kalla, D. Sanjeev Kumar, Shreekantha Sil, Ashok Chatterjee. "Double refraction of electron spin across a metalsemiconductor junction with Rashba and Dresselhaus spin-orbit interactions: A stronger spin-filtering effect", Superlattices SCHOOL OF PHYSICS UNIVERSITY OF HYDERABAD and Microstructures, 2021

HYDERABAD - 500 046. INDIA

Publication

Manasa Kalla, Narasimha Raju Chebrolu, Ashok Chatterjee. "Magneto-transport properties of a single molecular transistor in the presence of electron-electron and electron-phonon interactions and quantum dissipation", Scientific Reports, 2019 Publication

UNIVERSITY OF HYDERAB HYDERABAD - 500 046, INL

www.ncbi.nlm.nih.gov

Internet Source

2%

assets.researchsquare.com

Internet Source

Manasa Kalla, Ch. Narasimha Raju, Ashok Chatterjee. "Magneto-transport properties of a single molecular transistor: Anderson-

Holstein-Caldeira-Leggett model", AIP Publishing, 2019

Publication

Filippo Furfaro. "A Probabilistic Framework for Building Privacy-Preserving Synopses of Multi-dimensional Data", Lecture Notes in Computer Science, 2008

<1%

Publication

Manasa Kalla, Narasimha Raju Chebrolu, Ashok Chatterjee. "Quantum transport in a single molecular transistor at finite temperature", Scientific Reports, 2021

<1%

Singiresu S. Rao. "Vibration of Continuous Systems", Wiley, 2019

<1%

Publication

Ch. Narasimha Raju, Ashok Chatterjee.
"Quantum dissipative effects on nonequilibrium transport through a singlemolecular transistor: The AndersonHolstein-Caldeira-Leggett model", Scientific
Reports, 2016
Publication

<1%

Manasa Kalla, Ashok Chatterjee. "Magnetotransport in an interacting single molecular transistor using Anderson-Holstein model", AIP Publishing, 2018

<1%

Publication

Submitted to University of Hyderabad, Hyderabad

<1%

12	Ch Uma Lavanya, Ashok Chatterjee. "Persistent charge and spin currents in the 1D Holstein-Hubbard ring at half filling and at away from half filling by Bethe-ansatz approach", Physica E: Low-dimensional Systems and Nanostructures, 2021 Publication	<1%
13	Ch. Narasimha Raju, Ashok Chatterjee. "Specific heat of a localized magnetic impurity in a non-magnetic host: A spectral density method for the Anderson–Holstein model", Physica B: Condensed Matter, 2015 Publication	<1%
14	www.freepatentsonline.com Internet Source	<1%
15	www.sciencegate.app Internet Source	<1%

Exclude quotes On Exclude matches < 14 words

Exclude bibliography On

The total Similarity index is 23%

The total Similarity index is 23%

out of which 17% is from the own

papers. So the effective similarity

papers is 6% which is whi

HYDERABAD - 500 046, INDIA